



Ghent University

Faculty of Engineering and Architecture

Department of Structural Engineering and Building Materials

Academic Year 2019-2020

**THE EFFECT OF FREE AREA SIZE AND DISTRIBUTION OF A PERFORATED FALSE
CEILING ON SMOKE AND VENTILATION DESIGN**

Student: Adina Arymbayeva

Promoter: Prof. Bart Merci

Master thesis submitted in the Erasmus+ Study Programme

International Master of Science in Fire Safety Engineering

DISCLAIMER

This thesis is submitted in partial fulfilment of the requirements for the degree of *The International Master of Science in Fire Safety Engineering (IMFSE)*. This thesis has never been submitted for any degree or examination to any other University/programme. The author(s) declare(s) that this thesis is original work except where stated. This declaration constitutes an assertion that full and accurate references and citations have been included for all material, directly included and indirectly contributing to the thesis. The author(s) gives (give) permission to make this master thesis available for consultation and to copy parts of this master thesis for personal use. In the case of any other use, the limitations of the copyright have to be respected, in particular with regard to the obligation to state expressly the source when quoting results from this master thesis. The thesis supervisor must be informed when data or results are used.

Read and approved,

31.07.2020

A handwritten signature in black ink, appearing to be 'M. J. J.', written over a horizontal line.

IMFSE Master Thesis Declaration

This form has been developed in the context of the unforeseen circumstances due to Covid-19, necessitating a reduction of practical project work (whether it be laboratory based, computational, or fieldwork) during the master thesis semester. It acts as a record of the impact on the master thesis. The form has been completed by the student and verified by the supervisor. **A copy of the signed form is included behind the abstract in the dissertation.**

Name: Adina Arymbayeva

Work completed

All items of wholly, or partially completed work must be listed, indicating the percentage completion for each task. **Please take care to provide a full detailed list of all work done.**

All work is complete as intended

Work not commenced

Any items of outstanding work that have not been started should be listed here.

No impact

Declaration

To the best of our knowledge, this form is an accurate record of the project status on _____ 31.07.2020

Student: Adina Arymbayeva _____



Supervisor: _____

Abstract

False ceiling installations are a popular solution to hide mechanical extraction systems in building spaces. Current guidance suggests a “rule-of-thumb” of a minimum 25% free area so that the smoke can flow through the perforations unhindered, which was based on experimental study. This threshold value is often misused in a wide range of false ceiling designs, although the original experimental work was carried out only for evenly distributed perforations in the false ceiling. To address the effects of the perforated false ceiling on the smoke and heat control system, a Computational Fluid Dynamics study was conducted using a Fire Dynamics Simulator. Firstly, this study examined the effects of the false ceiling with evenly distributed perforations on the gas temperatures and visibility inside the compartment where the smoke and heat control system is installed. Next, numerical simulations were carried out to see how the size and distribution of the openings in the false ceiling would affect the effectiveness of the smoke and heat control system, compared to false ceilings with evenly distributed perforations. The numerical results showed that for a fire as large as 2 MW the minimum of 40% free area will not hinder a significant amount of smoke from flowing through the false ceiling if the false ceiling is at the same level as the downstand. For free areas between 40 and 25%, extending the downstand below the false ceiling should be considered if the criterion is to contain the smoke within the compartment on fire. Evaluation of designs with various degrees of openness showed that the smoke above and below the false ceiling is dependent on the size and distribution of the openings and should be evaluated case by case in real-life applications. The numerical study demonstrated that taking the “rule-of-thumb” for designs that depart from the original experimental results gives rise to an ineffective smoke and heat control system which could result in high temperatures and loss of visibility at the escape routes.

Abstract in Qazaq (Түйіндеме)

Үйдің ішіндегі көтерме төбені орнату түрлі жайларда ауа тазартқыш (механикалық) жүйелерді жасырудың кең тараған шешімінің бірі. Қазіргі басшылық, эксперименттік зерттеулерге негізделген, түтіннің кедергісіз саңылаулардан өтуі үшін кем дегенде 25% бос аумақты «басқарудың ережесін» ұсынады. Бастапқы эксперименттік сынақ жұмысы тек ішінара тегіс аспалы төбе түрлерімен зерттелгенімен, күнделікті дизайн жұмыстарды жүзеге асырғанда осы ереже сақтала бермейді. Сонымен, аспалы төбені орнатқанда түтін мен жылудың бақылау жүйесінің жұмысын ойдағыдай атқаруын қадағалау үшін, оттың жану динамика симуляторының (FDS) көмегімен сұйықтықтың динамикасын зерттеу жүргізілді. Біріншіден, осы зерттеудің барысында аспалы төбенің теп-тегіс болуының әртүрлі мөлшердігі температураның қалыптылығын және ішкі көрінісін қалыпты жағдай дәрежесіне байланысты зерттелді. Содан кейін жалған төбедегі тесіктердің мөлшері мен таралуы әр түрлі дизайнерларын салыстырғанда түтін мен жылуды басқару жүйесінің тиімділігіне қалай әсер ететінін білу үшін сандық модельдеу жүргізілді. Сандық модельдеу нәтиже көрсеткендей, егер 2МВт-қа дейінгі өрт оқиғасы бола қалған жағдайда кем дегенде еркін алаңның 40% аспалы төбеден түтіннің өтуіне кедергі келтірмейді, егер аспалы төбесі бөлменің табалдырығымен бірдей деңгейде болса. Егер аспалы үйдің төбесі осындай деңгейде болған жағдайда өрт қауіпсіздігі сақталады. 40-тан 25% дейінгі еркін алаң үшін үйдің табалдырығының дейінгі аспалы төбеден төмендей болуы керек. Бұл өрт бола қалған жағдайда түтіннің мөлшерін іште шектеудің өлшемі болып табылады. Әр түрлі дизайнерларды бағалауда түтіннің аспалы төбенің үстінен және одан төмен қозғалуы саңылаулардың мөлшері мен таралуына байланысты екенін және оларды жеке-жеке бағалау керек екенін көрсетті. Көптеген есептік зерттеулер көрсеткендей, бастапқы эксперимент нәтижелерінен ауытқитын дизайнерлар үшін «бас ережесін» қолдану нәтижесіз түтін мен жылуды бақылау жүйесіне әкеліп соқтырады. Бұл қашу жолдарының бойында жоғары температура мен эвакуациялауға кедергі келтіріп, көрінуді жоғалтуына әкелуі мүмкін.

Abstract in Russian (Аннотация)

Установка подвесных потолков - популярное решение для скрытия механических вытяжных систем в различных помещениях. Текущее руководство предлагает «практическое правило» минимум 25% свободной площади, чтобы дым мог беспрепятственно проходить через отверстия, которое было основано на экспериментальном исследовании. Это пороговое значение часто неправильно используется в широком спектре конструкций подвесного потолка, хотя первоначальная экспериментальная работа проводилась только для равномерно распределенных перфораций в подвесном потолке. Чтобы учесть влияние перфорированного подвесного потолка на систему контроля дыма и тепла, было проведено исследование вычислительной гидродинамики (CFD) с использованием симулятора динамики огня (FDS). Во-первых, в этом исследовании изучалось влияние подвесного потолка с равномерно распределенными перфорациями на температуры горячего газа и видимость внутри помещения, где установлена система контроля дыма и тепла. Затем было проведено численное моделирование, чтобы увидеть, как размер и распределение отверстий в подвесном потолке влияют на эффективность системы контроля дыма и тепла по сравнению с подвесными потолками с равномерно распределенными перфорациями. Численные результаты показали, что при пожаре до 2 МВт минимальная свободная площадь 40% не будет препятствовать прохождению значительного количества дыма через подвесной потолок, если подвесной потолок находится на том же уровне, что и ветрина помещения. Для свободных площадей от 40 до 25% следует рассмотреть вопрос о расширении нижней части ниже подвесного потолка, если критерий должен ограничивать дым внутри помещения при пожаре. Оценка конструкций с различной степенью открытости показала, что дым выше и ниже подвесного потолка зависит от размера и распределения отверстий и должен оцениваться в каждом конкретном случае отдельно. Численное исследование продемонстрировало, что принятие «практического правила» для конструкций, которые отклоняются от первоначальных экспериментальных результатов, приводит к неэффективной системе контроля дыма и тепла, которая может привести к высоким температурам и потере видимости на путях эвакуации.

Acknowledgement

I would like to express my deepest appreciation to Prof. Bart Merci for support, guidance, and valuable advice during my final year and thesis semester. I am eternally grateful for your encouragement and profound belief in my work.

I would also like to extend my deepest gratitude to Dr Roger Harrison from the Building Research Establishment (BRE) for support, insightful suggestions, and constructive feedback on my work. Thank you for your invaluable insight into the subject matter that I will take with me beyond this master thesis.

I am extremely grateful to the Management Board of IMFSE, Prof. Bart Merci, Prof. Grunde Jomaas, Prof. Patrick Van Hees, Lies, and others for choosing me for this incredible program. Thank you for making the IMFSE a diverse, supportive, and fun family.

Big shoutout to my besties Karim and Sandesh with whom I spend three amazing semesters together. Thank you to Karim for the unparalleled support, encouragement, affection during these two years. Thank you to Sandesh for endless optimism, keenness for adventures, and group study sessions (videocall study sessions during the 2020 lockdown) together. I hope the special friendship bond between the three of us will last forever.

Many thanks to Dan, Kevin, Reyalen, Danny, Karim, and Sandesh for making the first semester memorable, as well as Ewana, Waqas, Maryam, Paolo, and Chamith for making Edinburgh, Lund, and Ghent feel like a home away from home.

Last but not least, I am extremely grateful for having such wonderful and supportive parents and siblings without whom I would not be able to reach what I have now. Thank you for encouraging me to chase my dreams and sharing my love for travels and adventures.

~This journey during IMFSE has been an incredible adventure that I will cherish forever~

Table of Contents

Abstract.....	iii
Abstract in Qazaq (Түйіндеме).....	iv
Abstract in Russian (Аннотация)	v
Acknowledgement	vi
List of Figures.....	viii
List of Tables.....	x
1 Introduction	1
1.1 <i>Background</i>	1
1.2 <i>Objectives</i>	8
2 Methodology.....	9
2.1 <i>Modelling setup (FDS simulations)</i>	11
2.2 <i>Mesh sensitivity analysis</i>	16
2.3 <i>Assessment of CFD modelling predictions</i>	17
2.3.1 <i>Description of the experimental study</i>	18
2.3.2 <i>Description of the numerical modelling</i>	20
2.4 <i>Configurations of evenly distributed perforated false ceiling</i>	26
2.5 <i>Configurations of uneven openings in the false ceiling</i>	27
3 Results and Discussion	32
3.1 <i>Part I: Perforated false ceiling</i>	32
3.1.1 <i>Temperature</i>	32
3.1.2 <i>Velocity</i>	39
3.1.3 <i>Visibility</i>	44
3.2 <i>Part II: Uneven openings in the false ceiling</i>	44
3.2.1 <i>Temperature</i>	45
3.2.2 <i>Visibility</i>	55
3.2.3 <i>Additional simulation</i>	57
3.3 <i>Design implications</i>	58
3.4 <i>Uncertainty</i>	61
4 Conclusion.....	62
4.1 <i>Recommendations for future work</i>	64
5 References	65
6 Appendix A: Slice files from all test runs	67
7 Appendix B. Design extraction rate calculation.	95
8 Appendix C: Additional simulations.....	98
9 Appendix D. FDS input for 40% free area uneven openness in the false ceiling. Design #5.....	102

List of Figures

Figure 1. Copied from [8]. Leaky false ceiling design where ceiling screens are extended above the false ceiling ..4	4
Figure 2. Copied from [8]. Perforated false ceiling with sufficient free area.....4	4
Figure 3. Compartment geometry used for this study.....12	12
Figure 4. Comparison of time and space averaged temperature values at various locations for 500 kW and 2 MW fires. (averaging time 100s) ..17	17
Figure 5. Copied from [10]. The geometry of the experimental model of 1/10 scale ..19	19
Figure 6. The geometry of the FDS models based on the experimental study [10]. Left: Natural ventilation model. Right: Mechanical ventilation model.21	21
Figure 7. Comparison of experimental and numerical data for temperature change in the compartment of fire. Experimental data is from [10], and numerical data is taken from FDS time-averaged steady-state result (50 s. of the averaging period). Locations of thermocouples are shown in Figure 5.....24	24
Figure 8. Comparison of experimental and numerical data for temperature change in at shopfront downstand (fascia). Experimental data is from [10], and numerical data is taken from FDS time-averaged steady-state result (50 s. of the averaging period). Locations of thermocouples are shown in Figure 5.....24	24
Figure 9. Comparison of experimental and numerical data for temperature change at the mall ceiling. Experimental data is from [10], and numerical data is taken from FDS time-averaged steady-state result (50 s. of the averaging period). Locations of thermocouples are shown in Figure 5.....25	25
Figure 10. Temperature fields of compartment with perforated false ceiling of 25% free area for 500 kW fire. Slice cut at X=7.5 m: 500kW (left) and 2MW (right). Time-averaged steady-state results (50 s. of the averaging period).....33	33
Figure 11. Temperature fields of compartment with perforated false ceiling of 25% free area for 500 kW fire. Slice cut at X=7.5 m: 500kW (left) and 2MW (right). Time-averaged steady-state results (50 s. of the averaging period).....33	33
Figure 12. Time and space averaged temperature change from thermocouples located 10 cm above and 10 cm below perforated false ceiling. Time-averaged steady-state results (50 s. of the averaging period). Locations of thermocouples are shown in Figure 3 ..35	35
Figure 13. Time and space averaged temperatures from thermocouples located at the ceiling. Time-averaged steady-state results (50 s. of the averaging period). Locations of thermocouples are shown in Figure 335	35
Figure 14. Time and space averaged temperatures rise from thermocouples located at the floor. Time-averaged steady-state results (50 s. of the averaging period). Locations of thermocouples are shown in Figure 337	37
Figure 15. Time and space averaged temperature change from thermocouples located below fascia (four shopfronts in total). Time-averaged steady-state results (50 s. of the averaging period). Locations of thermocouples are shown in Figure 3 ..39	39
Figure 16. Air entrainment pattern at the height of (a) 0.5 m (left) and (b) 1.5 m (right) Velocity vector horizontal slice. The time averaged result (the averaging time of 50 seconds).....40	40
Figure 17. Flow pattern of the plume deflected from the point of origin towards the openings for 40% free area. Velocity vector horizontal slice at the height of 2.2 m. The time averaged result (the averaging time of 50 seconds).....41	41
Figure 18. Flow pattern of the plume deflected from the point of origin towards the openings. (Left) Temperature horizontal slice at the height of 2.3 m. (Right) Velocity vector horizontal slice at the height of 2.2 m. The time averaged result (the averaging time of 50 seconds).....41	41
Figure 19. Flow pattern of the plume deflected from the point of origin towards the openings. Velocity vector horizontal slice for 15% free area at the height of 2.2 m. The time averaged result (the averaging time of 50 seconds).....42	42
Figure 20. Comparison of temperature changes for perforated false ceiling with 6, 10, 15, 25, and 40% free area and uneven openness of 40% with various designs. Temperature readings are from thermocouples located at each of the four shopfront downstands. TCF1, TCF2, TCF3, and TCF4 are thermocouple names. Time-averaged steady-state results (50 s. of the averaging period).....45	45
Figure 21. Temperature slice cut at 2.5 m (Y-axis) for uneven openness of 40% Design #1. Black line on the slice is false ceiling location.....46	46

Figure 22. Comparison of ambient temperature changes for perforated false ceiling with 6, 10, 15, 25, and 40% free area and uneven openness of 40% with various designs. Temperature readings are from thermocouples located at the floor level. TCA1, TCA2, TCA3, and TCA4 are thermocouple names. Time-averaged steady-state results (50 s. of the averaging period)	47
Figure 23. Comparison of temperature changes at the false ceiling level for perforated false ceiling with 6, 10, 15, 25, and 40% free area and uneven openness of 40% with various designs. Temperature readings are from thermocouples located 10 cm below the false ceiling (2.3 m from the floor). TFM1, TFM2, TFM3, and TFM4 are thermocouple names. Time-averaged steady-state results (50 s. of the averaging period).....	47
Figure 24. Horizontal temperature fields for Design #2 (left) and Design #3 (right) of 40% uneven openness at the height of 2.0 m above floor.	48
Figure 25. Velocity field of 40% Design #7 at 7.5m of Y-axis. Hot gases are flowing out of the compartment at velocity higher than 1.6 m/s.	51
Figure 26. Horizontal temperature fields for Design #7 of 40 per cent uneven openness at the height of 2.0 m (left) and 2.3 m (right) above floor.	52
Figure 27. Comparison of temperatures for perforated false ceiling with 6, 10, 15, 25, and 40% free area and uneven openness of 25% with various designs. Temperature readings are from thermocouples located at each of the four shopfront downstands. TCF1, TCF2, TCF3, and TCF4 are thermocouple names. Time-averaged steady-state results (50 s. of the averaging period).....	54
Figure 28. Comparison of temperature changes at the false ceiling level for perforated false ceiling with 6, 10, 15, 25, and 40% free area and uneven openness of 25% with various designs. Temperature readings are from thermocouples located 10 cm below the false ceiling (2.3 m from the floor). TFM1, TFM2, TFM3, and TFM4 are thermocouple names. Time-averaged steady-state results (50 s. of the averaging period).....	54
Figure 29. Visibility fields at 2 m for 40%. (a) Design #3 (left). (b) Design #5 (right). Time-averaged steady-state results (50 s. of averaging period).....	56
Figure 30. Visibility fields at 2 m. From left to right: (a) 6% even perforations. (b) 40% Design #7. (c) 25% Design #7. Time-averaged steady-state results (50 s. of averaging period).....	57
Figure 31. Comparison of temperatures for perforated false ceiling with 6, 10, 15, 25, 40, 50, and 60% free area and uneven openness of 40% with various designs. Temperature readings are from thermocouples located at each of the four shopfront downstands. TCF1, TCF2, TCF3, and TCF4 are thermocouple names. Time-averaged steady-state results (50 s. of the averaging period).....	99
Figure 32. Comparison of temperatures for perforated false ceiling with 6, 10, 15, 25, 40, 50, and 60% free area and uneven openness of 25% with various designs. Temperature readings are from thermocouples located at each of the four shopfront downstands. TCF1, TCF2, TCF3, and TCF4 are thermocouple names. Time-averaged steady-state results (50 s. of the averaging period).....	100
Figure 33. Comparison of temperatures for perforated false ceiling with 6, 10, 15, 25, 40, 50, and 60% free area and uneven openness of 40% with various designs. Temperature readings are from thermocouples located 10 cm below false ceiling. TFM1, TFM2, TFM3, and TFM4 are thermocouple names. Time-averaged steady-state results (50 s. of the averaging period)	100
Figure 34. Comparison of temperatures for perforated false ceiling with 6, 10, 15, 25, 40, 50, and 60% free area and uneven openness of 25% with various designs. Temperature readings are from thermocouples located 10 cm below false ceiling. TFM1, TFM2, TFM3, and TFM4 are thermocouple names. Time-averaged steady-state results (50 s. of the averaging period)	101

List of Tables

Table 1. Boundary condition in the FDS model.....	11
Table 2. Approximate estimation of open and closed cells in the matrix to design for numerical simulations using PyroSim.....	13
Table 3. Conditions modelled in this study.....	15
Table 4. Boundary condition in the FDS model.....	20
Table 5. The geometry of the false ceiling in the numerical model. Dark grey represents perforations in the false ceiling.....	22
Table 6. Description of the simulations compared with the experimental data.....	22
Table 7. Modelling of the evenly distributed perforated false ceiling with different free areas (dark blue filling represents perforations).....	26
Table 8. Modelling of the uneven openings in the false ceiling for 25% and 40% free areas with various designs (dark blue/grey filling represents opening in the false ceiling).....	28
Table 9. The radial distance of 100°C and higher temperatures that spread 10 cm above and 10 cm below the false ceiling for 2 MW fire.....	34
Table 10. Temperature change difference from thermocouples readings that are located at 2.5 m and 3.9 m height for 2 MW fire.....	36
Table 11. Comparison of velocity contour of 0.35 m/s for 100 and 60% free area. Vertical slices at the locations (from top to bottom) 7.5, 5.0, and 2.5 meters.....	37
Table 12. Maximum ceiling jet velocity and radial distances for 2 MW fire. 7.5 m is the maximum confined radial distance at the ceiling level. Unconfined – meaning at this velocity, the ceiling jet travels beyond the compartment.....	43
Table 13. Effectiveness (in terms of average temperature rise) at the shopfront and below the false ceiling of 40% uneven openness designs compared to 40% and 6% perforations. A positive value means an increase in the average temperature rise (less effective); a negative value means the design is more effective than even perforations in the false ceiling.....	50
Table 14. Effectiveness (in terms of average temperature rise) at the shopfront and below the false ceiling of 25% uneven openness designs compared to 25% and 6% perforations. A positive value means an increase in the average temperature rise (less effective); a negative value means the design is more effective than even perforations in the false ceiling.....	53
Table 15. Horizontal temperature fields of additional simulations for uneven openness in the false ceiling. Slice cut is at Z=2.3 m (10 cm below false ceiling). Time-averaged steady-state results (50 s. of the averaging period).....	58
Table 16. Temperature, velocity, and visibility scales for the following tables of horizontal and vertical planes...67	67
Table 17. Temperature slices at various locations with truncated temperatures below 30°C for 2 MW fire. Time-averaged steady-state results (50 s. of the averaging period). Slice cut is at 2.5 m on the X-axis. Blackline on the temperature slices is false ceiling locations. Colour bar scale is given in Table 16.....	68
Table 18. Temperature and velocity fields of perforated false ceilings for 500 kW design fire. Time-averaged steady-state results (50 s. of the averaging period). Slice cut is at 2.5 m on the X-axis. The black line on the temperature slices is false ceiling locations. Colour bar scale is given in Table 16.....	69
Table 19. Temperature and velocity fields of perforated false ceilings for 500 kW design fire. Time-averaged steady-state results (50 s. of the averaging period). Slice cut is at the middle of the fire source (X=7.5 m). A black line on the temperature slices is false ceiling locations. Colour bar scale is given in Table 16.....	70
Table 20. The temperature on horizontal fields at 2.0, 2.3, 2.5, and 3.0 m heights for perforated false ceilings with 500 kW design fire. Time-averaged steady-state results (50 s. of the averaging period). Colour bar scale is given in Table 16.....	71
Table 21. Temperature and velocity fields of perforated false ceilings for 2 MW design fire. Time-averaged steady-state results (50 s. of the averaging period). Slice cut is at 2.5 m on the X-axis. Blackline on the temperature slices is false ceiling locations. Colour bar scale is given in Table 16.....	73
Table 22. Temperature and velocity fields of perforated false ceilings for 2 MW design fire. Time-averaged steady-state results (50 s. of the averaging period). Slice cut is at the middle of the fire source (X=7.5 m). Blackline on the temperature slices is false ceiling locations. Colour bar scale is given in Table 16.....	74

Table 23. The temperature on horizontal fields at 2.0, 2.3, 2.5, and 3.0 m heights for perforated false ceilings with 2 MW design fire. Time-averaged steady-state results (50 s. of the averaging period). Colour bar scale is given in Table 16	75
Table 24. Visibility on horizontal fields at 2.0, 2.3, 2.5 m heights for perforated false ceilings with 500 kW design fire. Time-averaged steady-state results (50 s. of the averaging period). Colour bar scale is given in Table 16	77
Table 25. Visibility on horizontal fields at 2.0, 2.3, 2.5 m heights for perforated false ceilings with 2 MW design fire. Time-averaged steady-state results (50 s. of the averaging period). Colour bar scale is given in Table 16	79
Table 26. Velocity vector slices at 1.5 m and 2.2 m for 50, 40, 25, 15% for 2 MW fire. Time-averaged steady-state results (50 s. of the averaging period). Colour bar scale is given in Table 16	81
Table 27. Temperature and velocity fields of uneven openings in the false ceilings for relative openness of 40% (2 MW design fire). Time-averaged steady-state results (50 s. of the averaging period). Slice cut is at 2.5 m on the Y-axis. The black line on the temperature slices is false ceiling locations. Colour bar scale is given in Table 16	82
Table 28. Temperature and velocity fields of uneven openings in the false ceilings for relative openness of 40% (2 MW design fire). Time-averaged steady-state results (50 s. of the averaging period). Slice cut is at 7.5 m on the Y-axis. The black line on the temperature slices is false ceiling locations. Colour bar scale is given in Table 16	83
Table 29. Temperature and velocity fields of uneven openings in the false ceilings for relative openness of 25%. Time-averaged steady-state results (50 s. of the averaging period). Slice cut is at 2.5 m on the Y-axis. The black line on the temperature slices is false ceiling locations. Colour bar scale is given in Table 16	84
Table 30. Temperature and velocity fields of uneven openings in the false ceilings for relative openness of 25%. Time-averaged steady-state results (50 s. of the averaging period). Slice cut is at 7.5 m on the Y-axis. The black line on the temperature slices is false ceiling locations. Colour bar scale is given in Table 16	85
Table 31. The temperature on horizontal fields at 2.0, 2.3, 2.5, and 3.0 m height for uneven openings in the false ceilings for relative openness of 40%. Time-averaged steady-state results (50 s. of the averaging period). Colour bar scale is given in Table 16	87
Table 32. The temperature on horizontal fields at 2.0, 2.3, 2.5, and 3.0 m height for 25% uneven openings in the false ceilings. Time-averaged steady-state results (50 s. of the averaging period). Colour bar scale is given in Table 16.....	89
Table 33. Visibility on horizontal fields at 2.0, 2.3, and 2.5 m height for uneven openings in the false ceilings for relative openness of 40%. Time-averaged steady-state results (50 s. of the averaging period). Colour bar scale is given in Table 16.....	91
Table 34. Visibility on horizontal fields at 2.0, 2.3, and 2.5 m height for uneven openings in the false ceilings for relative openness of 25%. Time-averaged steady-state results (50 s. of the averaging period). Colour bar scale is given in Table 16.....	93
Table 35. The geometry of additional performed simulation.....	98

List of abbreviations

BRE – Building Research Establishment

BSI – The British Standards Institution

CFD – Computational Fluid Dynamics

DNS – Direction Numerical Simulations

FC – False ceiling

FDS – Fire Dynamics Simulator

HRR – Heat Release Rate

HRRPUA – Hat Release Rate Per Unit Area

LES – Large Eddy Simulation

NFPA – National Fire Protection Association

SFPE – Society of Fire Protection Engineers

SHEVS – Smoke and Heat Exhaust Ventilation Systems

SOFIE – Simulation of Fire in Enclosure

SVLES – Simple Very Large Eddy Simulation

VLES – Very Large Eddy Simulation

1 Introduction

1.1 Background

Public buildings, such as shopping malls and airports, that accommodate a large number of people could become an area where there is a rapid spread of smoke and other combustion products in the event of a fire, that could hinder the escape routes and endanger people's lives [1]. By design, these places might have large elongated areas (a mall or street) that open up into many individual compartments and shops. Morgan et al. state that considerations for the means of escape for individual shops and shops within shopping complexes in general fall into the same category. This means that the means of escape from individual shops into the shopping malls are not considered as being part of the enclosed space, but rather an escape to an open street. However, when people exit the individual shops into the corridor of the mall, this area is another potentially unsafe zone. As a result, additional fire safety measures need to be provisioned for shopping streets in which people still have to exit by travelling down the mall [2].

According to NFPA Standards, smoke management systems in a shopping mall or atrium are required to achieve the following performance objectives [3] [4,5]:

- Maintain tenable conditions along the egress path within the mall and atrium during an evacuation
- Limit the spread of smoke within the smoke reservoir or space
- Limit the movement of smoke into adjacent compartments in the mall or atrium
- Maintain tenable conditions within the mall or atrium for firefighting operations.

Preventing the spread of smoke is achieved with one of a number of smoke management strategies for malls and individual shops. These include smoke and heat exhaust ventilation, depressurisation, temperature control ventilation, smoke filling, and others [6,7]. The main focus of this work is smoke and heat control systems.

In large areas such as malls, atria and large undivided shops, when physical separation and segregation of the space through compartmentation (walls and doors) is not desirable, area smoke and heat control systems are employed [6]. Such systems are used in order to vent out the smoke that is collected in the smoke reservoir of the mall or particular shop so that life safety objectives are achieved - people have enough time to evacuate, and firefighting

operations can be conducted without any interruption and complications. This is because large malls inherently accommodate people who might not be familiar with the building and its means of egress, so in case of emergency, visitors tend to exit through the same route as they arrived. This would mean that unintentionally, visitors might take a longer route to evacuate. Because smoke can have fatal effects on humans, the smoke management system should be designed to allow visitors enough time to evacuate through the mall corridors. In settings such as large malls with shops, one of the best design options would be to prevent or allow only minimal smoke to escape into the mall corridor from the shop in the fire. Ideally, this is done by installing smoke and heat control systems in each shop within the shopping mall. It is challenging to achieve and expensive to install separate extraction systems in each shop, so the preferred option, in this case, would be to install a common smoke and heat control system in the mall. However, in particular circumstances, smoke and heat control systems in each shop are unavoidable, for example, if a smoke and heat control system cannot be installed in the mall corridor due to constructive restrictions of the mall [2]. Additional protection measures are required for shops larger than 1000 m² for natural ventilation and 1300 m² for mechanical ventilation [2]. There should be a compromise between design and economic considerations and limiting the extent of the smoke layer. Sufficient ventilation needs to be provided for each smoke reservoir based on the smoke production of the specific fire size. As Hinkley recommends, the maximum area for the reservoir should be not more than 1000 m² or the size of the shop if it is less than 1000 m². If the shop is less than 1000 m², the walls and deep shopfront downstand over the shop front should be acting as a reservoir [8].

Extraction systems are used to limit the spread of smoke to other areas. Significant accumulations of smoke cannot be avoided unless the ventilation system installed is large enough to cope with the plume mass flow rate in the shop. However, this approach is not feasible in terms of practicality of the installation since, in reality, the formation and presence of a smoke layer are inevitable. As a result, the design of a smoke and heat control system that will ensure that the spread of smoke is restricted and minimise the mixing with fresh air is a practical and feasible approach. This, according to Hinkley, can be achieved if four elements are considered in the design process [8]:

1. Strictly controlling the size of the fire to restrict the smoke production rate. Ideally, this is achieved by limiting the combustible content of the shop, but this is not always possible. So, a standard practice to control the fire is the use of sprinkler systems.
2. Smoke reservoirs, which are generally areas underneath the ceiling that are restricted by smoke screens extending from the ceiling towards the floor or design features that will act as a reservoir.
3. Presence of a ventilation system, either natural or mechanical, to extract the smoke without significant accumulation.
4. Introduction of fresh air in order to replace extracted smoke.

According to Morgan, statistically, the vast majority of the fatalities from fire incidents occur because of the effects of smoke [2]. As a result, life safety is an essential objective in shopping malls and buildings similar to long shopping malls (i.e. airports). It is essential to ensure that, depending on the regulation of the particular jurisdiction, the accumulation of thermally buoyant smoky gases can be kept at the clear smoke layer height from escape routes. The author also noted the importance of ensuring that the smoke ventilation design is capable of performing for the period required, not only for people to evacuate, but also to ensure uninterrupted access for firefighters [6].

False ceilings are a frequently used solution in malls and shops for aesthetic reasons to hide the mechanical and electrical works under the ceiling. If the false ceiling is air-tight and unbroken, it must be considered as the top of the smoke layer [2]. On the other hand, if the false ceiling is porous or not air-tight, this means that smoke screens need to be extended below the false ceiling to form smoke reservoirs. Since false ceilings are rarely air-tight and fire-resistant, in order to avoid smoke leakage through the false ceiling, the ceiling screens need to be continued above the suspended ceiling [2,8,9]. This is illustrated in Figure 1. If the false ceiling has sufficient free area space above, it can be considered as a smoke reservoir provided that the depth of the reservoir meets the design requirements and is not obstructed by construction elements [8,10]. This is illustrated in Figure 2

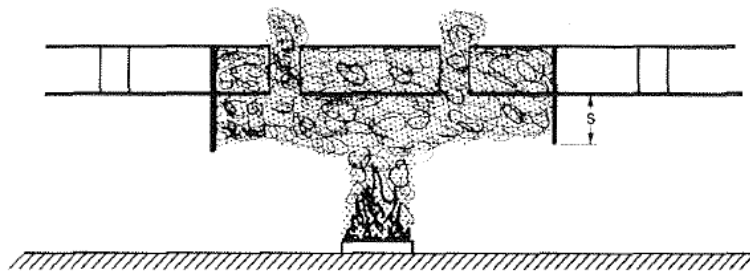


Figure 1. Copied from [8]. Leaky false ceiling design where ceiling screens are extended above the false ceiling

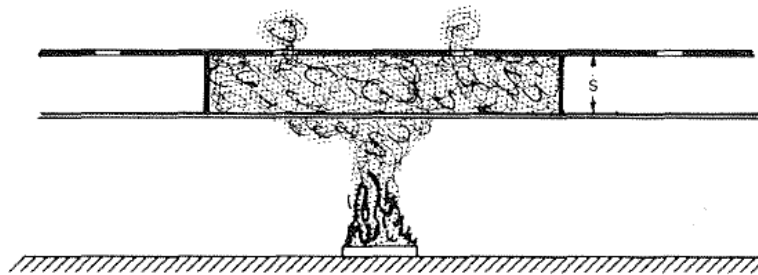


Figure 2. Copied from [8]. Perforated false ceiling with sufficient free area

If a particular design project considers the use of a false ceiling, in order for the smoke to be unhindered by it in the event of a fire, it must have sufficient free area of perforations [1,8]. The smoke and heat control system needs to be effective in removing the smoke and ensure the minimal escape of the smoke into the mall or atrium, even in the presence of a false ceiling.

There are a limited number of studies available related to the false ceiling in the case of fire. Experimental work was done by DELTA Electronics Testing, which investigated the effects of the perforated false ceiling's porosity on smoke detection [11]. Regulations in Denmark require fire detection systems to be installed above and below the false ceiling when the free area of the false ceiling exceeds 10%. However, detection above the false ceiling is not required for perforations below 10% and below the false ceiling for perforations exceeding 50%. Detection installers, fire authorities, and building owners have often contemplated whether these requirements are an optimum solution for reliability, cost and maintenance. Hence, this investigation was conducted to observe the permeability of a suspended ceiling with various free areas. Besides, detection times for ionization and optical detectors were monitored. The openings in the suspended ceiling that were monitored were 0, 5, 10, 15, 20, 25, 30, and 50%. The general observations from this test are as follows:

- Smoke density measurements were higher below the suspended ceilings where the openings did not exceed 20%

- Between openings of 20 and 30%, the smoke density measured by the MIC chambers showed similar results for both above and below the suspended ceiling.
- Smoke density measurements were higher above the suspended ceiling when the opening was 50%.

CFD simulations were carried out by Swedish National Testing and Research Institute to investigate whether the results from the previously mentioned study could be reproduced for the optimal locations of detectors in rooms with perforated suspended ceilings [11] [12]. The initial simulations were performed using JASMINE modelling software. The experimental results were compared with CFD modelling in terms of the temperature profiles inside the testing room for 10, 15 and 50% openings, with very small openings, and the velocities were too small to be able to determine the most suitable type of false ceiling. In general, based on the temperature rise measurements, 15 and 50% of openings showed the expected results and good agreement between the experimental data and CFD simulations. As expected, the temperature rise was higher below the suspended ceiling for 15% and lower for 50%, and vice versa above the suspended ceiling. The experimental data for the 10% free area resulted in the highest temperature rise above the suspended ceiling, which deviates from the expectation. The other method, smoke density measurement from the experimental data compared with the smoke density calculated with the oxygen depletion correlation [12], demonstrated adequate results that are in line with the predictions. It was noted that there are variations between the experiment and modelling when comparing the smoke model results in terms of temperature correlation, as it tends to overestimate. On the other hand, the smoke model based on the oxygen depletion demonstrated adequate agreement when comparing the two [12].

The conclusion drawn from the abovementioned CFD study is that indeed locating the detector above the false ceiling is good for a highly porous ceiling, and conversely that detection is faster below the false ceiling when the porosity is sufficiently low [11]. However, it was found that the smoke distribution above and below the suspended ceiling depends greatly on the geometry of the installation, particularly the size, distribution and spacing of the suspended ceiling panels. Nonetheless, based on the comparison of the experimental results with CFD simulations, the outputs indicate good agreement between the two, which indicates the potential benefits of CFD simulations when doing a qualitative investigation, to find the

most desirable positions by doing a parametric study when the detector types and fire sources are unknown [11, 12].

The aim of the following study [13] was to see how the thermal environment in the compartment changes when there is no suspended ceiling as opposed to a suspended ceiling made of timber and how the sprinkler activation time is affected by it. A full-scale experiment with a perforated suspended ceiling was conducted in a room 3.6 m x 2.4 m x 4.5 m to see the differences in temperature above and below the false ceiling for two separate fire sizes and locations. Also, the sprinkler activation time at the ceiling and the false ceilings heights were measured. This experiment was done on a 70% free area perforated false ceiling made of wood. The results of the tests with perforated false ceilings were compared with the test without a false ceiling, and it was concluded that perforations affect the distribution of the temperature across the ceiling and false ceiling.

When the false ceiling was present, the formation of two spaces separated by the false ceiling and the accumulation of hot gases below and above the false ceiling were observed. In the presence of the false ceiling, the hot gas temperature decreased with increasing height. Consequently, the sprinkler activation time is also affected by the presence of the false ceiling, fire size, location, and burning duration. The observation from the test with no false ceiling concluded that sprinkler heads located at the false ceiling level activated when the burning period was longer and for a bigger fire size. From the temperature data for tests with a false ceiling present it was concluded that, despite the accumulation of hot gases below the false ceiling, the maximum temperature rise would still not be enough to activate the sprinkler heads. As indicated, the fire sizes tested in this study represent the magnitude of the fire that would take place in the early stages of an accidental fire. This is useful to see the activation times of the detection and suppression installations. However, to understand the fire hazards and the heat of combustion of the combustible false ceiling and their effect on the sprinkler activation time, further studies should be carried out [13].

In earlier works, it was mentioned that a false ceiling with a 40% free area of perforations would not have significant effects on the flow of hot gases [8]. Later, Morgan hypothesised that a minimum of 25 % free area would probably be sufficient in most circumstances, noting that the openings should be well distributed across the whole area of the false ceiling rather than having a few large openings with large solid obstructions [14]. The earliest and

fundamental experimental study on the effects of the free area on the effectiveness of smoke extraction systems was carried out by Marshall et al. [10]. It became a “rule-of-thumb” for perforated false ceiling installations for spaces that have either natural or mechanical ventilation systems. Although the “rule-of-thumb” is widely used in the industry, the experiment was conducted on a 1/10 scale model, and no further full-scale experiments or CFD modelling were attempted to investigate the results. In addition, it was mentioned in the paper that the experiments were carried out for false ceilings with evenly distributed perforations of various free areas. It is known that, although current design methods use the recommended minimum free area of the false ceiling derived from this study, current designs of perforated false ceiling installations do not always follow the patterns of even distribution of perforations. As a result, it is uncertain if having various openings in a false ceiling would have the same effect on smoke extraction as evenly distributed perforations. The following work is carried out to investigate the results of the study mentioned above, in terms of the effect of both the size and the distribution of openings in the false ceiling on the smoke ventilation system.

1.2 Objectives

Since the experimental work that was conducted more than three decades ago has not been validated with full-scale experiments for financial and feasibility reasons, it was known that the experiments conducted on the 1/10 scale model would still hold the assumptions made for full-scale shops [10]. The results of the experiment are used to this day as a basis for the design of smoke and heat control systems where a false ceiling is fitted. From the experimental results, it was concluded that a minimum of 25% free area across the perforated false ceiling would allow smoke to flow through unhindered for mechanical extraction system design. It is essential to see if the results from the experiment would apply to a standard size (typically less than 280 m² [15]) small retail shop located within a mall or an airport when the perforations in the false ceiling are evenly distributed. This leads to the first objective: using numerical modelling to assess the minimum free area in the perforated false ceiling that would allow the smoke to flow through unhindered.

It is known that current designs of false ceiling installations do not always follow the patterns of even distribution of perforations. In modern buildings such as airports, often false ceilings with unconventional designs and openings are employed. The experimental conclusions drawn based on the evenly distributed perforated false ceiling are used as the basis of designs that depart from the original conditions that were examined by Marshall et al. [10]; as a result, it is uncertain if having various openings in the false ceiling would have the same effect on smoke extraction as evenly distributed perforations. This leads to the second objective of the work: to investigate the results of the numerical study mentioned above, in terms of the effects of both the size and distribution of openings in the false ceiling on the smoke ventilation system when the false ceiling has 25 and 40 % openness relative to the total area of the false ceiling to see how the results might differ from those of a perforated false ceiling with evenly distributed openings.

2 Methodology

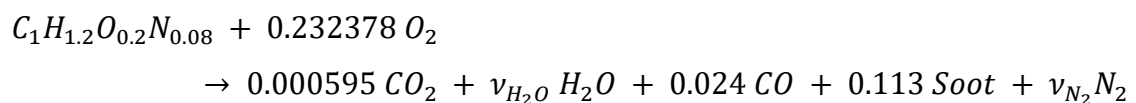
In the present work, Computational Fluid Dynamics (CFD) simulations were carried out with Fire Dynamics Simulator (FDS) version 6.7.0 and PyroSim. CFD is a computational tool that is based on the conservation of mass, momentum and energy laws that govern fluid motion. With the help of computer modelling, it gives quantitative predictions of fluid motion [16]. FDS is a CFD model that was developed by the National Institute of Standards and Technology for fire-driven fluid flow. It numerically solves Navier–Stokes equations for low-speed and thermally driven flow, with the emphasis on smoke and heat transport from fires [17].

As defined by Thunderhead Engineering, PyroSim is a graphical user interface for the FDS which gives immediate input feedback and can provide an accurate format of the FDS files [18]. Additionally, it gives more flexibility to work with different geometries, allows additions of background images for sketching, and allows the use of features for copying and moving various details. In the current work, the FDS codes were generated with the help of PyroSim because of the relative complexity of false ceiling geometry, which required a large quantity of obstruction and hole elements that were modelled to create perforations of the false ceiling with the required free area and relatively even distribution. Smokeview, a software used to visualise the numerical simulation done by FDS [19], was used to extract computational results on the horizontal and vertical planes for the purposes of comparison between different false ceiling setups. Smokeview gives the visual representation of the smoke and other fire attributes by displaying two- and three-dimensional plots, temperature contours, flow vectors and visibility on the horizontal and vertical planes [19].

In FDS, there are four modes of operation that manage the physical and numerical parameters in order to resolve the accuracy of the numerical model. These are Direction Numerical Simulations (DNS), Large Eddy Simulation (LES), Very Large Eddy Simulation (VLES), and Simple Very Large Eddy Simulation (SVLES) [17]. In this study, Large Eddy Simulation was employed because it is capable of capturing the turbulent buoyant nature of the fire that is contained in large scales of motion. At the same time, the smaller scales of motion are solved with empirical correlations. In LES, the smallest resolvable length scale is determined by the grid size and the time scale is determined by the timestep. Since scales of motion smaller than the grid size are solved with a sub-grid scale model, when the grid gets coarser, FDS becomes more reliant on the sub-grid scale model, which is based on the empirical model [17,20]. Due

to the nature of the current study, employing LES modes for the studies gives a good compromise among the resolution of the turbulent energy, time consumption and computing power.

In FDS, there are two ways to specify the burning process: through gas-phase combustion – the fuel vapour and oxygen reaction, or solid-phase pyrolysis – the generation of fuel vapour at solid or liquid surfaces. Since it is computationally demanding to use both methods to solve transport equations for multiple fuels, the default setting in FDS is simple chemistry, a mixing-controlled combustion model. Although combustion can be modelled in two ways: mixing-controlled and finite-rate, for practical application, the mixing-controlled combustion model is commonly used. Mixing-controlled refers to the reaction of fuel and oxygen controlled by the mixing process. When the fuel species consists of primarily carbon, hydrogen, oxygen, and nitrogen atoms that react with oxygen and form H₂O, CO₂, CO, and soot, it is called the “simple chemistry” combustion model. In more complex situations when C, O, H, and N are not the only components involved in the reaction, complex stoichiometry is used. This requires a more significant amount of detailing, where gas species or species mixtures need to be specified along with the stoichiometry reaction. A finite-rate combustion model is recommended when FDS needs to be run in DNS mode. Due to the specificity of LES calculation where the temperature is spread over the mesh cell, the reaction parameters need to be modified to take account of the lower cell-averaged temperatures when the finite-rate combustion model is used in such mode [17]. In the current study, a “simple chemistry” single-step, mixing-controlled combustion model was chosen. Based on Equation (15.1) in the FDS User Guide [17], the following reaction was taken as a base for the modelling:



In order to evaluate and compare the experimental data conclusions with CFD simulations, first, the accuracy of the FDS predictions was checked by running simulations based on the original work by Mashall et al. [10]. This was achieved by modelling the experimental model, running simulations of the mall, and checking how accurate the results are compared to the experiments. A detailed explanation of the experimental work and numerical model can be found in Section 2.3 **Error! Reference source not found.**. Then the main part of this study was divided into two parts. The first part runs a set of simulations on FDS to determine the

minimum acceptable free area of a perforated false ceiling to ensure that hot gases will flow unhindered and will not escape the shop. CFD simulations were carried out for a typical shop setting with false ceiling perforations with 60, 50, 40, 25, 15, 10, and 6% free area. In addition, these various free area models were run for small and large design fires of 500 kW and 2 MW HRR, respectively. The second part of the study focuses on false ceilings that have openness of 25 and 40% relative to the total ceiling area and different shapes. According to the earlier studies available, 40% is considered to be a case when the presence of the false ceiling would not cause any disturbance of the smoke extraction in the compartment [8]. In comparison, 25% is considered as the minimum acceptable free area for life safety purposes [2,9,10]. The primary purpose of the second part of the study is to see if the claims of the 40% and 25% free areas will have the same effect on smoke movement and the efficiency of the smoke extraction system if the false ceiling does not consist of conventional perforations, but instead has 40 and 25% openness relative to the total ceiling area.

2.1 Modelling setup (FDS simulations)

To evaluate the ‘rule-of-thumb’ that was identified by the experimental data [10], a typical full-scale shop layout was chosen.

Boundary conditions were left out as a default in the FDS model.

Table 1. Boundary condition in the FDS model

Description	Value
Ambient temperature	20.0 °C
Ambient pressure	101325 Pa
Ambient oxygen mass fraction	0.232378 kg/kg
Ambient carbon dioxide mass fraction	0.000595 kg/kg
Relative humidity	40 %

Compartment geometry. As it is essential to see if the “rule-of-thumb” would apply to a standard size (typically less than 280 m² [15]) small retail shop located within a mall or an airport. So, the shop is chosen to be 15 m x 15 m with identical and symmetrical doors on all sides of the wall. The doors are 4.2 m wide. The shop is 4 m in height, and the depth of the fascia was chosen to be 2.4 m from the ceiling. The compartment plan, side view, and elevation are given in Figure 3.

Building construction. The building geometry is given in Figure 3. Since no attempt was made to model heat losses in the shop, the walls and false ceiling construction were chosen to be adiabatic. As Marshall states, in practice ventilation systems are designed assuming the steady-state condition and any heat losses would be considered as a deviation to the steady-state condition [10].

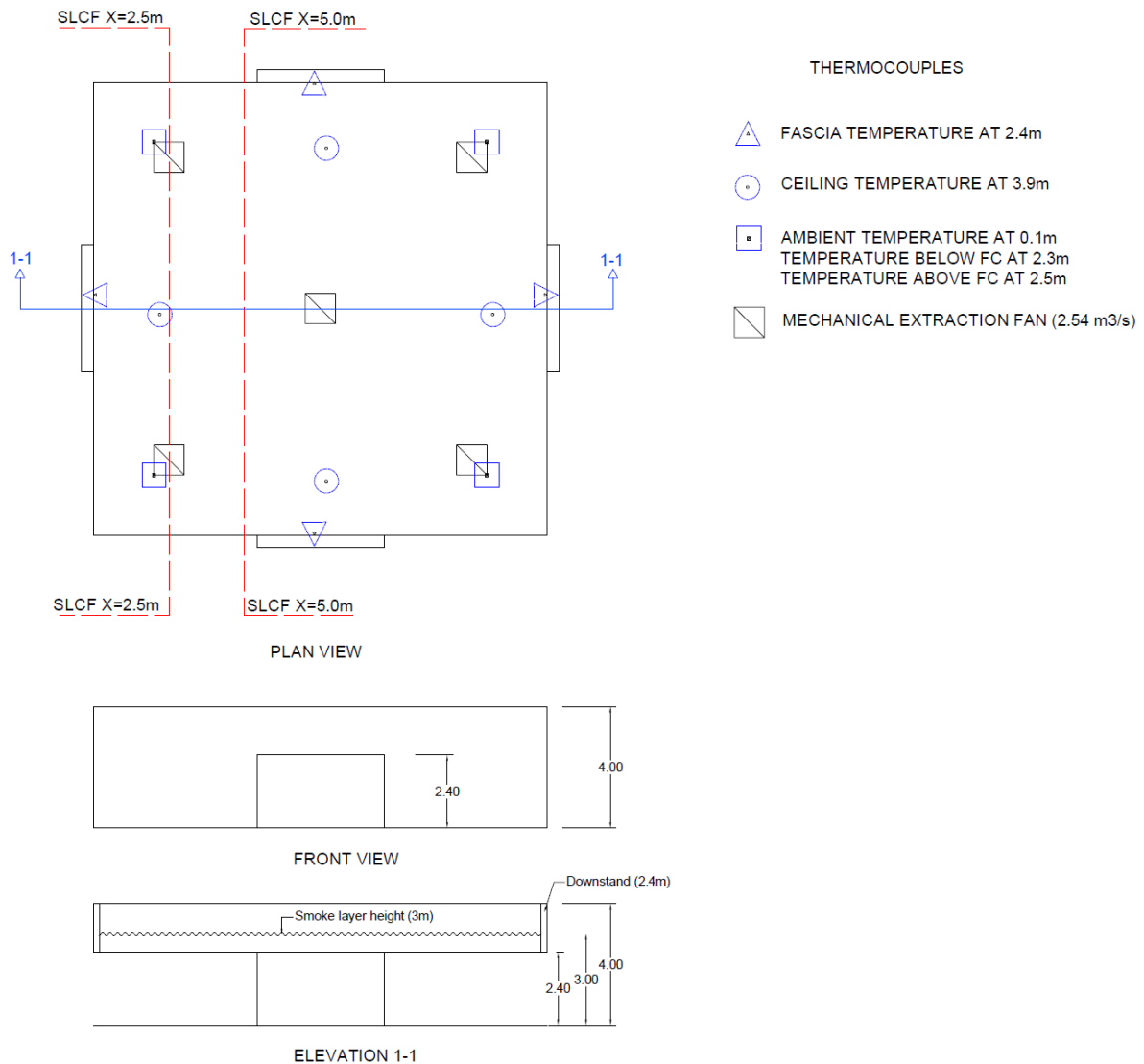


Figure 3. Compartment geometry used for this study

False ceiling. The false ceiling is located at 2.4 metres. Perforations of the false ceiling were designed with 20 cm x 20 cm grids. In order to design the false ceiling, the total area potentially covered by the false ceiling was divided into a matrix of tiles. So for the compartment of 225 m², there were 5625 cells (75 x 75) of 0.04 m² each. Then, corresponding to each free area, the matrixes were designed to be either closed or open for 60, 50, 40, 25, 15, 10, and 6%. For example: to achieve 40% perforation, the matrixes were distributed in such

a way as to have approximately 2250 cells open and 3375 cells closed. Design of the even distribution of the perforation was achieved with AutoCAD for each free area.

Table 2. Approximate estimation of open and closed cells in the matrix to design for numerical simulations using PyroSim.

Free area %	Open cells (represent perforations in the false ceiling)	Closed cells (represent false ceiling construction)
60	3375	2250
50	2812	2813
40	2250	3375
25	1406	4219
15	844	4781
10	562	5063
6	338	5287

In FDS, the open and closed cells that make up the false ceiling were achieved with obstructions and holes. Each open cell in the matrix designed using AutoCAD was treated as a hole, whereas each closed cell was treated as an obstruction. The obstruction is treated as adiabatic.

Table 7. Modelling of the evenly distributed perforated false ceiling with different free areas (dark blue filling represents perforations). Table 7 gives the geometry of evenly distributed perforated false ceiling design with various free area sizes.

Table 8 gives the geometry of uneven openings for 40 and 25% with various configurations.

Smoke extraction. In order to achieve a design smoke layer height of 3 metres above the floor, the smoke extraction rate for mechanical ventilation was calculated using equations from Section 5 of [6]. Detailed calculation is given in Appendix B. Design extraction rate calculation.

Design fire. The design fire for this study was chosen based on the Heat Release Rate per Unit Area (HRRPUA) of 500 kW/m², which is a reasonable assumption for the fire load for retail premises [6,21]. The fire is located in the middle of the room. Two fire sizes were considered in the first part of the study, with the evenly distributed false ceiling: a 1 m x 1 m fire with HRR of 500 kW and a 2 m x 2 m fire with HRR of 2 MW. Since the primary purpose of this study is to observe the effectiveness of the smoke exhaust system and the permeability of the perforated false ceiling when different free areas are given, it was essential to see if different fire sizes would affect the severity of the smoke accumulation and the efficiency of the extraction

system. This is observed in the evenly distributed perforated false ceiling part. NOTE: the design exhaust rate was calculated for the large fire (2 MW).

A parametric numerical study [22] that looked into different soot yield (ranging from 0.01 g/g to 0.2 g/g) and its effect on visibility concluded that there is a hyperbolic trend due to the increase in the soot yield. The hyperbolic trend of the numerical analysis in this soot yield study [22] explained that the soot yield can produce a consistent change in visibility for a soot yield below 0.10 g/g and a negligible change in visibility for a soot yield above 0.10 g/g. This would indicate that, unless the exact material properties are known during the design process, a soot yield value below 0.10 g/g should be used with great caution when assessing the ASET/RSET. Since the design criteria for smoke exhaust design are to fulfil life safety requirements, determining the minimum free area of the false ceiling that would not hinder smoke from going through and not severely affect visibility is essential. Since visibility is one of the main parameters compared in this study, the soot yield was chosen to give the worst-case scenario. As discussed in the previous paper [22], visibility is profoundly affected by the soot yield, so that a soot yield of more than 0.10 g/g would give conservative results. Hence, the fuel chosen for this numerical simulation is POLYURETHANE_GM37, which is one of the default fuel characteristics available in PyroSim, having a soot yield greater than 0.10 g/g. All characteristics, including soot yield, CO yield, and others are kept at the default settings because the values are taken directly from the SFPE Handbook. The following characteristics are inputted in the fuel reaction: carbon atoms – 1.0, hydrogen atoms – 1.2, oxygen atoms – 0.2, nitrogen atoms – 0.8, CO yield – 0.024 g/g, soot yield – 0.113 g/g, radiative fraction – 0.35, hydrogen fraction – 0.1 [23].

Temperature measurements. Temperature readings were done with the help of thermocouples. The bead diameter of all the thermocouples is 5 mm and their locations are given in Figure 3. In total, five groups of thermocouples were employed in the model to monitor the temperatures of the hot gases leaving the shop at each opening (right below the fascia) at the height of 2.4 m. The temperature of the hot gases at the ceiling was monitored with four thermocouples at several locations. The ambient temperature was monitored at the floor level (0.1 m). Temperatures right above and below the false ceiling were monitored with four thermocouples at 2.3 m and four thermocouples at 2.5 m.

Description of FDS simulations.

In total, 32 simulations were performed. Part I is the study focuses Runs 1-16, which are false ceiling with even perforations. Part II, Runs 17-32 are for uneven openness in the false ceiling with various designs.

Table 3. Conditions modelled in this study

Run No.	Design fire	Type of false ceiling	Free area of the FC
1	500 kW	N/A	100
2	2 MW	N/A	100
3	500 kW	Even perforation	60
4	2 MW	Even perforation	60
5	500 kW	Even perforation	50
6	2 MW	Even perforation	50
7	500 kW	Even perforation	40
8	2 MW	Even perforation	40
9	500 kW	Even perforation	25
10	2 MW	Even perforation	25
11	500 kW	Even perforation	15
12	2 MW	Even perforation	15
13	500 kW	Even perforation	10
14	2 MW	Even perforation	10
15	500 kW	Even perforation	6
16	2 MW	Even perforation	6
17	2 MW	Uneven openings	40
18	2 MW	Uneven openings	40
19	2 MW	Uneven openings	40
20	2 MW	Uneven openings	40
21	2 MW	Uneven openings	40
22	2 MW	Uneven openings	40
23	2 MW	Uneven openings	40
24	2 MW	Uneven openings	25
25	2 MW	Uneven openings	25
26	2 MW	Uneven openings	25
27	2 MW	Uneven openings	25
28	2 MW	Uneven openings	25
29	2 MW	Uneven openings	25
30	2 MW	Uneven openings	25
31	2 MW	Uneven openings	25
32	2 MW	Uneven openings	25

2.2 Mesh sensitivity analysis

In order to obtain accurate results in numerical simulations without compromising on computational time, a mesh sensitivity analysis was carried out. The methodology used to identify the most appropriate cell size followed the FDS User Guide. The guide suggests looking into the non-dimensional expression $D^*/\delta x$, which is the ratio of a characteristic fire diameter to the nominal size of a mesh cell [17]. D^* is found with the following formula:

$$D^* = \left(\frac{\dot{Q}}{\rho_{\infty} c_p T_{\infty} \sqrt{g}} \right)^{\frac{2}{5}}$$

where \dot{Q} is the total heat release rate of the fire.

As explained in the guide, a cell size of 10 cm would be appropriate for the study of the smoke spreading through the building from appropriate size fire.

Moreover, the FDS Validation Guide Table 3.31 gives a summary of the numerical parameters for the simulations of different test setups. UL/NIST Vent Experiments with fires of 500 kW to 2 MW were conducted in a room with dimensions of 6.1 m x 4.3 m x 2.4 m. The D^* (m) and $D^*/\delta x$ values used for FDS validation purposes varied in the range of 0.7–1.2 and 7–12 respectively. As suggested in the FDS Validation Guide, the greater the value of the Plume Resolution Index, $D^*/\delta x$, the better the fire dynamics is resolved [24].

Based on the calculations for the given fire sizes in this study, the following table was created:

kW	500	2000
D*	0.73	1.28
δx		
0.2	3.67	6.39
0.1	7.34	12.78
0.05	14.68	25.57

Compared with the Validation of UL/NIST Vent Experiments, for this study it would be appropriate to use a 10 cm cell size without losing the resolution of the numerical results while saving on computational time.

FDS simulations for the mesh sensitivity study were conducted for mechanical ventilation with no false ceiling present with cell sizes of 20, 10, and 5 cm. Figure 4 shows the temperature readings from thermocouples at various locations for the given cell sizes. It is important to

note that since the false ceiling perforations in the FDS model were modelled as holes with the smallest dimension of 20 cm x 20 cm, the degree of accuracy of the flow through those holes was not evaluated and some deviations are expected.

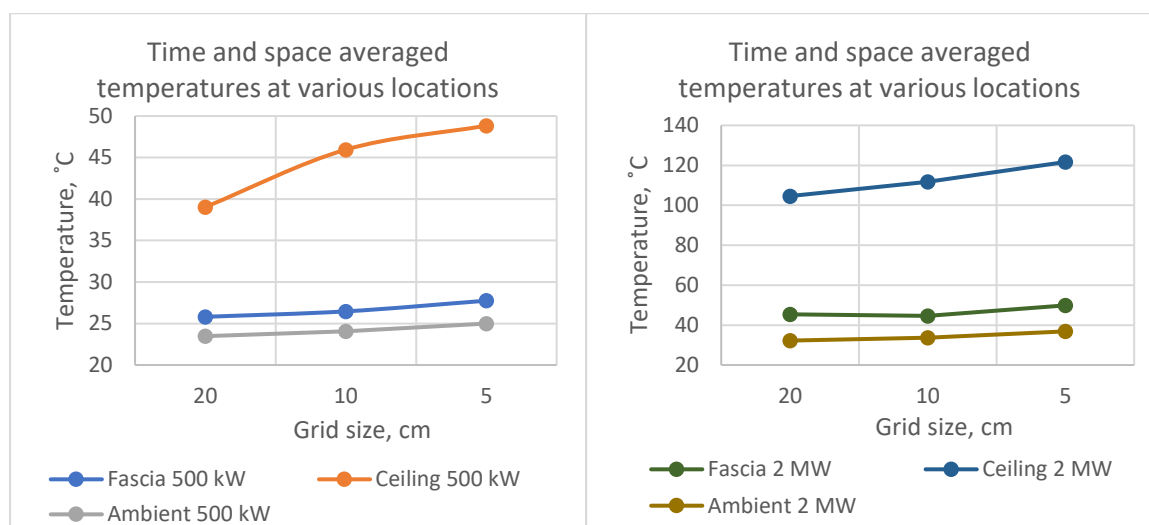


Figure 4. Comparison of time and space averaged temperature values at various locations for 500 kW and 2 MW fires. (averaging time 100s)

Based on the temperature results from the thermocouples, it seems that using a mesh with a size of 10 cm is adequate for the simulation, because there are only minor differences between the 10 cm and 5 cm cell sizes. The computational time for the simulations using high-performance computing (with 16 cores) for 20 cm, 10 cm, and 5 cm was roughly 15 minutes, 4 hours, and 80 hours, respectively. As a result, the compromise between the accuracy of the results and the computational time was to use the 10 cm cell size. In total, the computational domain involved close to 930 000 cells.

2.3 Assessment of CFD modelling predictions

The scope of this study includes the numerical modelling of the 1/10 scale shopping mall based on the study by Marshall et al. [10] to assess the quality of the CFD modelling. Conducting a numerical simulation based on the experimental data available and comparing the results of the two will help to understand the agreement between the CFD modelling and experimental data and the accuracy of the CFD predictions. Then, these results are applied to a typical full-scale shop compartment with a perforated false ceiling, with openings of varied size and distribution.

In order to assess the quality of the CFD modelling, the experimental work done by Marshall et al. [10] was carried out using FDS. Due to the relative complexity and feasibility of false ceiling geometry, PyroSim, a graphical user interface software for FDS, was employed.

The following is the description of the original work by Marshall et al. and the experimental test setup.

2.3.1 Description of the experimental study

The experimental study was carried out to determine the minimum possible free area of a perforated false ceiling that would not obstruct the movement of smoke through the smoke and heat control system. This was done on a 1/10 scale model of an enclosed one-storey shopping mall that had a false ceiling with the free area varying between 6, 10, 14.4, 24, and 40%. These free areas were examined for both natural and mechanical ventilation systems, and the work was divided accordingly.

Experimental setup

The model was constructed of two parts, the mall and compartment shop with the fire. The mall was made of a steel frame and chipboard sheets that had four Perspex windows on the sides. Ceramic fibre insulation blankets were used in the interior of the walls and ceiling in order to minimise the heat losses. The fire compartment construction and shopfront downstand were made of ceramic fibre insulation board with a steel frame. At the open end of the mall, a perspex screen was installed.

Square-section aluminium extraction ducting was provided with four rectangular inlet ducts that were connected to the fan unit with varying extraction ranges for mechanical ventilation. Natural ventilation was done by removing the mechanical ventilation and enlarging four vent holes in order to provide the same ventilation capacity as the mechanical ventilation.

The false ceilings that were investigated in the experiment had evenly distributed free area openings of 40, 24, 14.4, 10, and 6%. The elements were made of 1.2 mm (18 gauge) mild steel that was installed on the steel angle frame along the two sides of the mall in the model setup.

Two fire sizes were used in the experiment, 15.8 kW and 6.8 kW, which correspond to 5 MW and 2.2 MW fires in full-scale. In total 22 experimental runs were performed: from 1 to 12 with mechanical ventilation, and 13 to 22 with natural ventilation. For both ventilation systems first

cases with no false ceiling were analysed, followed by false ceilings with 40, 24, 14.4, and 10% evenly distributed perforated free areas. Additionally, a 6% evenly distributed perforated free area was used for mechanical ventilation only.

Several thermocouples were in the mall and the shop at various heights. These were located 10 mm below the fascia to observe the temperatures leaving the shop. Several thermocouples were located 10 mm below the ceiling of the mall to observe the hot gases reaching the mall. The outputs from these measurements were averaged to observe the mean layer temperature. Two thermocouples were in the ceiling of the fire compartment and four thermocouples were located centrally at each exhaust duct outlet. Several thermocouples were also used to observe the ambient temperatures of the shop at the floor level, located at the height of 120 mm above the floor.

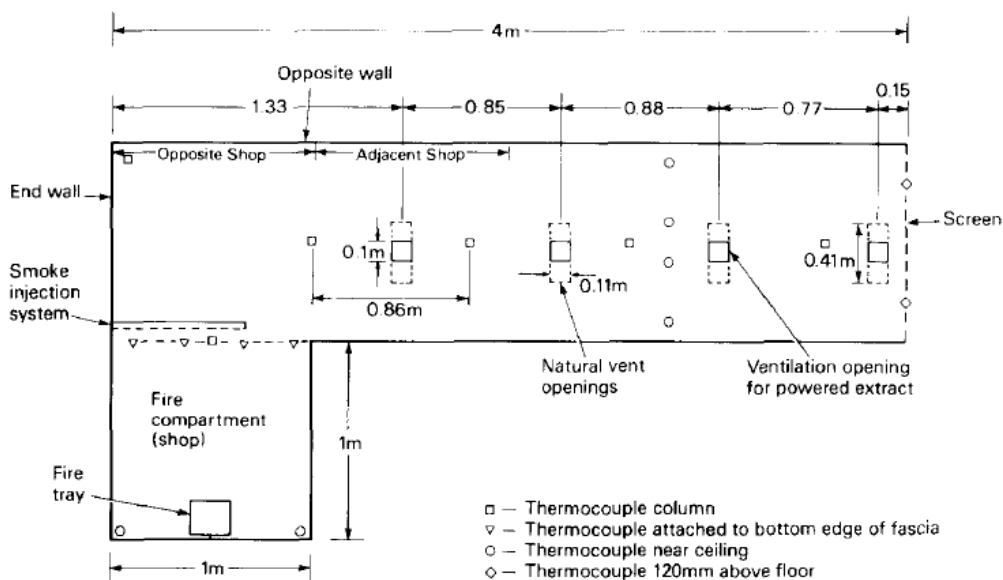


Fig. 1. The model mall (plan).

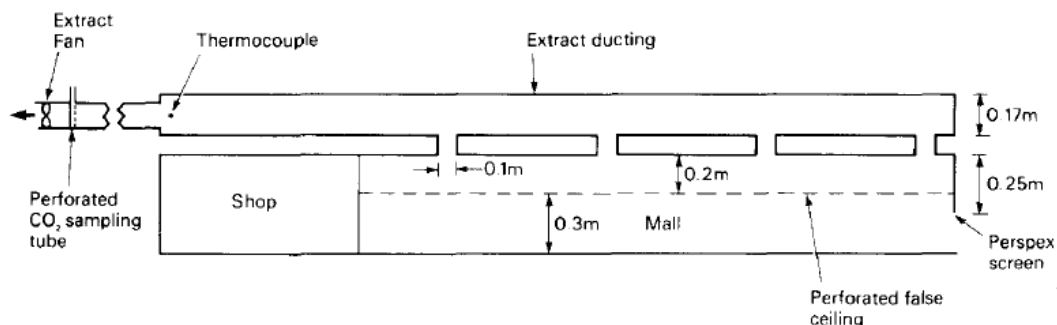


Figure 5. Copied from [10]. The geometry of the experimental model of 1/10 scale

Results

The runs that were done for both types of ventilation and fire sizes with no false ceiling (a 100% free area) had similar results in terms of the smoke flow patterns and smoke layer height in the mall. This was a clear indication that the total mass flow of gases leaving the smoke reservoir was similar for both mechanical and natural ventilation.

It is expected that the spread of the hot gases will depend on the free area of the perforated false ceiling. From the experimental results, it is possible to see that a 40% free area is enough to extract the hot gases unhindered, which is also possible with smaller free areas, although those would make the extraction system less effective. Hence the hot gases do not reach the opposite wall when the false ceiling has perforations of 40%, according to the experimental results. As the free area gets smaller and the smaller, a greater amount of hot gases impinge against the wall.

Concluding remarks

In general, for the mechanical ventilation systems where the false ceiling is located at the same height as the bottom side of the shopfront, a minimum perforated free area of 25% should be used in most applications, whereas for natural ventilation this minimum value should be 30%.

2.3.2 Description of the numerical modelling

Boundary conditions and geometry

Due to the limited availability of the information from the original work, some boundary conditions and settings had to be adjusted accordingly. The following boundary conditions were chosen for the numerical model.

Table 4. Boundary condition in the FDS model

Description	Value
Ambient temperature	20.0 °C
Ambient pressure	101325 Pa
Ambient oxygen mass fraction	0.232378 kg/kg
Ambient carbon dioxide mass fraction	0.000595 kg/kg
Relative humidity	40 %

The experiments specified that the fuel was the industrial methylated spirit, with no further details. Since no detailed specifications could be found for such fuel, ethyl alcohol was chosen from SFPE Handbook [23] with the following characteristics: Heat of Combustion – 27.7 kJ/g, CO yield – 0.001g/g, soot yield – 0.008 g/g.

Because it was specified in the experiment that insulation blankets were used to minimise the heat losses, the construction and extraction ducts in the numerical simulation were chosen to be adiabatic.

Due to the limits in the time and computing power, numerical simulations were conducted for 6.8 kW fire (corresponds to 2.2 MW fire in full-scale) for both mechanical and natural ventilation. The fire source was specified as 0.1 m x 0.1 m obstruction with HRRPUA of 680 kW/m² located at the far end of the compartment (locations is given in Figure 6).

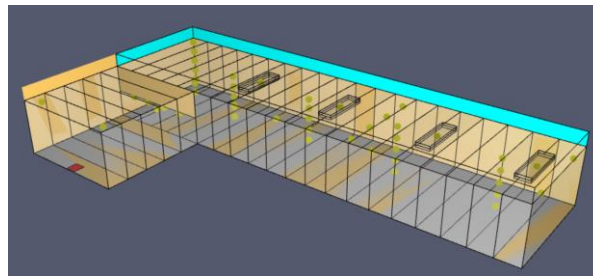
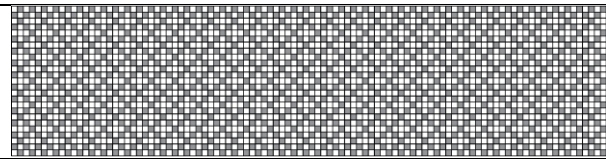
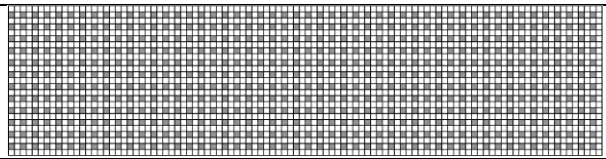
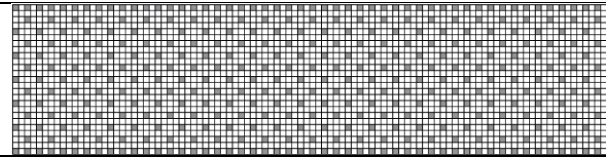
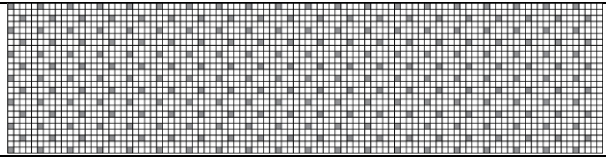
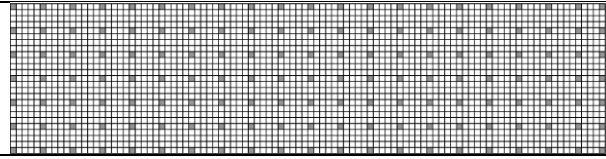


Figure 6. The geometry of the FDS models based on the experimental study [10]. Left: Natural ventilation model. Right: Mechanical ventilation model.

The total area covered by the false ceiling was 4 x 1 meter. The sizes of each perforation were not specified in the experiment. The perforations in the numerical study were modelled with 40 x 40 cm. 40 cm was chosen as an optimal dimension due to the complexity and dimensions of the false ceiling area. The geometry of the false ceiling perforations is given in Table 5.

Table 5. The geometry of the false ceiling in the numerical model. Dark grey represents perforations in the false ceiling.

40%	24%
	
15%	10%
	
6%	
	

Numerical simulations were conducted for 5 mechanical and 5 natural ventilation for 6.8 kW fire.

Table 6. Description of the simulations compared with the experimental data.

Run No.	Smoke extraction method	Free area of perforated FC	Extraction rate (kg/s)
1	Natural	100	
2	Natural	40	
3	Natural	24	
4	Natural	15	
5	Natural	10	
6	Mechanical	100	0.069
7	Mechanical	40	0.06
8	Mechanical	24	0.068
9	Mechanical	15	0.073
10	Mechanical	10	0.078

Mesh sensitivity

In order to identify optimal grid size to obtain accurate in the following numerical study, $D^*/\delta x$ dimensionless expression was studied. Based in the computations, for 6.8 kW fire, the expression for 5 cm, 2 cm, and 1 cm grid sizes would be 2.63, 6.58, and 13.16, respectively. Although the grid size of 1 cm would give accurate results for the purposes of this assessment, due to unknown reasons, the simulations kept showing errors upon starting. As a result, the simulation was run with 2 cm grid size. There were a total number of around 390k cells in natural ventilations and 480k cells in mechanical ventilation. The computational time for the

simulations using High-Performance Computing (with 16 cores) was around 30 hours for each simulation.

Limitations of the numerical assessment in comparison with available experimental data

- Unknown parameters such as boundary conditions and fuel characteristics had to be modelled as a reasonable assumption
- Size of perforations in the false ceiling was not mentioned in the experiment. As a result, in order to keep the design of the perforations simple, 40 x 40 holes with various free areas were designed as a reasonable assumption for evenly distributed perforations
- Simplifications of the geometry, especially for the mechanical ventilation
- Grid size (coarse)

Results

Due to the limited availability of data from experiments and simplifications in the numerical model, the only parameter that could be compared between the two is temperature change at three locations taken from the thermocouple readings. It should be pointed out that ambient temperature in the compartment is not known; as a result, in the numerical simulations, the ambient temperature was taken as 20°C. Other parameters that were presented in the experiment are largely done by visual observation of the smoke layer spread, which was done using a commercial smoke generator. The numerical simulations were conducted only for 6.8 kW fire, which is equivalent to 2.2 MW fire in full-scale.

In general, natural ventilation 40, 24, 14, and 10% and mechanical ventilation 40% showed adequate results that are in line with experimental data (Figure 7, Figure 8, Figure 9). The results of temperature change in the compartment in the experiments and FDS simulations varied between 3-18 degrees (Figure 7) for natural ventilation and 35 degrees for mechanical.

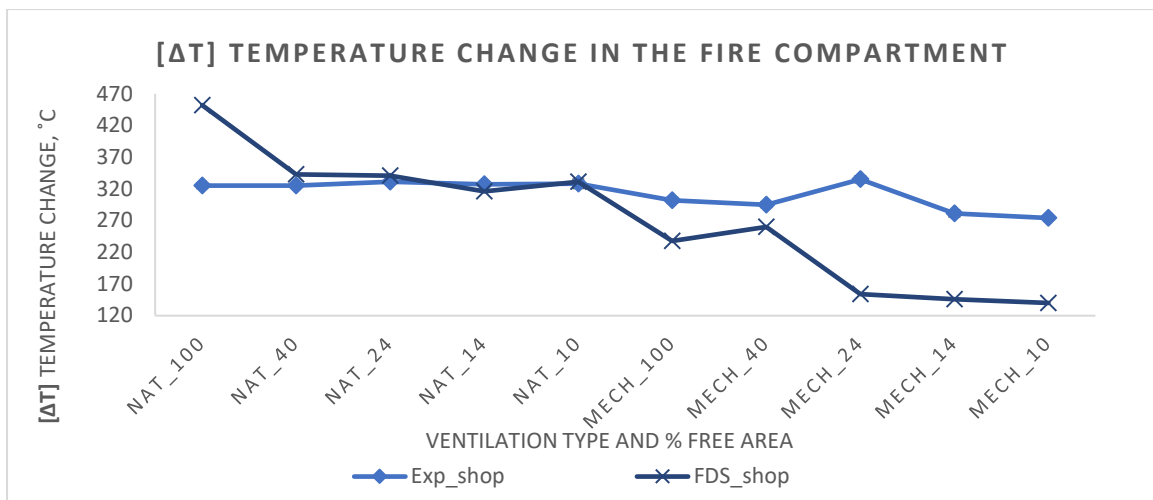


Figure 7. Comparison of experimental and numerical data for temperature change in the compartment of fire. Experimental data is from [10], and numerical data is taken from FDS time-averaged steady-state result (50 s. of the averaging period). Locations of thermocouples are shown in Figure 5.

Similar to the previous comparison, the temperature changes at the shopfront (Natural Ventilation 40, 24, 14, and 10% and mechanical ventilation 40%) show that FDS results are in line with experimental results (Figure 8). Although in the graph, the FDS results are lower than experimental ones, they are within the uncertainty margin with was reported by the experimental data.

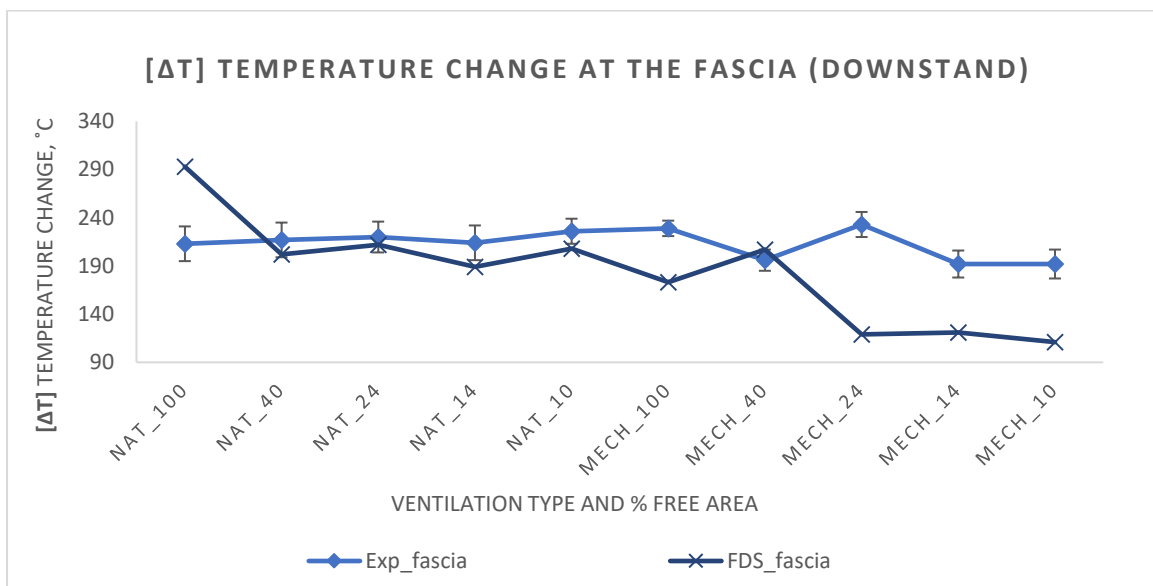


Figure 8. Comparison of experimental and numerical data for temperature change in at shopfront downstand (fascia). Experimental data is from [10], and numerical data is taken from FDS time-averaged steady-state result (50 s. of the averaging period). Locations of thermocouples are shown in Figure 5.

Temperature changes at the ceiling of the mall at the end of the corridor vary between 3-32 degrees for natural and 20 degrees for mechanical ventilation (Figure 9) for Natural Ventilation 40, 24, 14, and 10% and mechanical ventilation 40%. Unlike previous comparisons, the temperature at the ceiling at the end of the corridor carries significant uncertainty level when

comparing experimental and numerical results. This is because perforations in the experimental test are not known and in numerical model are big due to the simplification of the geometry. Nonetheless, it is possible to conclude that for these runs, the numerical simulations present consistent results with experimental data.

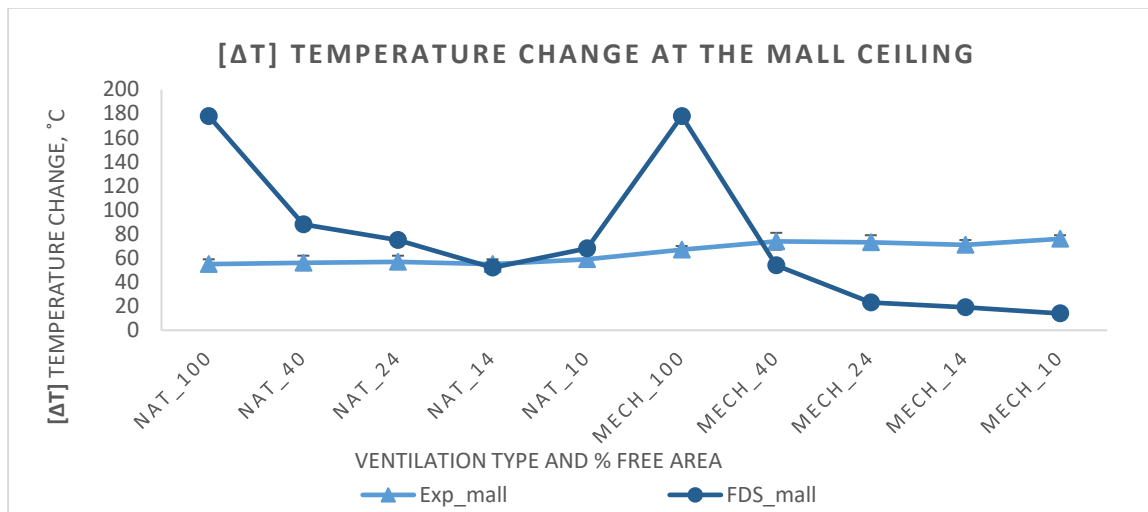


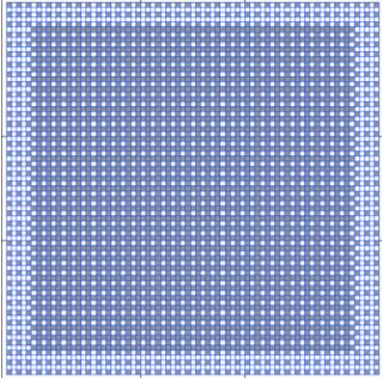
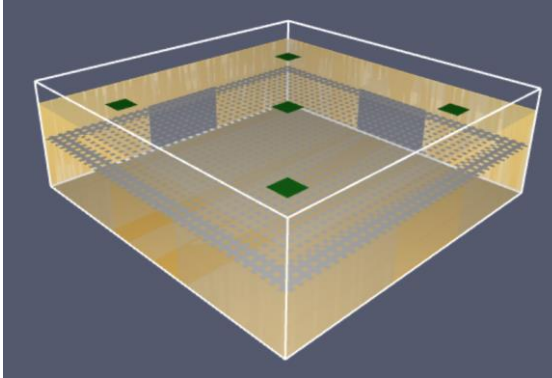
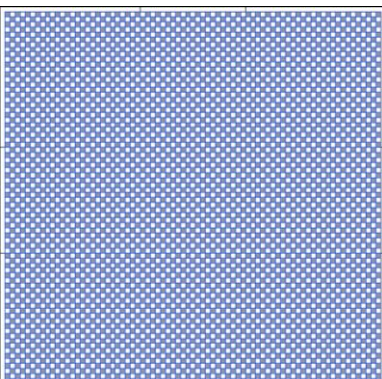
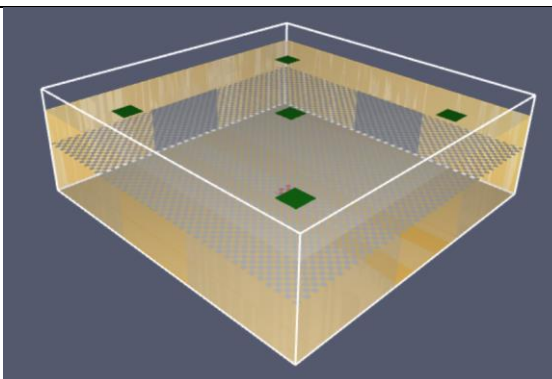
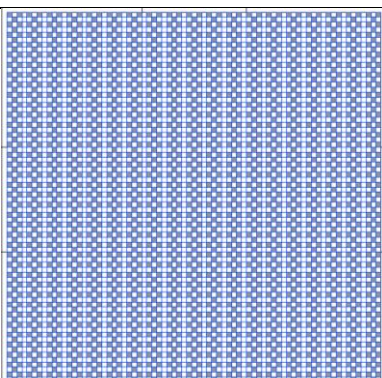
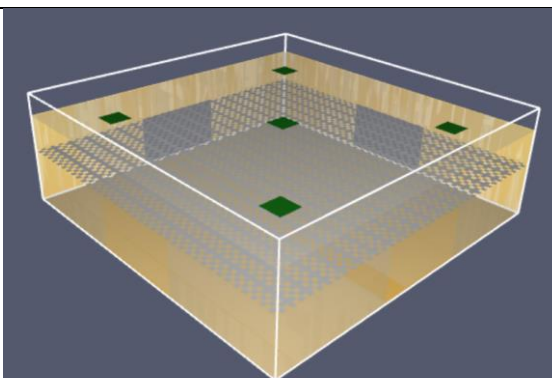
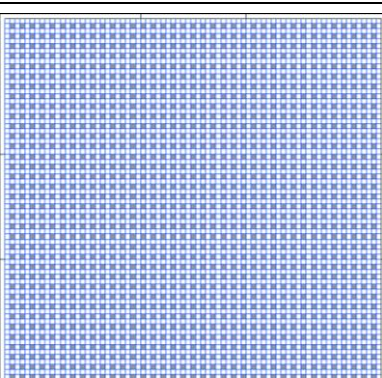
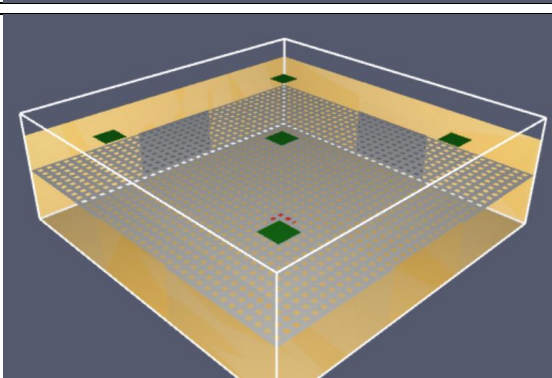
Figure 9. Comparison of experimental and numerical data for temperature change at the mall ceiling. Experimental data is from [10], and numerical data is taken from FDS time-averaged steady-state result (50 s. of the averaging period). Locations of thermocouples are shown in Figure 5.

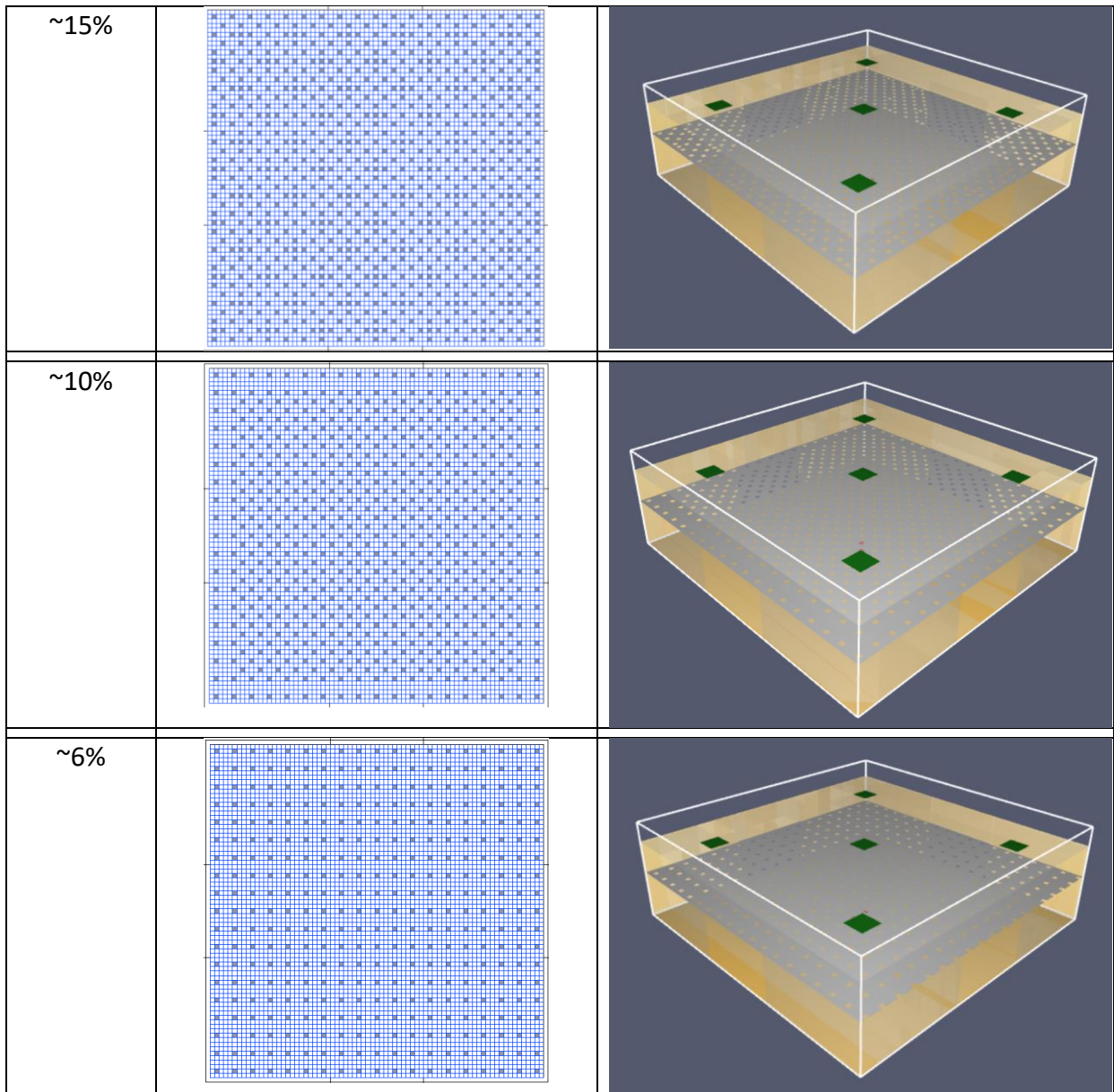
The simulations for natural ventilation with free area 100% (no false ceiling) showed overestimated results. The temperature changes were 127 degrees in fire compartment, 80 degrees at the shopfront downstand, and 123 at the ceiling of the mall. The last two values are counterintuitive because thermocouples closer to the fire compartment would register a higher temperature than thermocouple at the ceiling of the mall. Similarly, mechanical ventilation with no false ceiling showed overestimated temperature changes. On the other hand, free areas of 24, 14, and 10 showed underestimated temperature changes. These temperature changes should not be taken into account as a possibility in these designs because during the evaluation of the temperature slice cuts in the middle of the fire source showed no flames (in other word flame temperature was as low as ~140°C), hence very low temperatures. Several simulations have been performed to identify who there is no flame present in those designs, which leads to the need for further investigations.

In summary, based on the simulations with natural ventilation of 40, 24, 14, and 10% and mechanical ventilation of 40%, it is possible to conclude that FDS demonstrates the ability to predict the behaviour of fire plume transport adequately. Further analysis should be performed for the simulations that showed counterintuitive and faulty results.

2.4 Configurations of evenly distributed perforated false ceiling

Table 7. Modelling of the evenly distributed perforated false ceiling with different free areas (dark blue filling represents perforations).

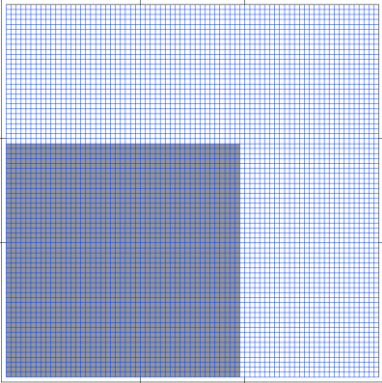
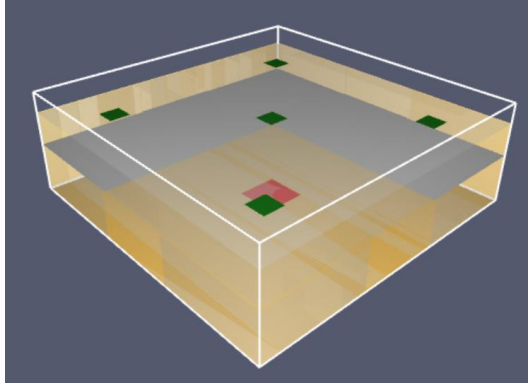
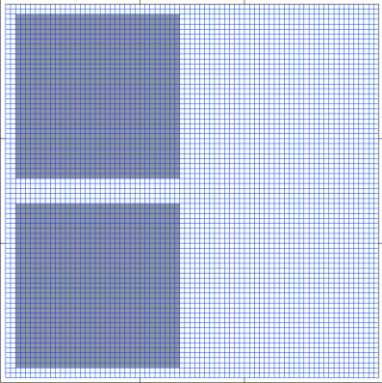
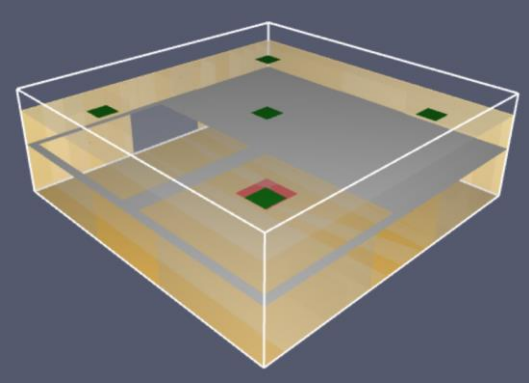
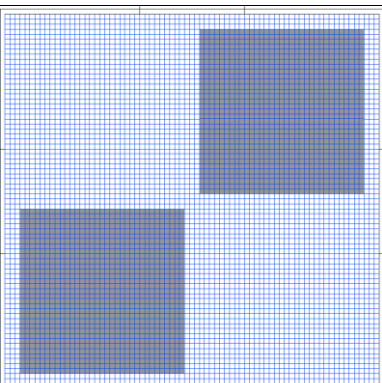
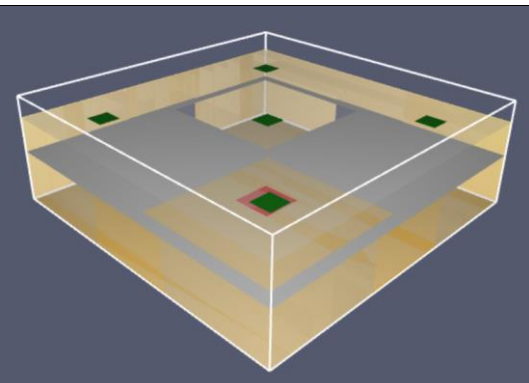
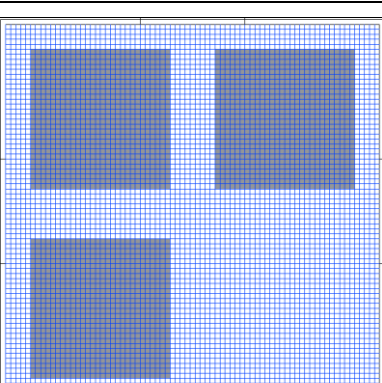
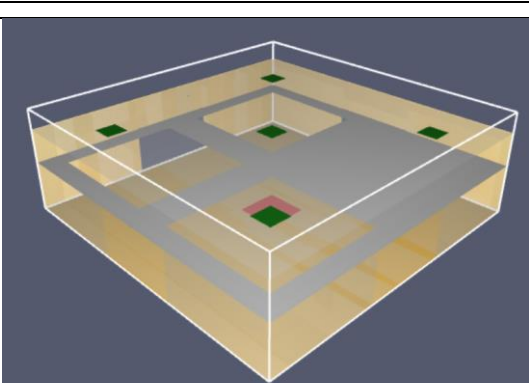
Free area	Geometrical drawing	Modelling (in PyroSim)
~60%		
~50%		
~40%		
~25%		

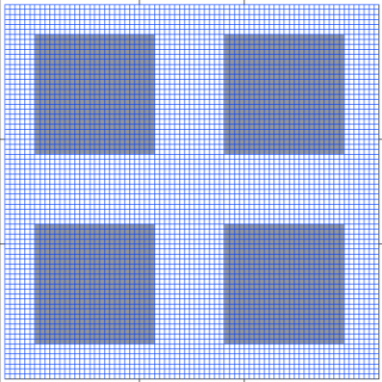
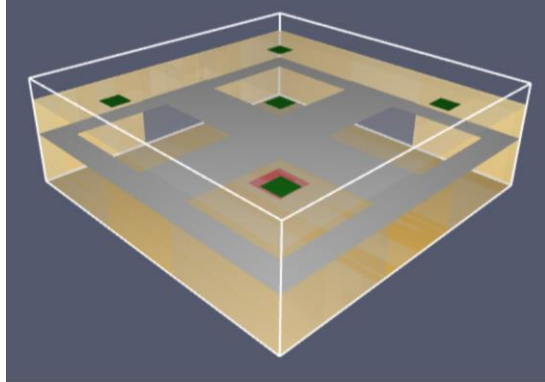
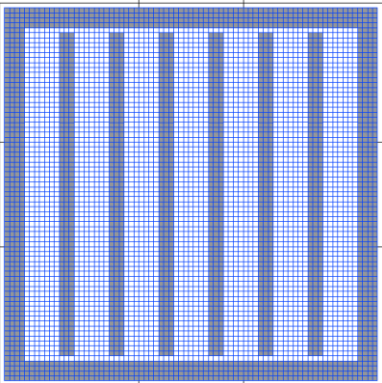
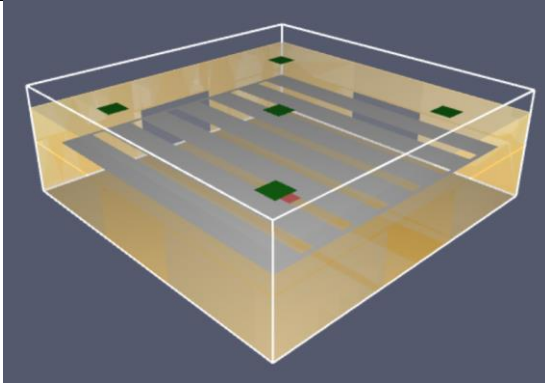
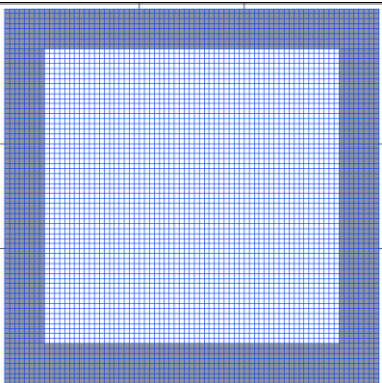
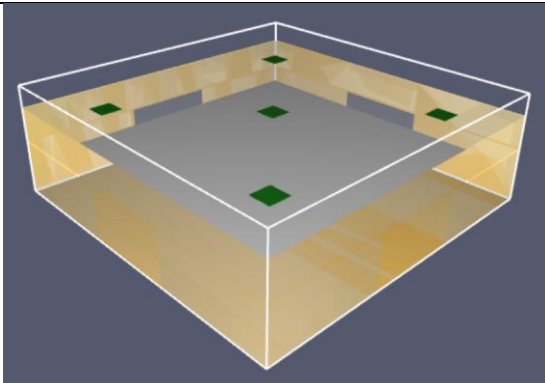
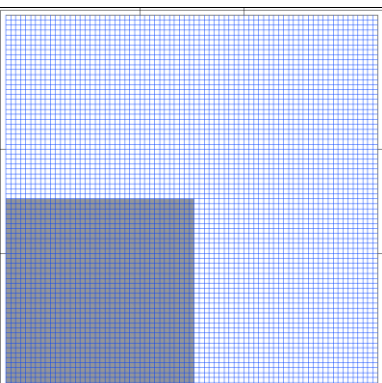
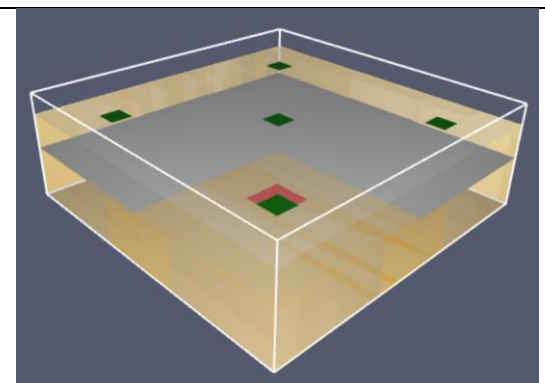


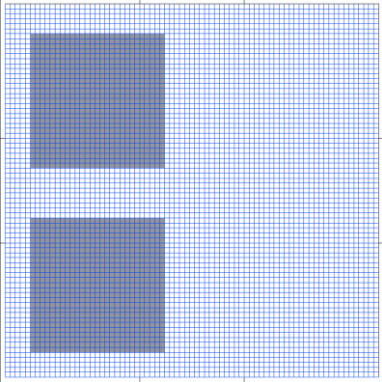
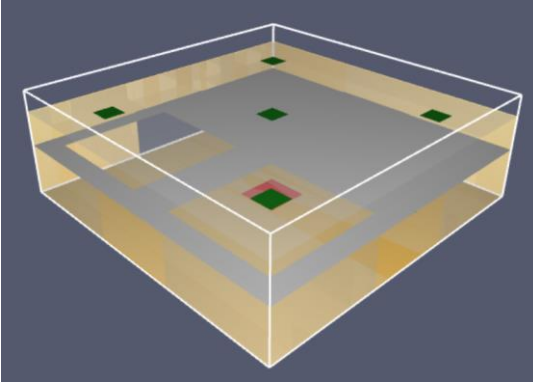
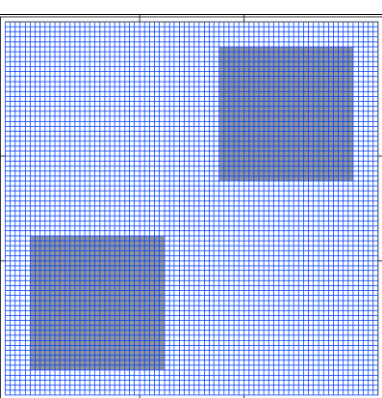
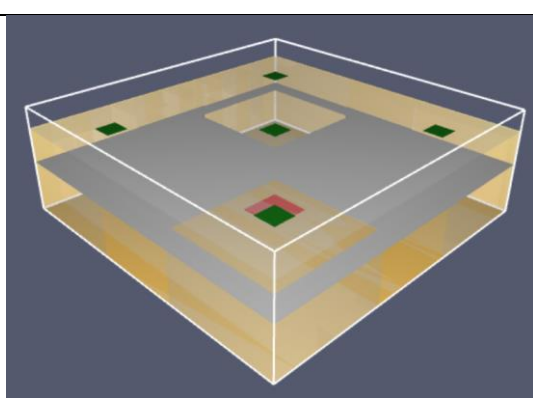
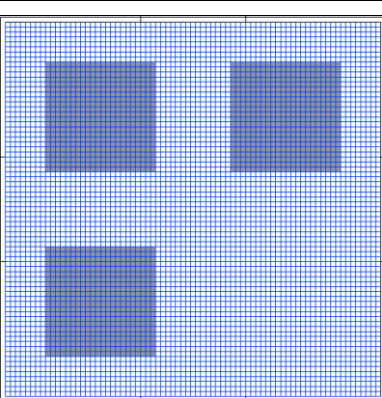
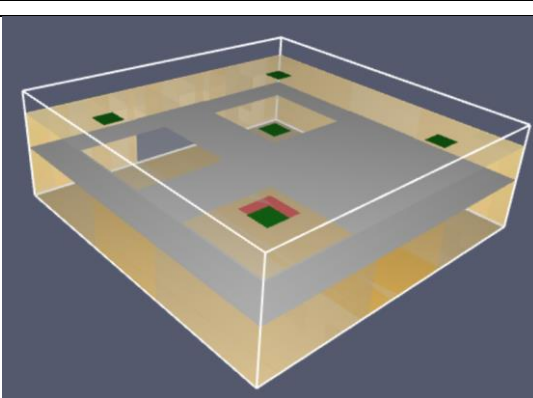
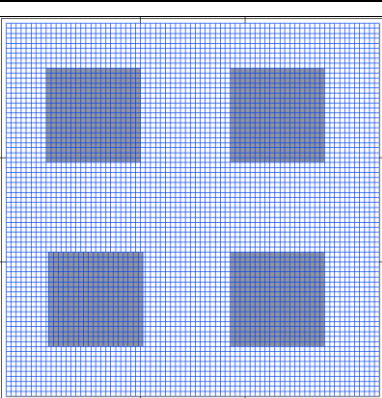
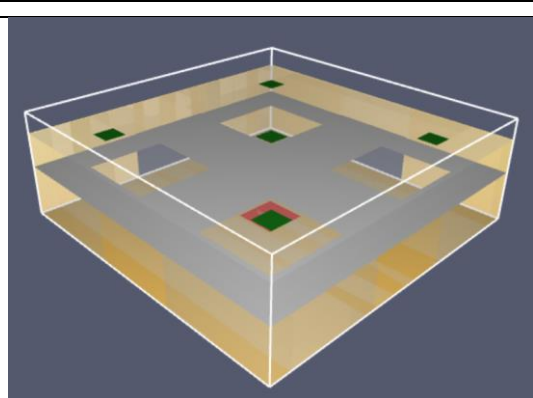
2.5 Configurations of uneven openings in the false ceiling

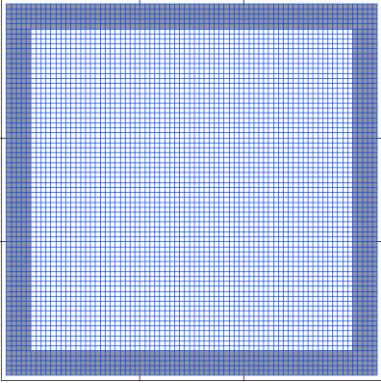
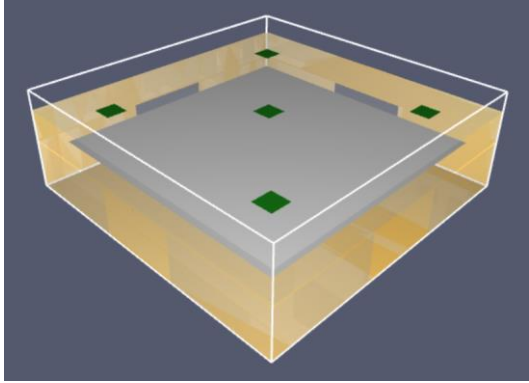
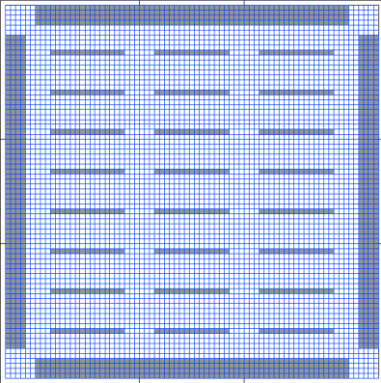
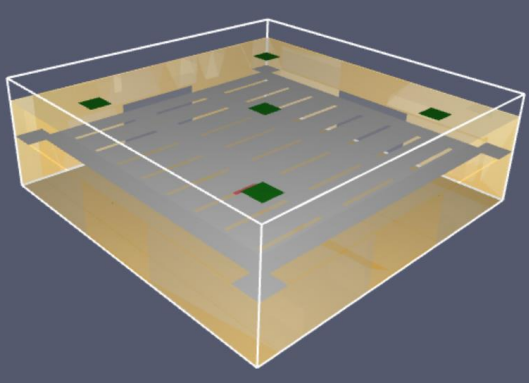
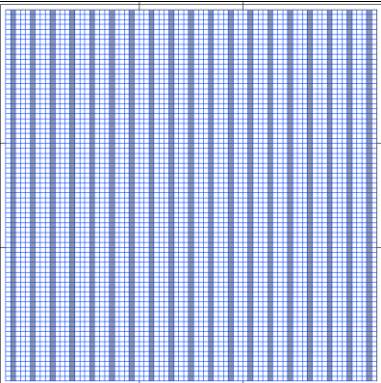
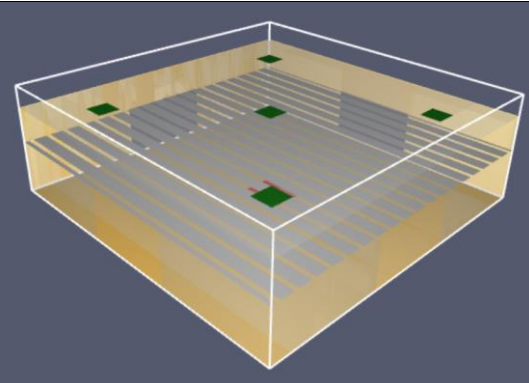
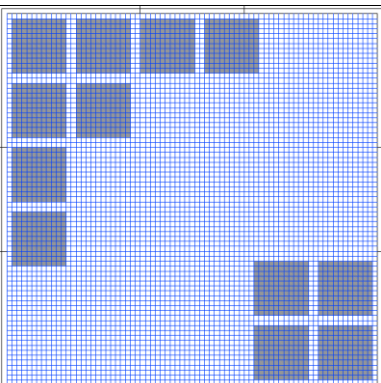
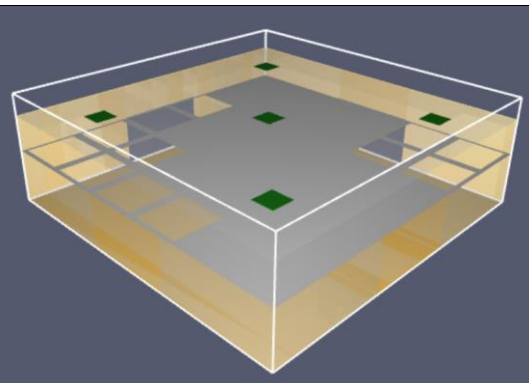
Free areas chosen for this part of the study were 40 and 25% with various designs. The general approach was to start with one opening and systematically change the openness of the false ceiling to become increasingly more distributed and symmetric. This will allow the identification of any patterns or trends that influence the performance of the smoke and heat control system. For both the 40 and 25% free areas, the false ceiling designs #1 to #5 are similar in pattern, whereas the remaining designs are taken from some real-life design applications of false ceilings from various sources.

Table 8. Modelling of the uneven openings in the false ceiling for 25% and 40% free areas with various designs (dark blue/grey filling represents opening in the false ceiling).

Free area	Geometrical drawing	Modelling (in Pyrosim)
<p>~40% (Design #1)</p>		
<p>~40% (Design #2)</p>		
<p>~40% (Design #3)</p>		
<p>~40% (Design #4)</p>		

<p>~40% (Design #5)</p>		
<p>~40% (Design #6)</p>		
<p>~40% (Design #7)</p>		
<p>~25% (Design #1)</p>		

<p>~25% (Design #2)</p>		
<p>~25% (Design #3)</p>		
<p>~25% (Design #4)</p>		
<p>~25% (Design #5)</p>		

<p>~25% (Design #6)</p>		
<p>~25% (Design #7)</p>		
<p>~25% (Design #8)</p>		
<p>~25% (Design #9)</p>		

3 Results and Discussion

The CFD simulations were performed for the steady-state fire, which allows the prediction of the final height of the smoke layer as well as the trajectory and spread of the smoke plume. The steady-state analysis gives the worst-case scenario where the smoke and heat control system needs to operate [25].

A test simulation was performed to identify when the steady-state condition is reached for the given boundary conditions and settings. Initially, a 400 second simulation was done, which showed the steady-state condition to be reached at about 150 seconds. As a result, all other succeeding simulations were performed until 200 seconds, in which the last 50 seconds were averaged in time.

3.1 Part I: Perforated false ceiling

3.1.1 Temperature

The smoke and heat control system was designed to have a 3-metre smoke layer height with a design fire of 2 MW. Then, this design was checked with two different fire sizes (small fire – 500 kW and large fire – 2 MW) against various free areas of perforated false ceiling. Two benchmark simulations were denoted with a 100% free area, which means there is no false ceiling present in the test model. In Appendix A: Slice files from all test runs, Tables Table 17 - Table 23 show the temperature, velocity, and visibility profiles on the horizontal and vertical planes for all test runs.

Design smoke layer height and temperatures above the false ceiling

Based on the temperature profiles (Table 19- Table 22), the flow of hot gases has the same unhindered flow for 100, 60, and 50% free areas and the design smoke layer height is uninterrupted. For the 40% free area, the behaviour of the hot gases based on the temperature profile differs between the small and large fires. While the small fire has a negligible effect on the plume mass flow and formation of the uniform smoke layer, in the large fire hot gases travel radially before flowing through the false ceiling. This disturbance in the flow of hot gases through the false ceiling creates a lag in the plume flow rate and temperature distribution, which influences the design smoke layer height. For example, if the

temperature contour of 100°C and higher for the 50% free area shows a smoke layer thickness of about 0.5 metres, for the 40% free area it is approximately 0.8 metres. This would indicate that up to 40% free area is enough for the buoyancy-driven hot gas flow to be unhindered and this therefore does not affect the design smoke layer height and the effectiveness of the smoke and heat control system. From the 25% free area, the smoke layer height is no longer uniform for both fire sizes, especially close to the fire source, which is due to the impinging of

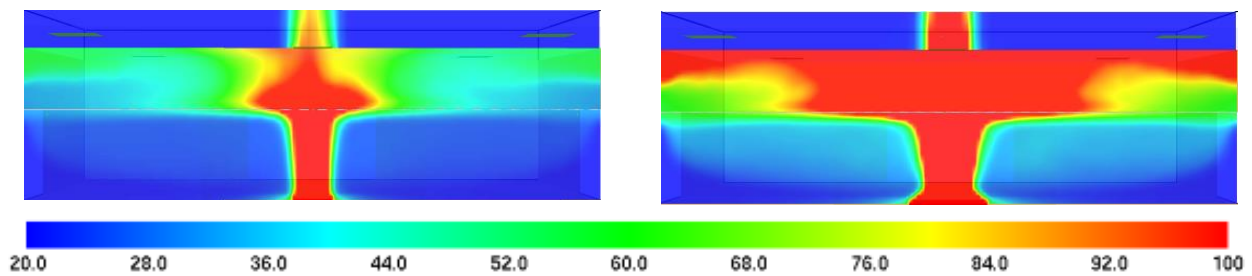


Figure 10. Temperature fields of compartment with perforated false ceiling of 25% free area for 500 kW fire. Slice cut at $X=7.5$ m: 500kW (left) and 2MW (right). Time-averaged steady-state results (50 s. of the averaging period).

the plume into the false ceiling (Figure 10). The 3-metre smoke layer height is still visible away from the fire source with 25% of free area for both fire sizes, although it is not entirely uniform for the large fire (Table 18, Table 21). In the case of the 500 kW fire, the design smoke layer height is still observable for the free areas of 15 and 10%, whereas the smoke occupies almost the entire volume of the smoke reservoir at 6% free area at the lower temperature due to the

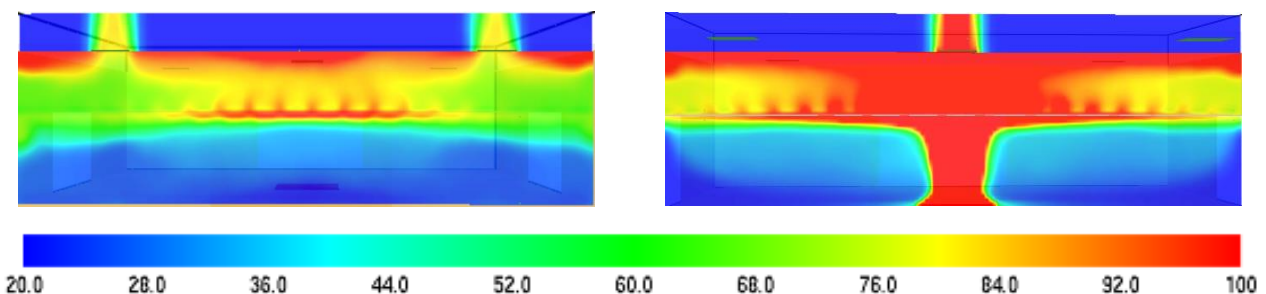


Figure 11. Temperature fields of compartment with perforated false ceiling of 25% free area for 500 kW fire. Slice cut at $X=7.5$ m: 500kW (left) and 2MW (right). Time-averaged steady-state results (50 s. of the averaging period).

smoke flowing out of the compartment (Figure 11). Since the lesser free area of the false ceiling acts as a barrier to the flow of hot gases, as mentioned before, some of the hot gases flow radially, occupying the entire area underneath the false ceiling, then flowing through the perforations due to the effect of buoyancy. This effect is more prevalent with the large fire (2 MW), starting from the free area of 15%. Due to the rapid production of the plume, the higher HRR, and fewer perforations in the false ceiling, the hot gases cannot be extracted immediately. As a result, some of the hot gases flow through the false ceiling directly, and some horizontally below the false ceiling before flowing through the perforations. The radial

distance of the spread below the false ceiling increases with decrease of the free area in the false ceiling (Table 19, Table 22). Because the high temperatures travel radially and mix with the ambient temperature, the overall temperature of the hot gases flowing through the false ceiling decreases. The radial distances (r) of temperatures higher than 100°C that spread 10 cm below and 10 cm above the false ceiling in Table 9 show that for 40 and 25% free area, the radial spread below the false ceiling is smaller than that above the false ceiling, whereas for 15% and below the opposite is true.

Table 9. The radial distance of 100°C and higher temperatures that spread 10 cm above and 10 cm below the false ceiling for 2 MW fire.

Free area, %	Radial distance (r) 10 cm below false ceiling	Radial distance (r) 10 cm above the false ceiling	Ratio $\left[\frac{r_{above FC}}{r_{below FC}} \right]$
40	1.5 m	2.7 m	1.8
25	2.9 m	3.9 m	1.3
15	4.8 m	4.6 m	0.96
10	5.0 m	3.8 m	0.76
6	6.7 m	3.7 m	0.55

This means that higher temperatures are trapped below the false ceiling, which makes the smoke layer above the false ceiling have an overall lower temperature that occupies the entire volume of the smoke reservoir. This can also be seen from the thermocouple readings in Figure 12. There, although the difference in the temperature changes above and below the false ceiling is minimal, it is still possible to see that for up to 25% the temperatures 10 cm above the false ceiling are higher, whereas at 15% and thereafter the temperatures are higher 10 cm below the false ceiling.

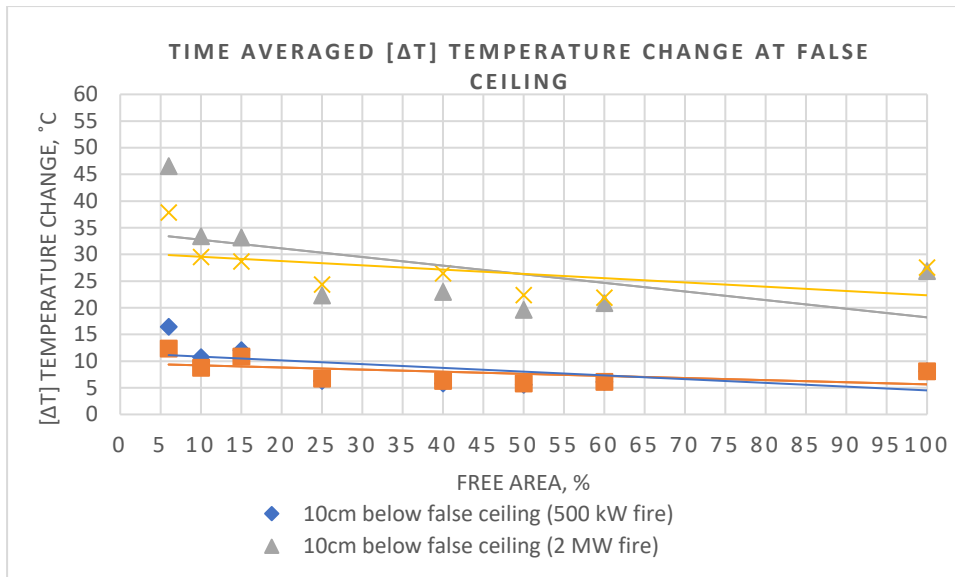


Figure 12. Time and space averaged temperature change from thermocouples located 10 cm above and 10 cm below perforated false ceiling. Time-averaged steady-state results (50 s. of the averaging period). Locations of thermocouples are shown in Figure 3

As mentioned before, if, until the 40% free area, the smoke layer height is uniform, and it is possible to see (Table 18 – Table 25) a clear distinction between temperatures higher and lower than 100°C, in the 25% case and thereafter the uniformity is lost, and the temperatures in the whole reservoir vary. In this case, the hot gas layer that is over 100°C is thinner compared to 40%, which is observable in Figure 13, where the temperature change is 110°C for 40% and 80°C for 25%.

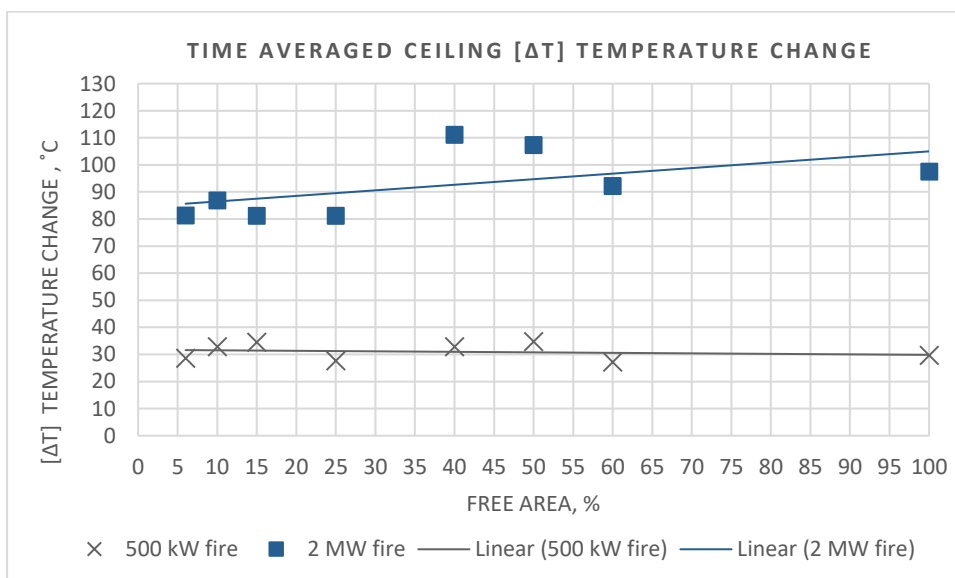


Figure 13. Time and space averaged temperatures from thermocouples located at the ceiling. Time-averaged steady-state results (50 s. of the averaging period). Locations of thermocouples are shown in Figure 3

Another way to look at this is through the comparison of the thermocouple readings at the ceiling and right above the false ceiling (Table 10). The difference in height for the two locations is 1.4 metres. The temperature difference between these two locations is similar for the 100, 60, 50, and 40% free area range between 70 and 85°C, whereas for 25, 15, 10, and 6% it is in the range of 43–57°C. This could indicate that when the difference of temperature is high, a significant amount of plume is transported to the ceiling unhindered.

Table 10. Temperature change difference from thermocouples readings that are located at 2.5 m and 3.9 m height for 2 MW fire.

Free area, %	$[\Delta T]_{FC}$ 10 cm above the false ceiling	$[\Delta T]_C$ 10 cm below the ceiling	$[\Delta T]$ difference
100	27	97	70
60	22	92	70
50	22	107	85
40	26	111	85
25	24	81	57
15	29	81	52
10	29	87	58
6	38	81	43

Ambient temperatures

The ambient temperature was monitored with four thermocouples located at the floor level (0.1 m). According to Figure 14, the time-averaged ambient temperature change is much higher for the case with no false ceiling and gradually decreases as the free area of the perforations decreases. This can also be observed from the temperature slices in Table 17, where the temperatures below 30°C were truncated in Smokeview for comparison reasons. Because the motion of the intermittent flame region has large instabilities at the boundary of the fire plume with cold air, fluctuations in this region create large eddies or vortexes. This phenomenon can be observed especially in the case with NO false ceiling. Since the velocities are the highest in the intermittent flame region [26], the large vortexes could be contributing to the temperature increase in the compartment due to increased mixing. The temperature rise at the floor level corresponds to 15°C above the ambient temperature when there is no false ceiling (Figure 14).

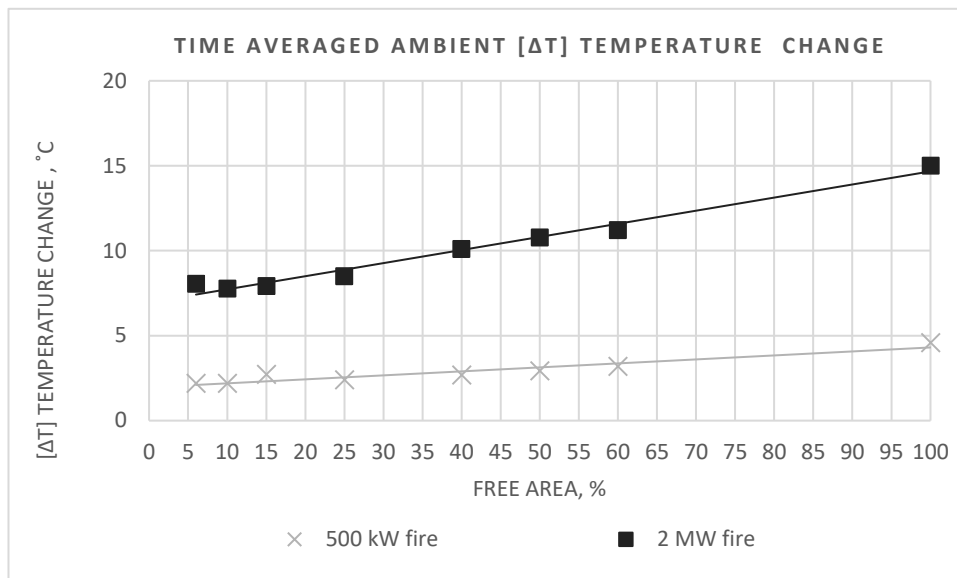
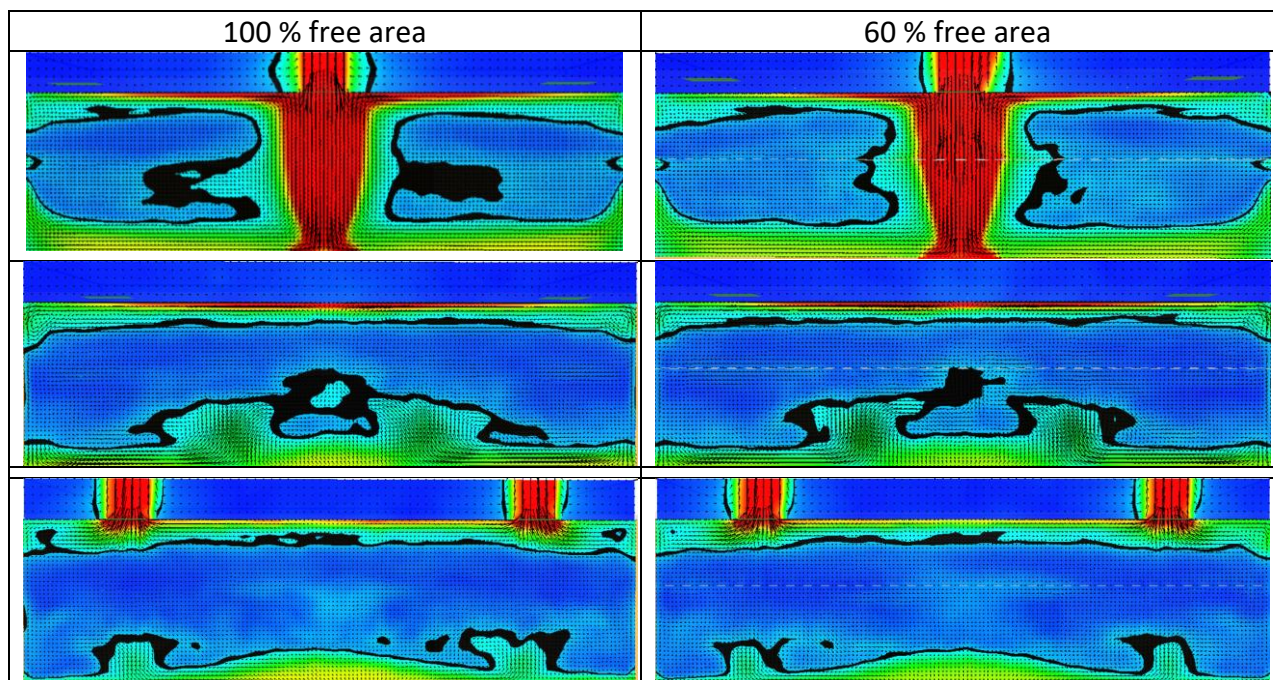


Figure 14. Time and space averaged temperatures rise from thermocouples located at the floor. Time-averaged steady-state results (50 s. of the averaging period). Locations of thermocouples are shown in Figure 3

Slightly better results are observed for the model when the false ceiling is introduced (Table 11 shows the comparison between 100 and 60%). The perforated false ceilings with 60 and 50% free areas have a slightly lower ambient temperature rise (compared to 100%), which can be attributed to the smaller vortices due to the introduction of the false ceiling as a barrier. The barrier disturbs large eddies and vortices in the oscillation region, thus creating a smaller area of mixing of the plume interface with cold air. Comparison of the temperatures on horizontal planes in Table 23 shows a significant difference between 100% and 60% for the 2 MW fire.

Table 11. Comparison of velocity contour of 0.35 m/s for 100 and 60% free area. Vertical slices at the locations (from top to bottom) 7.5, 5.0, and 2.5 meters.



For the 40 and 25% free areas, the ambient temperature rise is even lower, which is primarily due to the absence of large vortexes that would mix the hot gases with cold air in the whole compartment. Free areas between 40 and 25% effectively divide the height of the compartment into two layers. Buoyancy-driven hot gases, once risen, are trapped in the upper layer, and thus do not mix with cold air at the floor level. The vortexes are smaller and divided into two distinct layers, above and below the false ceiling. While free areas of 60 and 50% do not hinder any smoke flow movement, 40 and 25% only slightly hinder the hot gases from rising. The smaller ambient temperature rise for 25% could also be the consequence of the formation of a ceiling jet under the false ceiling. The small amount of hot gases that cannot penetrate through the false ceiling form a ceiling jet and spread in all directions. Since the fire source is axisymmetric and located in the middle of a compartment that has four symmetrical openings on the sides, the hot gases that form the ceiling jet lower the temperature of the plume under the false ceiling and escape from the compartment. As a result, not only are there smaller vortexes due to the division of the compartment height into two distinct regions, but also hot gases escape through the openings. As a result, the ambient temperature at the floor level decreases significantly. Free areas of 15, 10 and 6% have very close temperature rises which could also have a similar explanation to that for 25%, with the difference being only in the ceiling jets with higher temperatures, that is, under the false ceiling, escaping the compartment. As a result, more hot gases escape from the compartment, which contributes to the lower ambient temperature and lower temperature above the false ceiling. This can be observed in Figure 13, where the ceiling temperature rise is much lower for 15% and lower, and Figure 15, where the thermocouples are located at the shopfront downstand to monitor the temperatures of the hot gases leaving the compartment.

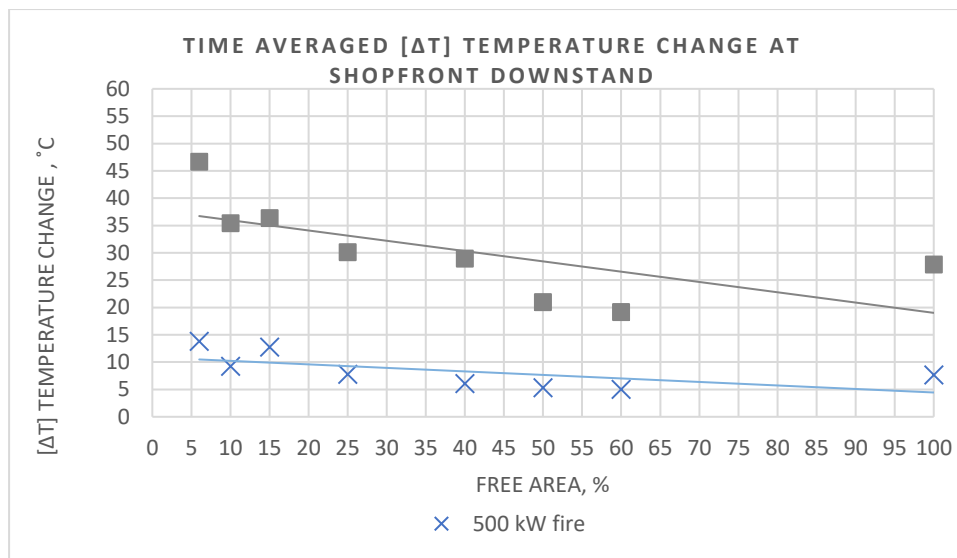


Figure 15. Time and space averaged temperature change from thermocouples located below fascia (four shopfronts in total). Time-averaged steady-state results (50 s. of the averaging period). Locations of thermocouples are shown in Figure 3

3.1.2 Velocity

Air entrainment

In unconfined axisymmetric plumes, there is no restriction of air entrainment and vertical movement of the flow. Since the surrounding surfaces largely influence the fire plume, when there is some form of obstruction, the air entrainment is reduced. In a compartment fire, the obstructions that could influence the rate of air entrainment are the walls or ceiling. When the fire plume impinges on the ceiling, it is deflected horizontally to form a ceiling jet, which is also with restricted air entrainment [27].

Since the fire in the current model is axisymmetric, the air entrainment into the fire plume occurs around the fire source and is transported until the plume impinges on the ceiling. Due to the absence of a false ceiling, the air entrainment is uninterrupted until the plume impinges on the ceiling. This is also the case for the 60 and 50% false ceilings. Judging by the information presented in Table 18 – Table 23, where the horizontal and vertical planes are shown for 500 kW and 2 MW fires, the air entrainment into the fire plume is uninterrupted for 60 and 50%. This indicates that having 60 and 50% perforations would have no or negligible influence on the air entrainment into the plume, mass flow rate, and ceiling jet velocities. Starting from 40%, the presence of the false ceiling divides the compartment height into two zones. A small portion of the fire plume is deflected by the false ceiling and travels radially before flowing through the perforations in the false ceiling. As a result, because the fire plume radius is more

significant due to the deflection by the false ceiling, the air entrainment into the fire plume below the false ceiling increases. This could mean that more air entrainment into the plume decreases the temperatures in the plume that is entering through the false ceiling. As the free area decreases, consequently the fire plume deflection under the false ceiling increases and more air is entrained into the plume, thus contributing to the lower temperatures above the false ceiling.

In general, the entrainment of fresh incoming air into the plume at a height of 0.5 metres has a similar pattern. Judging by the horizontal velocity planes, incoming fresh air entrains the fire source from four sides, and when the flows at the edges of the incoming flow meet, they deflect towards the fire source and corners (Figure 16-a). This is an idealised pattern because the building, openings and fire are symmetrical, which forms a star-shaped pattern. The velocities at 1.5 metres above the floor have a similar pattern for all cases, where the highest flow is coming from the corners of the compartment, whereas the flows from the opening are directed down to the floor and entrain the fire source from the bottom. At 1.5 metres above the floor, the air entrainment into the fire plume is coming from the corners, with a small portion being deflected towards the openings (Figure 16-b). As for the 0.5 metres height, the flow pattern is similar in all cases, with small variations between them. As the height increases,

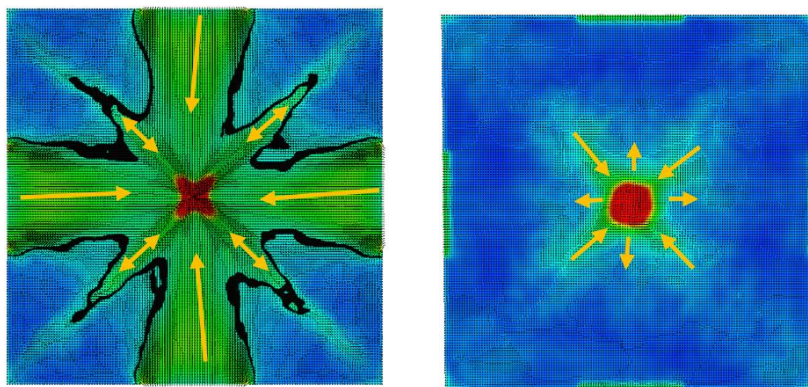


Figure 16. Air entrainment pattern at the height of (a) 0.5 m (left) and (b) 1.5 m (right) Velocity vector horizontal slice. The time averaged result (the averaging time of 50 seconds).

the flow pattern varies significantly depending on the free area of the false ceiling, and the spread of the flow under the false ceiling is more substantial due to the resistance of fewer perforations in the false ceiling. As mentioned before, the 60 and 50% free areas have negligible effects on the fire plume, whereas, starting from 40%, it is possible to see some differences in the flow patterns and temperatures under the false ceiling (Figure 17).

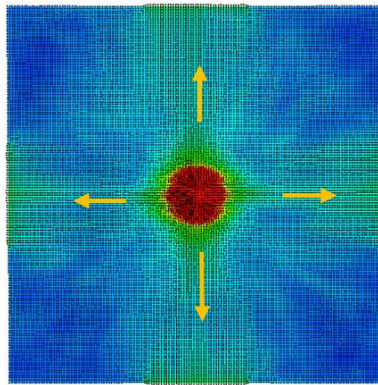


Figure 17. Flow pattern of the plume deflected from the point of origin towards the openings for 40% free area. Velocity vector horizontal slice at the height of 2.2 m. The time averaged result (the averaging time of 50 seconds).

The flows under the false ceiling are deflected away from the fire plume origin towards the openings. The star-shaped pattern can be noticed right below the false ceiling for free areas of 40 and 25%. Since the plume has enough free area to penetrate through the false ceiling after radial spread, the plume flow changes its trajectory to an inclined one, rather than flowing upward. The inclined flow follows the same route – towards the openings. This is probably because the corner zone is stagnant, so it is easier for the plume to follow the same trajectory

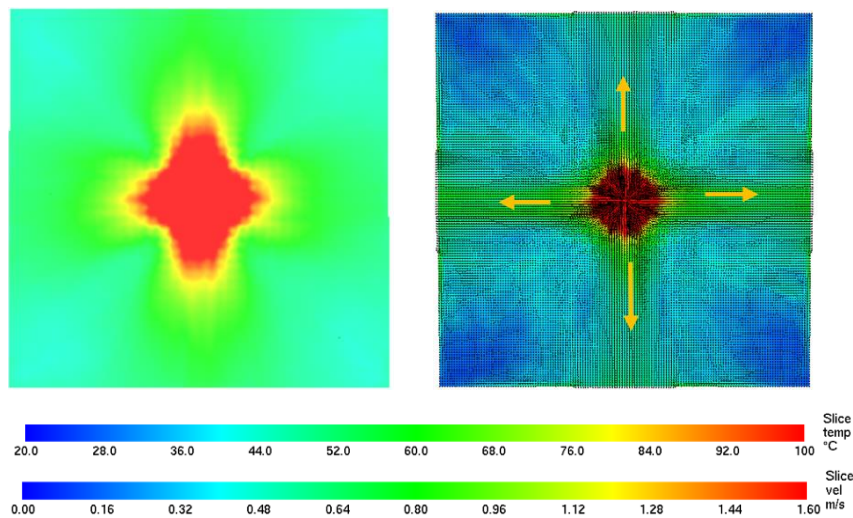


Figure 18. Flow pattern of the plume deflected from the point of origin towards the openings. (Left) Temperature horizontal slice at the height of 2.3 m. (Right) Velocity vector horizontal slice at the height of 2.2 m. The time averaged result (the averaging time of 50 seconds).

as the flows below the false ceiling. Besides, as the false ceiling free area decreases, there is less cold air to entrain into the plume above the false ceiling, which results in the spread of smoke in the entire volume of the space above the false ceiling. The velocity flow pattern reflects what can be seen from the temperature slices, where the temperature gradient is star-shaped. Because the flows are more substantial from the fire source towards the openings, gases with higher temperatures flow away from the source of origin, thus creating the star-shaped gradient (Figure 18).

The outflow under the false ceiling for the 15% false ceiling is much more significant in magnitude compared to 40 and 25%. This results in higher temperatures under the false ceiling rather than higher temperatures above the false ceiling. This occurs due to the outflow of hot gases from the fire compartment (Figure 19).

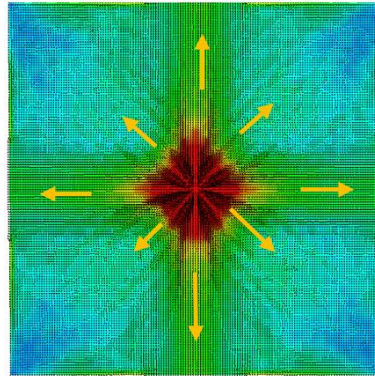


Figure 19. Flow pattern of the plume deflected from the point of origin towards the openings. Velocity vector horizontal slice for 15% free area at the height of 2.2 m. The time averaged result (the averaging time of 50 seconds).

Neutral plane

The neutral plane is characterised as the reference height where the pressure and velocity differences of the hot and cold gases are zero. The hot gases flow out of the compartment above the neutral plane, and cold air flows in below the neutral plane [26]. Since there are ventilation openings at the ceiling, for cases with 100, 60, and 50%, hot gases flow out of them without any disruption at the false ceiling level. Hence the flow from the shop openings is an inflow of cold air only. For 40% and less free area, the velocity difference across the openings is almost zero at the height of 2.1 metres. This means that for perforations of less than 40%, the spread of smoke outside the compartment of origin is expected, although the magnitude is different.

Ceiling jet

Ceiling jet is explained as a spread of hot gases radially once the fire plume impinges on the ceiling. According to Quintiere [26], the velocity of the ceiling jet will be zero at the ceiling boundary, and maximum close to the ceiling, which is typically 1% of the total height of the compartment. As the ceiling jet moves radially, its temperature decreases due to the air entrainment. Additionally, it is also cooled down by the heat transfer to the ceiling [26].

The ceiling jet is present at 100 and 60% free areas. This means that it is present only at the compartment ceiling and no ceiling jet forms at the false ceiling. It is formed under the false ceiling starting from the 50% free area. If for the 50% free area the maximum velocity under the false ceiling is 0.6 m/s and spreads to 2.7 m of radial distance, the constant velocity is 0.26 m/s and spreads to 4.8 m. This means that the ceiling jet formed under the ceiling does not leave the confinement. For 40%, on the other hand, the maximum velocity is 1.24 m/s with the radial distance of 4.6 m, whereas the constant velocity is 0.5 m/s with the radial distance not confined to the compartment. Similarly, 25% has a constant velocity of 0.5 m/s with an unconfined radial distance, whereas the maximum velocity is 1.36 m/s with a radial distance of 5.3 m. Table 12 shows the velocity and radial distance from the plume centreline at the ceiling and false ceiling heights. The readings are taken as visual observation of the velocity vectors and contour plots. The ceiling jet velocity decreases as the free area of the perforations decreases. The maximum ceiling jet velocity for the 40% free area is almost half of the velocity for 50%, whereas the velocity below the false ceiling is doubled. The ceiling jet velocity gradually decreases after the 40% free area because hot gases travel diagonally with lower velocity after penetrating through the lesser free area of the perforations, which happens because a ceiling jet forms underneath the false ceiling (Table 22). This ceiling jet allows the hot gases to escape through the openings. Although for 40 and 25% the radial distance at the maximum velocity is 4.6 and 5.3 metres, meaning within the compartment, the hot gases escape the compartment at lower velocity (Table 12). This can also be explained by the presence of a neutral plane at the 40% free area and lower.

Table 12. Maximum ceiling jet velocity and radial distances for 2 MW fire. 7.5 m is the maximum confined radial distance at the ceiling level. Unconfined – meaning at this velocity, the ceiling jet travels beyond the compartment.

Free area	Maximum ceiling jet velocity at the ceiling	Radial distance from plume centreline at the ceiling	Maximum ceiling jet velocity at the false ceiling	Radial distance from plume centreline at the false ceiling
100	2.0 m/s	3.7 m	N/A	N/A
60	2.0 m/s	3.6 m	NO ceiling jet formed	N/A
50	1.72 m/s	4.5 m	0.6 m/s	2.7 m
40	0.8 m/s	7.5 m	1.24 m/s	4.6 m
25	0.5 m/s	7.5 m	1.36 m/s	5.3 m
15	0.4 m/s	7.5 m	1.26 m/s	Unconfined
10	0.3 m/s	7.5 m	1.44 m/s	Unconfined
6	0.4 m/s	7.5 m	1.6 m/s	Unconfined

3.1.3 Visibility

Smoke production and visibility in FDS are controlled by three parameters, the soot yield, mass extinction coefficient, and visibility factor, and by default these are associated with the smoke that was defined by the chemistry model [17]. In addition, according to [22], the soot yield (Y_s) in the numerical study conducted showed significant differences between Y_s lower and higher than 0.1 g/g. The authors concluded that, when doing CFD assessment of the design, choosing $Y_s < 0.1\text{g/g}$ may lead to potential consequences of underestimating the smoke and heat control systems [22]. Based on these recommendations, the fuel chosen for this numerical study was POLYURETHANE_GM37 with $Y_s = 0.113\text{ g/g}$. For comparison purposes, the visibility benchmark taken was similar to [8] - 8 metres, which corresponds to the optical density of 0.1 over a 1-metre path length of the smoke on escape routes. Based on the horizontal visibility fields given in Table 24 and Table 25, for both small and large fires, 100, 60, 50, and 40% have maximum visibility at the escape route level – 2 metres from the floor. Although the 2% free area has maximum visibility during the small fire, for the large fire the visibility ranges between 2–4 metres at the stagnation areas. The visibility patterns are similar for the free areas of 15, 10, and 6% (Table 24, Table 25). For these cases, the worst visibility is at the stagnation zones and corresponds to 1 metre of visibility. The visibility is worst for these cases because not all of the plume mass can flow through the perforations in the false ceiling. As the smoke spreads below the false ceiling horizontally, some flows out of the compartment through the openings. Some more impinges on the walls and is deflected down to accumulate in the stagnant zones (corners).

3.2 Part II: Uneven openings in the false ceiling

In the following section, false ceilings with uneven openings for the relative free areas of 40 and 25% were examined for different designs. The benchmark for different designs was the perforated false ceiling design of 40 and 25% from the previous section. Designs #1 to #5 have a similar arrangement for both types of openings. Design #1 starts off with a large opening on one side of the total false ceiling area. Then, from Design #2 and thereafter, a systematic increase in the number of openings begins, becoming more evenly distributed. This will allow

us to see the trends associated with the unevenness of the openings and how it affects the effectiveness of the smoke and heat control system.

Appendix A: Slice files from all test runs contains the vertical and horizontal slices of temperature, velocity, and visibility for all test runs.

3.2.1 Temperature

40 %. Design #1

This false ceiling design is characterised as one large opening from one corner of the walls. In the current consideration, the fire was located in the middle of the compartment where no false ceiling hinders the flow of the plume to the ceiling. In terms of the hot gas flow and design smoke layer height, it has the same flow pattern and behaviour as the case with no false ceiling present.

In Figure 20, it is possible to see the comparison of temperatures at the shopfront downstand between evenly distributed perforations of 40% and below with designs of uneven openness. The temperature rise of Design #1, in this case, is lower than the temperature rise of the 40% perforations.

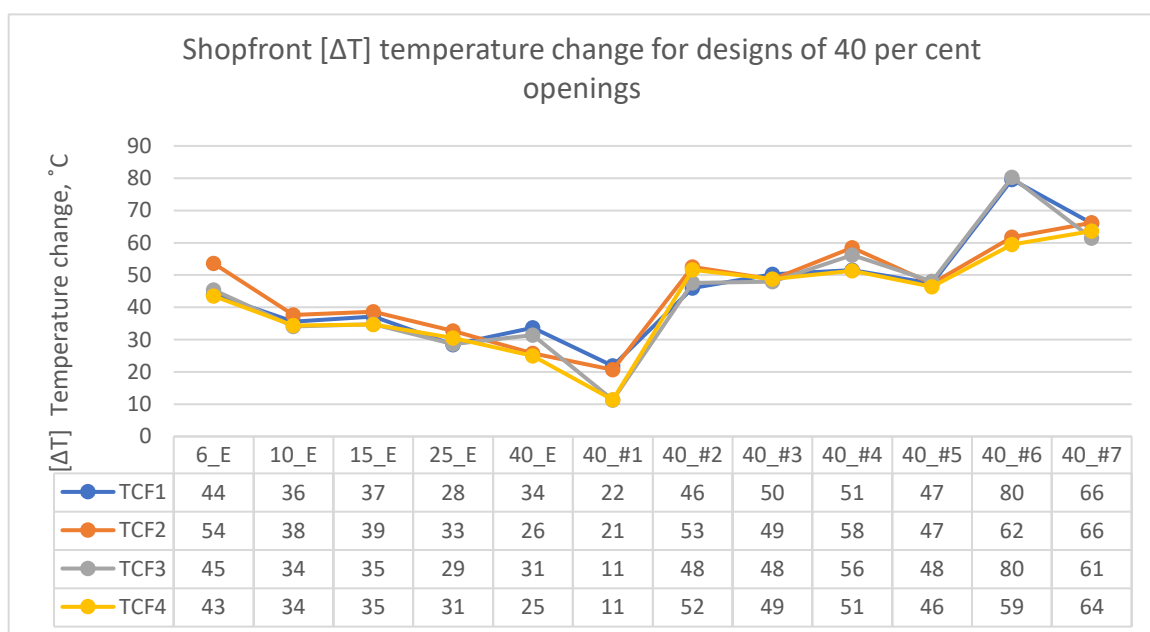


Figure 20. Comparison of temperature changes for perforated false ceiling with 6, 10, 15, 25, and 40% free area and uneven openness of 40% with various designs. Temperature readings are from thermocouples located at each of the four shopfront downstands. TCF1, TCF2, TCF3, and TCF4 are thermocouple names. Time-averaged steady-state results (50 s. of the averaging period)

As explained in the previous section, the free area of 40% perforations allows the formation of the ceiling jet and a neutral plane under the false ceiling, which would indicate that some smoke escapes through the lower openings. In Design #1, on the other hand, the fire plume is not hindered by the openness in the false ceiling, and the plume is free to be transported through the ventilation openings. This means that there is a clear formation of the design smoke layer height, which makes this design similar to the case with no false ceiling (Figure 21). However, since the remaining 60% of the false ceiling is a solid obstruction, the ambient temperature is lower compared to the 100% free area.

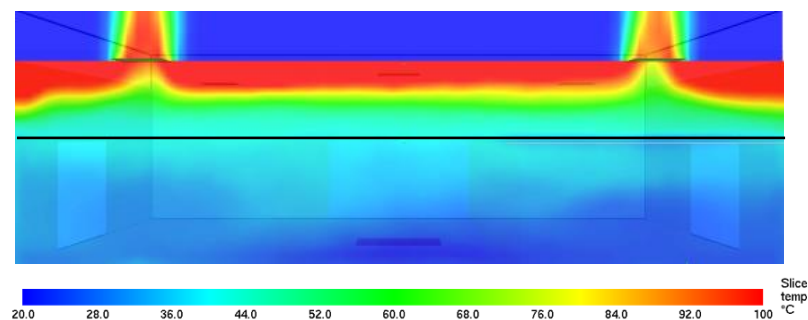


Figure 21. Temperature slice cut at 2.5 m (Y-axis) for uneven openness of 40% Design #1. Black line on the slice is false ceiling location.

In Figure 22, it is possible to see that the ambient temperature at one of the thermocouples is much higher than the 40% even perforations, whereas others are lower. This is due to the false ceiling acting as a barrier between the upper and lower part of the false ceiling, preventing mixing between the layers and large vortexes. TCA1 (Figure 22) was located on the side of the floor level where the false ceiling has a large opening, which supports the statement above: due to the large opening and no obstruction, large vortexes are created which mix the hot gases that are rising and the cold air at the floor level. It is important to note that this design is only applicable if the fire source is located in the open part of the free area. A parametric study needs to be conducted with various fire source locations. It is hypothesised that the temperatures below the false ceiling will be much higher if the fire source is located below the solid part of the false ceiling (similar to Design #2 or #3).

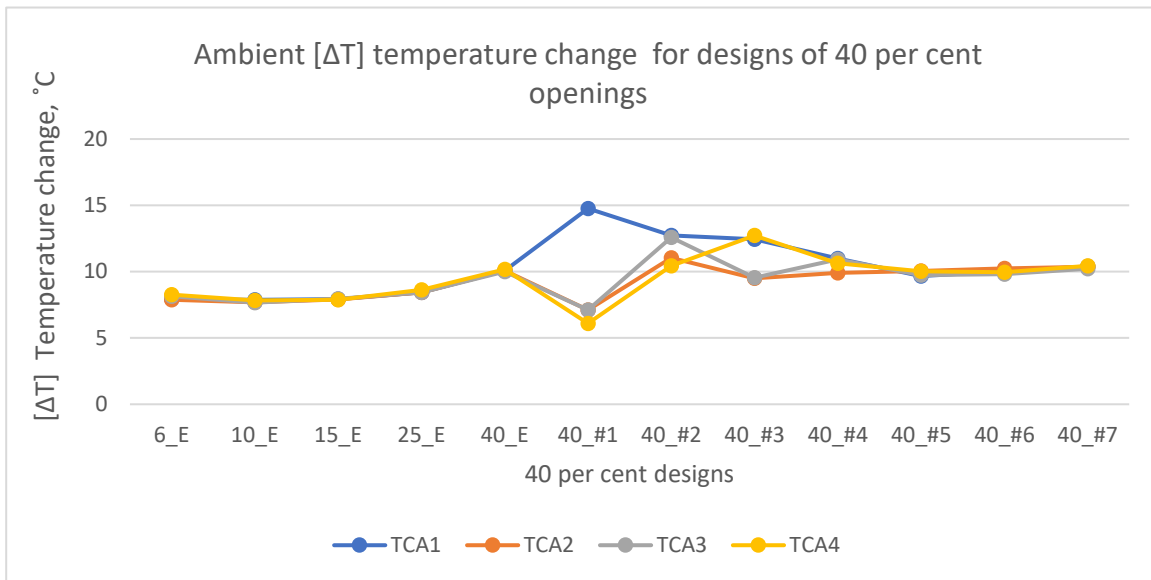


Figure 22. Comparison of ambient temperature changes for perforated false ceiling with 6, 10, 15, 25, and 40% free area and uneven openness of 40% with various designs. Temperature readings are from thermocouples located at the floor level. TCA1, TCA2, TCA3, and TCA4 are thermocouple names. Time-averaged steady-state results (50 s. of the averaging period)

40 %. Designs #2 and #3

Designs #2 and #3 have the same number of openings that differ only in the arrangement. While the Design #2 opening is located on one side of the compartment, the Design #3 openings are located on the opposite corners of the compartment. Judging by the thermocouple readings at various locations in (Figure 20, Figure 22, Figure 23) and the temperature fields (Table 27, Table 28, Table 31), Design #3 has slightly lower temperatures in the enclosure below the false ceiling and better uniformity of hot gases at the ceiling level.

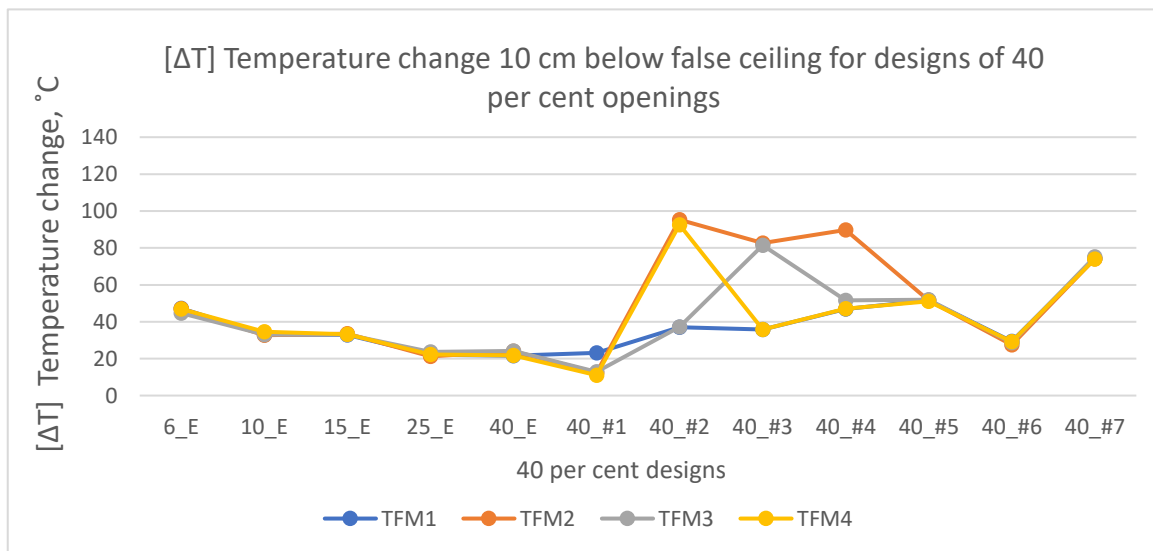


Figure 23. Comparison of temperature changes at the false ceiling level for perforated false ceiling with 6, 10, 15, 25, and 40% free area and uneven openness of 40% with various designs. Temperature readings are from thermocouples located 10 cm below the false ceiling (2.3 m from the floor). TFM1, TFM2, TFM3, and TFM4 are thermocouple names. Time-averaged steady-state results (50 s. of the averaging period)

However, these are far from ideal conditions for life safety purposes. For both designs, the ambient temperature changes are 20–40% higher than the ambient temperature of the lowest free areas of the evenly distributed perforations in the false ceiling. The temperature changes below the false ceiling are up to 50% higher than the results from even perforations (Figure 23). As expected, the highest temperatures are monitored below the solid parts of the false ceiling. When the plume impinges on the solid obstruction, it travels horizontally until it either exits the compartment or meets a transverse barrier. Theoretically, if we divide the compartment in half, Design #2 could be characterised as if one half is entirely open, while the second half is entirely closed. On the other hand, if the same principle is applied to Design #3, then both parts are 50% open and 50% closed. Since in Design #2, one side of the compartment is an entirely solid false ceiling, the plume that has impinged on the solid part of the false ceiling has a longer, uninterrupted distance to travel until an opening or transverse barrier. This contributes to the higher accumulation of the hot gases and local deepening in the stagnant zones (Figure 24). On the other hand, in Design #3, when the plume impinges on the solid part of the false ceiling, the horizontal travel distance under the false ceiling is shorter and is interrupted by the presence of the openings on either side of the compartment. As a result, the smoke and heat control system is more efficient in Design #3, with about 10–13% lower temperatures below the false ceiling (Figure 23) than Design #2.

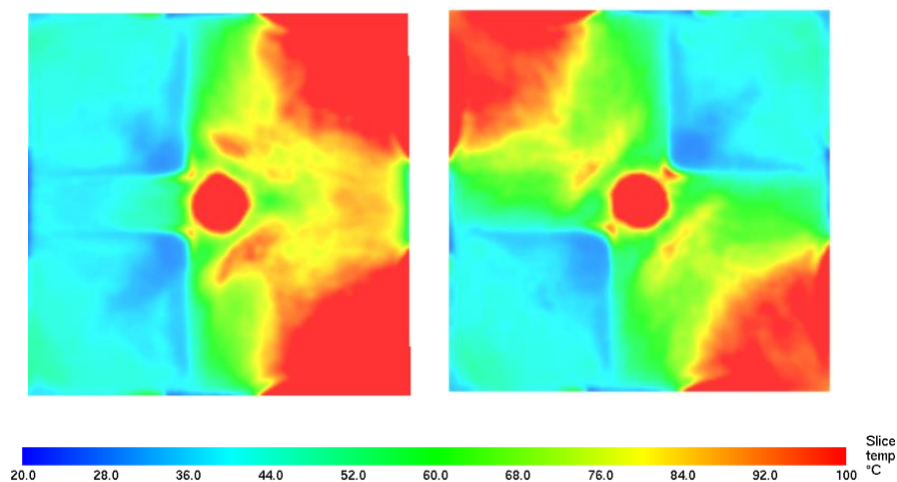


Figure 24. Horizontal temperature fields for Design #2 (left) and Design #3 (right) of 40% uneven openness at the height of 2.0 m above floor.

40 %. Designs #4 and #5

In the following designs, the number of openings is increased accordingly. Design #4 has three openings, whereas Design #5 has four openings that are evenly distributed compared to all previous designs. The ambient temperature and the temperature below the false ceiling gradually get better as the number of openings increases (Designs #2–#5). Looking at the ambient temperature changes at the floor level (10 cm above the floor) raises the speculation that having fewer large openings adversely affects the temperatures at the lower level of the compartment because larger openings accommodate more mixing and interaction between the colder lower layer and the hotter upper layer. Temperatures leaving the compartment are in the same range for all of these four designs, but Design #4 shows a slightly higher temperature rise than others. This is probably due to the specific opening locations. The solid parts of the false ceiling between openings are extended until the shopfront openings, which probably allows the plume that has impinged on the false ceiling to become a ceiling jet and exit the compartment. A similar range of temperatures leaving the compartment for Designs #2–#5 would indicate that, in these kinds of arrangements, a large amount of smoke and hot gases escapes from the compartment. Compared to 40% even perforations in the false ceiling, on average these designs (Designs #2–#5) have a 39–47% higher temperature rise at the shopfront downstand and 56–65% higher temperatures just below the false ceiling (Figure 20 and Figure 23). Another comparison could be made with 6% free area of even perforations. Based on the averaged thermocouples values from the same figures, Designs #2–#5 have 7–14% higher temperature rises of the hot gases leaving the compartment, whereas the temperature rises below the false ceiling range between 10–29% (Table 13). As a result, it is possible to see that having fewer openings in the false ceiling, even with 40% openness, does not necessarily mean that the effectiveness of the smoke and heat control system is guaranteed. The results from these designs show that they perform worse than the 6% free area perforations that are distributed evenly over the whole surface of the false ceiling. The closest design to 6% even perforations is Design #5, which has four openings distributed symmetrically.

Table 13. Effectiveness (in terms of average temperature rise) at the shopfront and below the false ceiling of 40% uneven openness designs compared to 40% and 6% perforations. A positive value means an increase in the average temperature rise (less effective); a negative value means the design is more effective than even perforations in the false ceiling.

Design description	(40% even distributed perforations) at shopfront.	(6% even distributed perforations) at shopfront.	(40% even distributed perforations) below FC	(6% even distributed perforations) below FC
Design #1	- 78 %	- 186 %	- 54 %	- 213 %
Design #2	42 %	7 %	65 %	29 %
Design #3	41 %	5 %	61 %	21 %
Design #4	47 %	14 %	61 %	21 %
Design #5	39 %	1 %	56 %	10 %
Design #6	59 %	34 %	20 %	- 62 %
Design #7	55 %	28 %	69 %	37 %

40 %. Designs #6 and #7

These designs were created to resemble real-life applications of the false ceilings that are fitted in malls and airports. Design #6 is characterised as open slits distributed over the entire surface of the false ceiling area, additional to the slits that surround the compartment. The slits are equidistant and span the entire length of the Y-axis. Since the openings are evenly distributed over the entire length of the false ceiling, the temperature rises monitored from thermocouples located at the same level show uniform readings. This is especially true for the ambient temperature, temperatures under the false ceiling, and at the ceiling. On the other hand, it is possible to note in Figure 20 that two thermocouples show higher temperatures. This is due to the specific geometry of the design. When the plume impinges on the false ceiling and spreads radially, long slits in the false ceiling allow the smoke to flow through, so that the plume impinged on the false ceiling can easily flow through the slits. On the other hand, a plume that is travelling perpendicular to the slits experiences more resistance from the solid sections of the false ceiling. As a result, the width of the slits and the solid parts in between the slits do not allow the hot gases to flow through, which makes the hot gases flow out of the compartment. This hypothesis can be noticed from the thermocouple readings in Figure 20. The thermocouples named TCF1 and TCF3, located perpendicular to the long slits that are evenly distributed over the entire surface of the false ceiling, have higher temperatures than the thermocouples parallel to the slits. However, even having this kind of design that has multiple openings that are distributed and parallel to each other does not make the design more effective. Although the overall temperatures at the evacuation level,

ambient temperatures at floor level, and temperatures below the ceiling are much better than other designs, the escape of hot gases is still expected. Compared to the performance of 40% even distributed perforations in terms of the temperatures at the shopfront downstand, in Design #6 the average temperature is 59% higher than the 40% free area and 34% higher than the 6% free area in the evenly distributed false ceiling. Temperatures below the false ceiling monitored for Design #6 showed a 20% higher temperature. On the other hand, compared to the 6% perforations, it had a 62% lower temperature rise (Table 13). This means, in terms of the temperature distribution under the false ceiling, that the temperature rise results were closer to the 15–25% evenly distributed perforations (Figure 23).

Design #7 is another example similar to real-life applications. In this setting, the openings at the false ceiling are located near the walls and surround the compartment. When the plume impinges on the false ceiling, it has to travel radially until it reaches the openings. Because the openings are located around the compartment, including corner zones, there are minimal accumulations of hot gases at the stagnant zones (Table 31). On the other hand, the effectiveness of the smoke and heat control system is the lowest (in terms of the extraction of hot gases) because the geometry, location of the openings, and extraction power are not enough for the plume flow to be extracted through the extraction system. The ceiling jet that is formed under the false ceiling does not have any obstruction or interruptions on the false ceiling, which gives the opportunity for the hot gases to flow out of the compartment at high velocity (Figure 25).

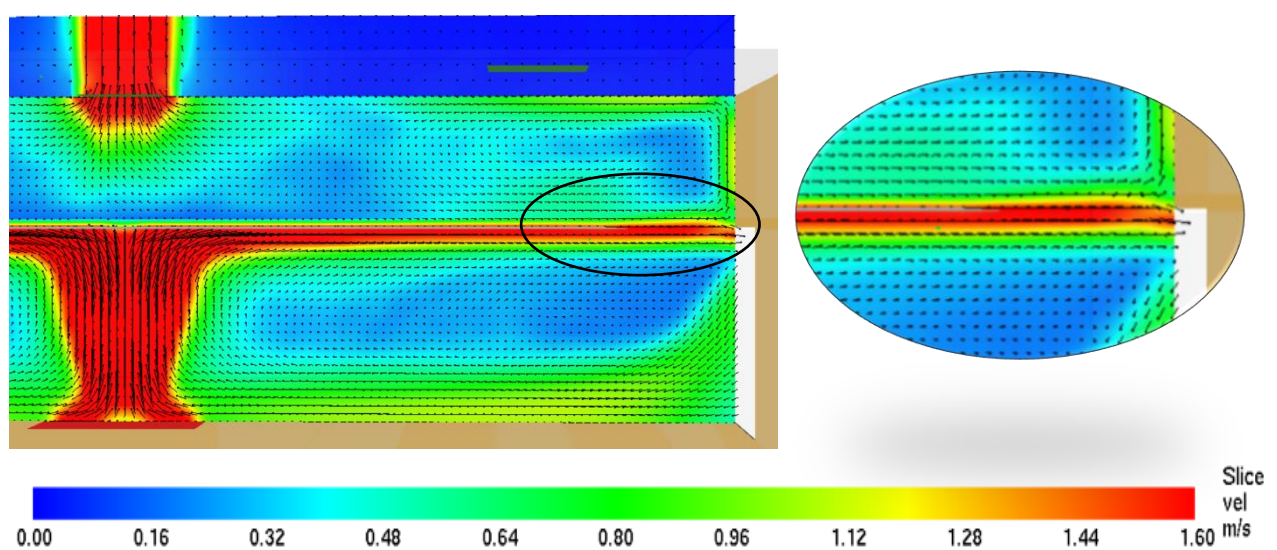


Figure 25. Velocity field of 40% Design #7 at 7.5m of Y-axis. Hot gases are flowing out of the compartment at velocity higher than 1.6 m/s.

This could mean that when the plume flows radially in all directions, some amount flows out of the compartment, whereas the amount that impinges on the vertical barrier flows through the openings on the edges of the compartment (Figure 26). In terms of the temperature distribution on the compartment, Design #7 shows the worst results. The average temperature rise below the false ceiling is 69% higher than the 40% free area evenly distributed perforations and 30% higher than the 6% even perforations. The gases flowing out of the compartment have a 55% higher temperature than the 40% free area and 28% higher than the 6% free area (Table 13). As a result, based on the thermocouples readings and contour plots from Smokeview, Design #7 performs the worst of all the designs.

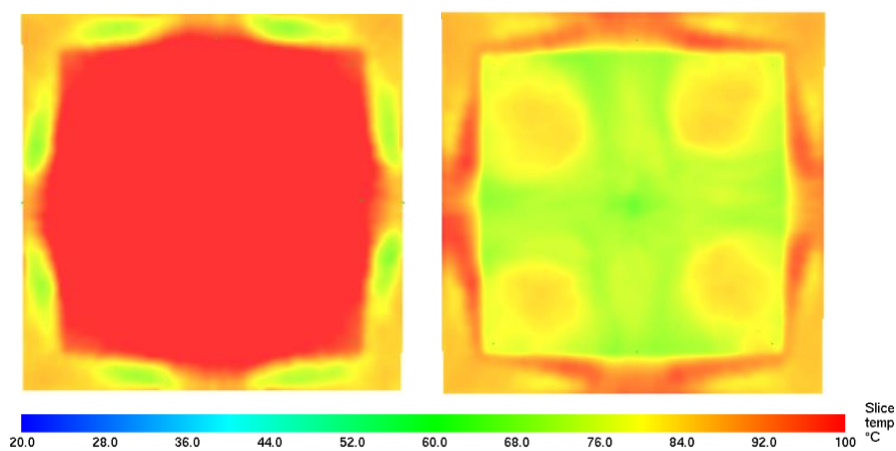


Figure 26. Horizontal temperature fields for Design #7 of 40 per cent uneven openness at the height of 2.0 m (left) and 2.3 m (right) above floor.

25 %. Design #1

The geometry pattern of the openness of the false ceiling design was similar to 40%, starting with one opening of 25%, then two openings that combined to give 25%, and so forth until four openings. Unlike the 40% Design #1, the axisymmetric position of the fire did hinder the plume transport for the 25% Design #1 because the opening was not large enough. As a result, on average, the accumulation of hot gases below the false ceiling is 61% more than for the 25% free area when the perforations are evenly distributed and 18% more than the 6% perforations (Table 14). In terms of hot gases leaving the compartment, the thermocouples located at the shopfront close to the openings in the false ceiling recorded a lower temperature rise compared to 25% even perforations, whereas the other two thermocouples recorded a similar temperature rise. Although there are accumulations of hot gases below the false ceiling, the temperature rise is not as high as Designs #2–#4 (Table 29, Table 30, Table 32).

Table 14. Effectiveness (in terms of average temperature rise) at the shopfront and below the false ceiling of 25% uneven openness designs compared to 25% and 6% perforations. A positive value means an increase in the average temperature rise (less effective); a negative value means the design is more effective than even perforations in the false ceiling.

Design description	(25% even distributed perforations) at shopfront.	(6% even distributed perforations) at shopfront.	(25% even distributed perforations) below FC	(6% even distributed perforations) below FC
Design #1	-12%	-74%	61%	18%
Design #2	36%	1%	66%	28%
Design #3	42%	10%	64%	25%
Design #4	37%	3%	56%	8%
Design #5	36%	1%	66%	28%
Design #6	51%	24%	70%	37%
Design #7	52%	25%	58%	13%
Design #8	21%	-22%	25%	-57%
Design #9	34%	-2%	68%	34%

25 %. Design #2–#5

The 25% Designs #2–5 have similar patterns to the 40% Designs #2–#5, the difference being in the percentage of openness in the false ceiling relative to the whole area. In terms of temperature behaviour, they are similar to the 40% openness designs. The ratios of the temperature rise below the false ceiling range between 56–66% higher than the 25% even perforations and 8–28% higher than the 6% even perforations. According to the temperature readings from the thermocouples located at the shopfronts, on average, the results are similar to the 6% even perforations (Figure 27). It is interesting to note for Designs #3 with both 40% and 25% that the thermocouple readings showed very similar temperatures at all the shopfront openings (Figure 20 and Figure 27). The temperature readings in Figure 28 vary greatly between thermocouples, which could be because of the locations of the openings and the unchanged positions of the thermocouples for all the designs.

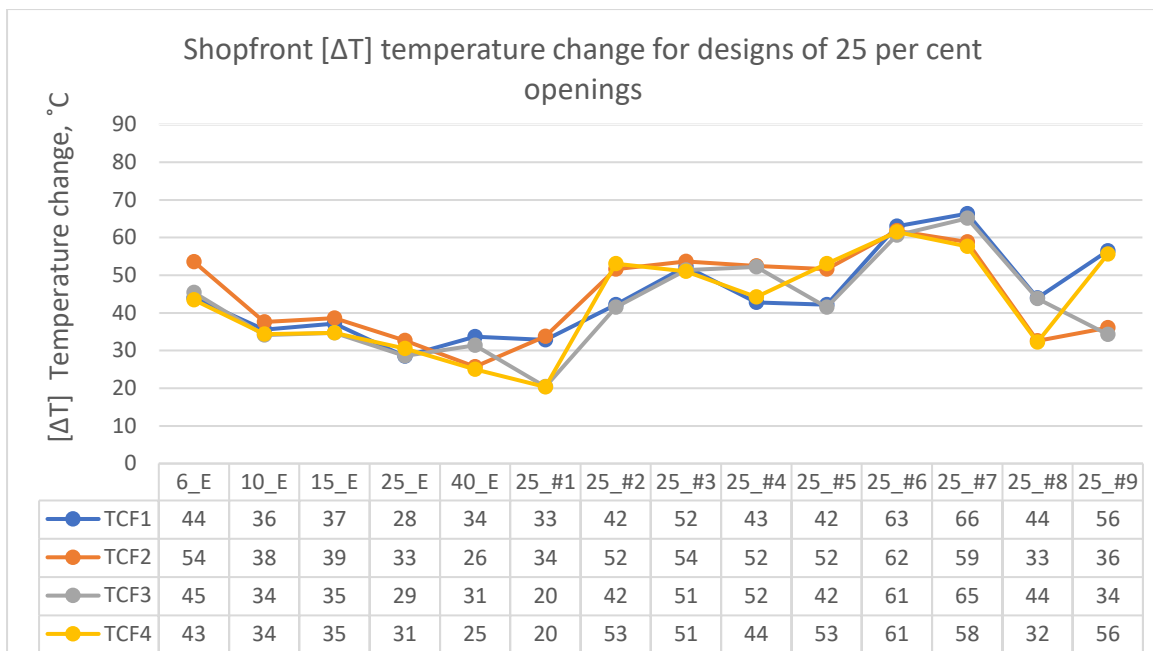


Figure 27. Comparison of temperatures for perforated false ceiling with 6, 10, 15, 25, and 40% free area and uneven openness of 25% with various designs. Temperature readings are from thermocouples located at each of the four shopfront downstands. TCF1, TCF2, TCF3, and TCF4 are thermocouple names. Time-averaged steady-state results (50 s. of the averaging period)

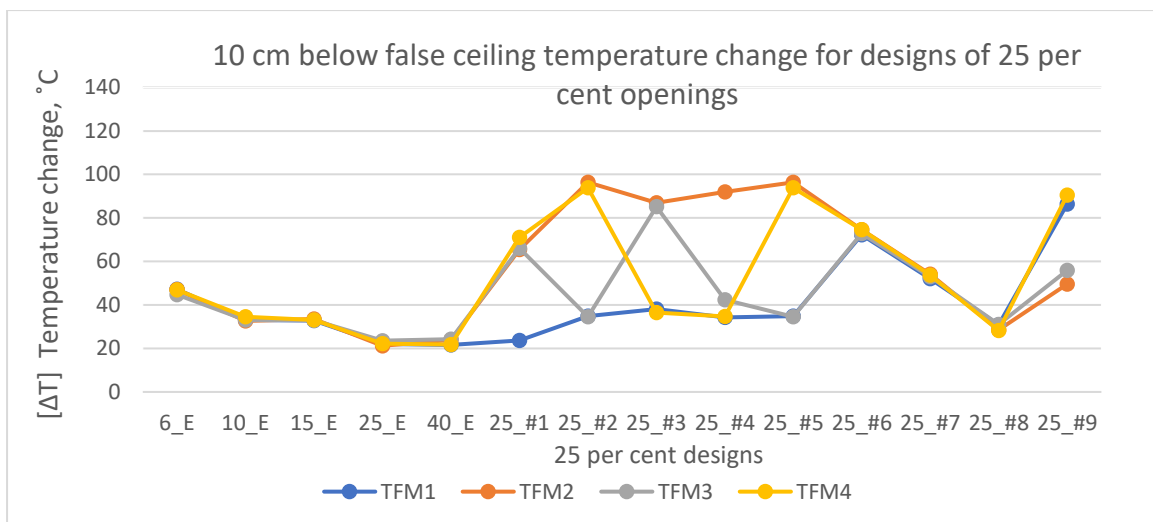


Figure 28. Comparison of temperature changes at the false ceiling level for perforated false ceiling with 6, 10, 15, 25, and 40% free area and uneven openness of 25% with various designs. Temperature readings are from thermocouples located 10 cm below the false ceiling (2.3 m from the floor). TFM1, TFM2, TFM3, and TFM4 are thermocouple names. Time-averaged steady-state results (50 s. of the averaging period)

25%. Designs #6–#9

The 25% Design #6 is similar to the 40% Design #7 in terms of its geometry: narrow slit openings around the compartment and a non-permeable central part. As mentioned before, although having openings at the stagnant zones helps with removing the smoke and hot gases from the area, the overall performance of the smoke and heat control system with this kind of design is not efficient. A large amount of smoke escapes from the compartment, and smoke that is being extracted from the compartment is at lower temperatures, which indicates that

hot gases are not necessarily reaching the smoke reservoir that is located above the false ceiling (Table 29, Table 30, Table 32).

Design #7 is another design similar to a real-life application. Similar to Design #6, bigger opening slits surround the compartment, but it also has smaller slits distributed across the entire surface of the false ceiling. Compared to Design #6, the presence of smaller slits across the false ceiling helps the flow of hot gases to the smoke reservoir, which means the smoke extraction system is more efficient. However, relative to the 25% even perforations, these designs are still not as efficient. For example, on average, the temperature rise below the false ceiling is 58% higher than with 5% even perforations and 13% higher than with 6% perforations (Table 14).

Design #8 is characterised as an equidistant slit that spans from one end of the compartment to the other along the Y-axis. Based on comparison of the average temperature rise (Table 14), the temperature rise for this design is 21% higher than with 25% even perforations at the shopfront and 25% higher below the false ceiling. From the average temperatures based on Figure 27 and Figure 28, this design is closer to 10 and 15% even perforations. As a result, it is possible to see that the geometry of the openings in the false ceiling plays a big role in the effectiveness of the flow through the false ceiling. The numerical results for Design #8 indicate that even if the 25% openness is in the form of long slits that are evenly distributed relative to each other, the effectiveness of the temperature accumulation and flow out of the compartment is similar to 10 and 15%, not 25%.

Design #9 is characterised as a series of smaller openings grouped together at opposite ends of the compartment. In total, there are four small openings in one corner and eight openings in the opposite corner. Similar to Designs #2–#4, the accumulation of hot gases is expected at the corners and stagnant zones where there is no opening in the false ceiling. By comparison, it has similar temperature rises below the false ceiling and at the shopfront to Design #5, although in Design #5 no hot gases accumulate at the lower levels.

3.2.2 Visibility

Similar to the previous visibility comparison, the results were compared for the height of 2 metres, which was taken as a benchmark for evacuation purposes from the compartment. The visibility threshold was taken to be 8 metres [8], when people can safely evacuate from the

compartment. As mentioned before, based on the numerical simulation results, when the perforations are evenly distributed with a free area of 40%, the maximum visibility was observed. In comparison, with the 25% free area of even perforation, the visibility ranges between 2–4 metres at the corner areas. The 40% Design #1 showed the best results because, as mentioned in the previous section, having one large opening in the setting where the fuel source is located right under the opening guarantees unhindered flow of the plume into the smoke reservoir.

For the 40% Designs #2–#4 and 25% Designs #1–#4, the visibility is less than 1 m under the impermeable (solid) parts of the false ceiling (Table 33 and Table 34). Unlike other cases, with the 40% Designs #2 and #3 the visibility was the maximum below large false ceiling openings where the width of the false ceiling edge near the walls is 0.4 and 0.6 metres (Figure 29-a).

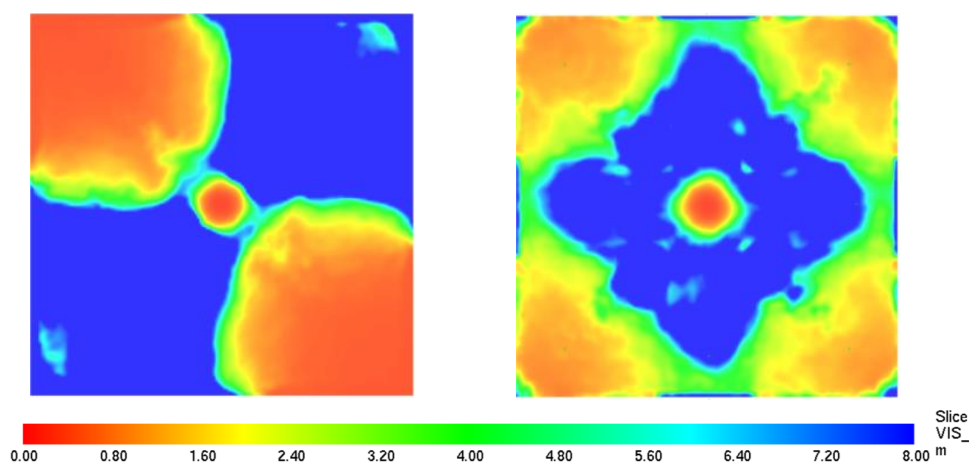


Figure 29. Visibility fields at 2 m for 40%. (a) Design #3 (left). (b) Design #5 (right). Time-averaged steady-state results (50 s. of averaging period).

In all other cases (40% Designs #4, #5 and 25% Designs #2–#5), the width of the false ceiling near the walls was 1 metre and the visibility under the false ceiling openings corresponded to 0–2 metres (Figure 29-b). This could mean that smoke could be accumulated in the corner and near the walls when large openings of the false ceiling are located at least 1 metre away from the wall. The 40% Design #6 has the best visibility results among all designs, having 40% even perforations with the openings as equidistant slits with a width of 0.6 metres that are 1.4 metres apart from each other. Among the designs with 25% free area, the best result in terms of visibility is Design #8 with 3–4 metres at the corners.

All other cases (40% Design #7, 25% Designs #6, #7, #9) have similar visibilities, where the corner zones have visibility less than 2 metres, and their patterns of visibility are the same as with 15, 10, and 6% free areas of evenly distributed perforated false ceiling (examples in Figure 30).

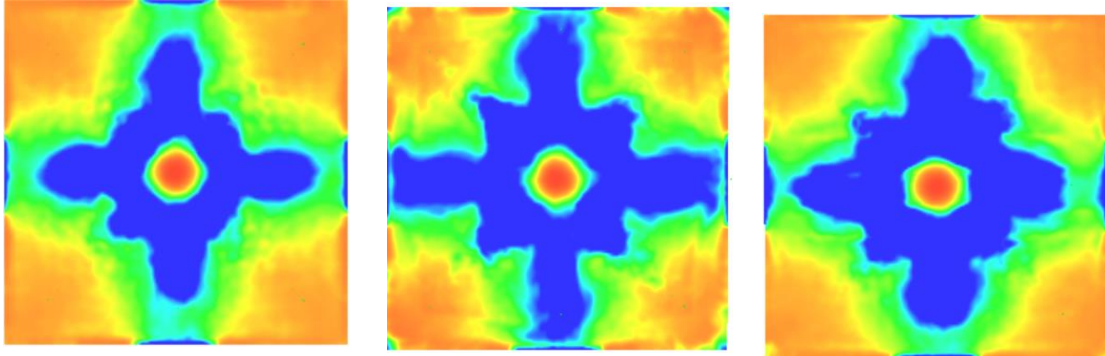


Figure 30. Visibility fields at 2 m. From left to right: (a) 6% even perforations. (b) 40% Design #7. (c) 25% Design #7. Time-averaged steady-state results (50 s. of averaging period).

3.2.3 Additional simulation

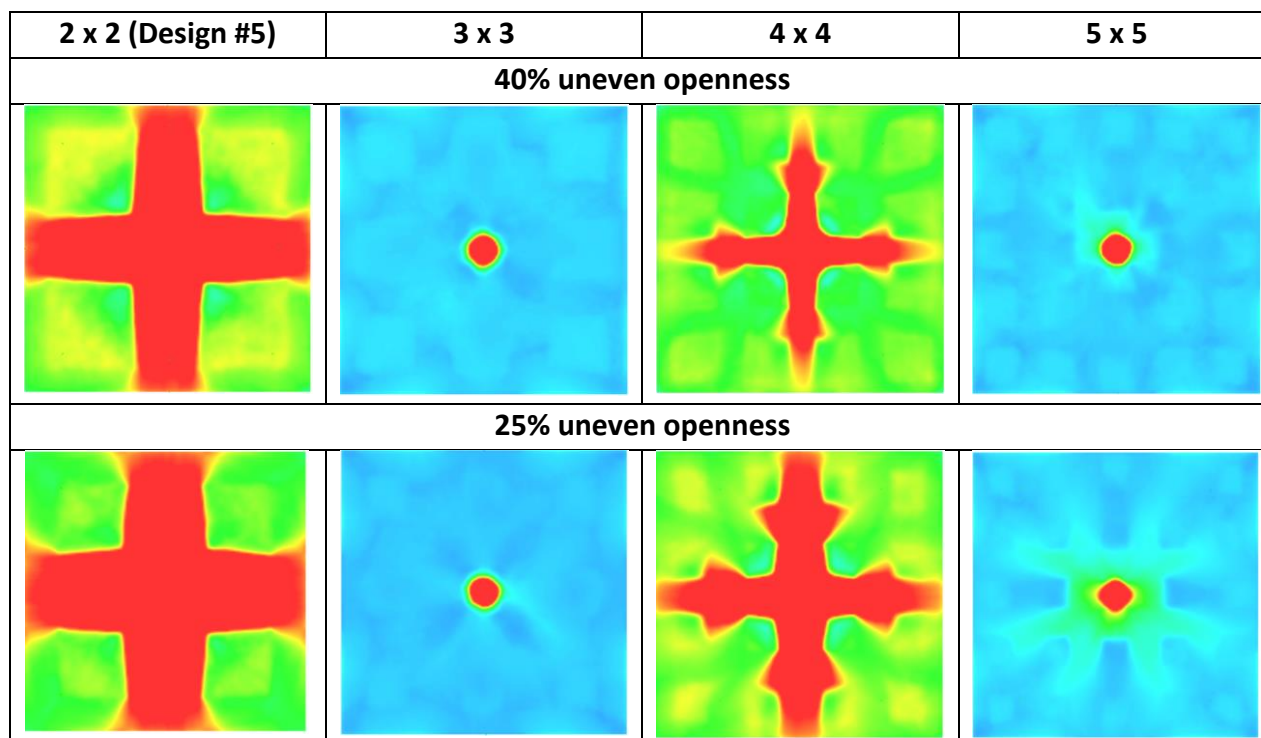
Additional simulation has been performed with the further refined false ceiling with increased numbers and symmetrical distribution. Detailed geometry and graphs are given in Appendix C: Additional simulations. The base for opening and distribution was from Design #5, that has four openings in total (2 x 2). Further models were performed for 9 openings in total (3 x 3), 16 openings (4 x 4), and 25 openings (5 x 5) for 25% and 40% openings in the false ceiling (Table 35).

These six additional simulations demonstrated that, for the given compartment geometry and fire location, the improvement of conditions inside the compartment is possible with further increase in the number of openings and evenness. Simulations with a total number of 9 and 25 openings total showed results better than 60% evenly distributed perforations in the false ceiling. The temperatures below the false ceiling and at the shopfront downstand monitored the lowest results among all other designs of uneven openness. This is due to the presence of an opening above the fire source.

The simulation with 16 openings registered higher temperatures than previously mentioned two models; however, compared to other models, it showed improvement (for both 20 and 40% openness). The higher temperatures are due to the obstruction above fire source where the plume cannot travel directly. As a result, it impinges on the obstruction, then flows

through the nearest openings. In terms of numerical comparison, this design came close to 10% evenly distributed openings in the false ceiling (Table 15).

Table 15. Horizontal temperature fields of additional simulations for uneven openness in the false ceiling. Slice but is at Z=2.3 m (10 cm below false ceiling). . Time-averaged steady-state results (50 s. of the averaging period).



A further parametric study with respect to ceiling design and fire location should be performed to see how these designs perform in different conditions. As it was mentioned in the previous sections, many of the uneven openings in the false ceiling could severely underestimate the temperatures, whereas in a few other cases it could actually perform better. Overall, these results ones again showed that evaluation of the false ceiling design should be carried out case by case because having large openings and uncertainty where the fire might occur increases uncertainty in the whole smoke and heat control design sharply.

3.3 Design implications

Depending on the objectives of smoke spread and containment, the minimum admissible free area of the false ceiling could be adapted to the particular design. In this study, the false ceiling was fitted at the same level as the shopfront of the compartment (false ceiling flush with shopfront downstand); hence the smoke reservoir was the space above it. The numerical results support the recommendations made by Hinkley [1], that having a false ceiling with a free area of 50% or more will not hinder the smoke flow through it. Moreover, based on the simulations conducted for the 500 kW fire, a 40% free area will also not hinder the smoke from

flowing through the openings, whereas 25% does not significantly affect the flow of the smoke. Based on the results from the 2 MW fire, even if there is a slight increase in the temperature under the false ceiling, in terms of visibility, the 40% free area showed much better results than 25%.

With reference to the current study, it appears that the false ceiling free areas of the evenly distributed false ceilings can be separated into three ranges:

1. Free area of 40% and more – no or insignificant influence of the smoke and heat control system. The position of the false ceiling does not play a role since, in the current setting smoke is not hindered by the presence of the false ceiling.
2. Between 40 and 25% – an amount of smoke escapes from the compartment, although based on the numerical results from the temperature readings, the temperatures above the false ceiling are higher than the temperatures below. This could imply that more hot gases are flowing through the false ceiling due to buoyancy than flowing out of the compartment.
3. Free areas below 25% – once the free area of the evenly distributed perforated false ceiling decreases from this threshold value, the gas temperatures are higher below the false ceiling than above it. This suggests that the accumulation of smoke and hot gases is significantly higher under the false ceiling than in the smoke reservoir.

Initially, Hinkley tentatively suggested [1] that the smoke reservoir could be considered as the space above the false ceiling when the false ceiling has a free area of 10% or more, and the depth of the smoke screens (downstand) extending down a bit. On the other hand, he suggested, if the leakage area is small (less than 10%), provisionally the downstand should be extended below the false ceiling to at least a 1 metre depth or 1/3 of the false ceiling height, and have a ducting system in place to remove the smoke [1]. Later, based on experimental results, Marshall et al. [10] recommended that for false ceilings with 14% free area or more, the downstand depth should be extended at least 0.3 metres below the false ceiling level plus 0.1 metre to allow fluctuations in the gas layer. In the cases where the downstands and shopfront downstands are at the same level as the false ceiling, it was suggested that for a large fire such as 5 MW, a 25% free area should be the minimum value for mechanical ventilation [10]. However, it is important to note that these recommendations are based on the criteria when the smoke ventilation system and the false ceiling were installed in the mall, and evaluation of the results was based on the observation that the shop adjacent to the shop

opposite the compartment on fire is smoke-free. As a result, the minimum 25% free area recommendation is based on the premise that when the fire happens in the shop when the mall has 25% perforations in the false ceiling, the shop next to the shop located opposite the compartment on fire is smoke-free. In the current numerical study, the criterion for the design is different: both mechanical extraction and a false ceiling are located in the compartment on fire. As a result, to keep the evacuation routes free from smoke and stop the hot gases flowing out of the compartment, a minimum 40% free area seems to be more feasible when the perforations are evenly distributed, whereas, between 40 and 25%, the downstands should be extended below the false ceiling in order to prevent the flow of hot gases out of the compartment. Unlike Hinkley's suggestion that the smoke reservoir should be extended below the false ceiling when 10% or less free area is employed, based on the numerical results, the smoke reservoir should be below the false ceiling, when the free area of the perforations is smaller than 25%. This suggestion is built upon the observation that the difference in temperatures and visibility is insignificant for the 15, 10, and 6% free areas for evenly distributed perforations.

As reported earlier, modern false ceiling design seldom includes perforations that are evenly distributed, but guidance for smoke and control systems does not specify that the minimum requirements suggested for openings do not include openings in the false ceiling that have different designs. The second part of this numerical study was to observe the differences in the efficiency of smoke extraction when the openings in the false ceiling are uneven. As seen from the previous section, having 40% or 25% openness in the false ceiling is not the same as having evenly distributed perforations in the false ceiling. From the numerical simulations, it can be seen that in the designs where the geometry of the openings in the false ceiling departs from the "original" evenly distributed perforations, the temperature distribution under the false ceiling and the flow of hot gases into the smoke reservoir were seriously underestimated. In some designs, the temperature and visibility outputs showed that even if the relative openness in the false ceiling is 40 or 25%, the flow of hot gases can be hindered by the design specifications of the false ceiling and could perform worse than the 6% evenly distributed perforations. In a few cases, the designs proved better than 6%; however, those cases could be considered as an exception to the general rule. The simulation outputs showed that the smoke distribution below and above the false ceiling depends on the size and spacing of the openings in the false ceiling and the position of the fuel source. In order to better understand the

influence of openness in the false ceiling and the relative position of the fire source, more numerical and possibly experimental studies should be performed.

3.4 Uncertainty

Although CFD is based on the fundamental conservation laws of mass, momentum, and energy, and is considered as a numerical solver of Navier-Stokes equations, it actually approximates it. This means that it involves simplification and assumptions [24]. FDS, as a tool for numerically predicting the combustion processes and plume transport, inherently carries the degree of uncertainty. Although it can provide useful insight into fire development, the end result of the numerical simulation is highly dependent on the input parameters, as well as the uncertainty embedded in the model itself.

Two terminologies are closely related to each other when talking about numerical analysis: uncertainty and error [28]. Although these two terms are used interchangeably, upon examination, it is possible to recognize the difference when referred to numerical studies. Uncertainty, in this case, referred to the lack of knowledge in the physical processes which can be determined through the sensitivity analysis. Errors, on the other hand, are characterized as acknowledged and unacknowledged. If acknowledged error refers to errors in the physical model, geometry, rounding-off, and iterative convergency errors, then unacknowledged refers to computer programming errors. The former can be found and eliminated, whereas the latter not [28].

As it was mentioned before, the output of the numerical simulations is dependent on the input parameters, such that changing certain parameters might influence the outcome. For the particular numerical study, for example, the parameters that carry uncertainty includes the geometry of the compartment, opening size and locations, fire size and location, properties of the obstructions (in here adiabatic), ambient temperature and other simplifications. Besides, there is always the degree of uncertainty related to the grid size in the simulations. Due to the limited availability of computing power and limitations in time, the compromise needs to be made with choosing the most suitable grid size.

As a result, largely, this study attempted to carry out quantitative analysis by comparing different free areas of the perforated false ceiling in terms of size and distribution. The data is compared among each other and relative to the benchmark simulations.

4 Conclusion

A false ceiling is a commonly used aesthetical solution in shopping malls and airports to hide mechanical works installed at the ceiling, such as mechanical extraction systems. For the smoke and heat control system to perform according to the design specifications, the installed false ceiling should not significantly hinder the flow of smoke and hot gases through it.

In earlier works, it was suggested that a 40% free area false ceiling would not significantly affect the flow pattern [8]. In the current design work, it is accepted to use a 25% free area as a “rule-of-thumb” design minimum for the false ceiling, based on the recommendations given by Marshall et al. [10]. According to the recommendation, in general, having a minimum of 25% free area in the false ceiling will not significantly hinder the smoke flow and the smoke and heat control system can function according to the design specification. However, this minimum design requirement for the false ceiling is often used for false ceilings that deviate from the original work on which those recommendations were based. As a result, if the experimental work was done for a false ceiling with evenly distributed perforations but which were not specifically mentioned, the minimum recommendations may be misused in a false ceiling that has unevenly distributed openings.

Firstly, this numerical study, conducted using FDS, attempted to assess the minimum free area of the false ceiling that allows smoke to flow through the perforations unhindered. Then, an attempt was made to see how the size and distribution of the openings in the false ceiling affect the effectiveness of the smoke and heat control system, compared to evenly distributed false ceilings.

In a general sense, the numerical simulations conducted are in conformity with earlier findings [8,10]. The simulations performed for the models with false ceilings with 50 and 60% free area showed that the flow of the plume is not hindered by the presence of the false ceiling, and showed very similar results to the model with no false ceiling, while a 40% free area does not significantly hinder the flow of the plume. Thereby, for design purposes, the smoke reservoir could be the space above the false ceiling and the false ceiling could be located at the same level as the downstand or shopfront.

Numerical results for models (with 2 MW fire) of false ceilings with between 40 and 25% free area showed that some amount of smoke could escape from the compartment into other

spaces. Depending on the design criteria for the particular model, if it is important that no smoke escapes from the compartment on fire, then the shopfront and false ceiling should not be at the same level, but rather the downstand should be extended down to a certain distance.

While Hinkley preliminarily suggested [1] that for a false ceiling with 10 % or less free area the downstand below the false ceiling should be extended down 1 metre, the numerical results suggest that there are negligible differences in the results for models with 15, 10, and 6 % free area. As a result, it is suggested that the recommendation should be reconsidered to include free areas of less than 25% with the downstand or shopfront extended below the false ceiling to form a smoke reservoir under the false ceiling.

The numerical results for uneven openings in the false ceiling demonstrated that having 40 and 25% evenly distributed perforations is not the same as having openings of different sizes and distributions. In the majority of the uneven designs, the temperature readings were significantly higher under the false ceiling than the evenly distributed perforations. These temperatures increased by as much as 70% in various regions when compared to evenly distributed false ceilings with 40 and 25% free area. In a few cases, the temperature readings were close to the numerical results taken from the 6% free area. Moreover, the vast majority of the numerical simulations demonstrated zero visibility in the compartment at the evacuation level.

Based on the evaluation of various designs of the same relative free area openness, the numerical outputs evidenced that indeed the smoke distribution and flow above and below the false ceiling are highly dependent on the size and distribution of the openings. Consequently, it is clear that uneven openings in the false ceiling should be evaluated case by case when employing them in a compartment with a smoke and heat control system. This numerical study attempted to show that taking the “rule-of-thumb” for designs that depart from the original experimental results gives rise to severely underestimated and ineffective smoke and heat control systems, which could result in high temperatures and loss of visibility at the escape routes.

4.1 Recommendations for future work

Evenly distributed perforations in the false ceiling

- The numerical model with a 500 kW fire showed that 40% free area perforations do not hinder any smoke from flowing through the perforations, whereas 25% free area showed insignificant flow under the false ceiling. However, for the 2 MW fire, some amount of smoke is expected to flow out of the compartment. Further analysis should be carried out in order to identify the depth to which the downstand should be extended for free areas between 40 and 25% in the compartment where a large fire is expected.
- As mentioned before, Hinkley's provisional suggestion [1] of at least a 1-metre depth of the downstand below the false ceiling is for perforations with less than 10% free area. This numerical study suggests that there is no significant difference in the temperature under the false ceiling and the visibility for false ceilings with 15, 10, and 6% free areas. As a result, it is recommended that if the free area is smaller than 25%, the smoke reservoir should be considered a space below the false ceiling. The depth of the downstand or shopfront should, therefore, be re-examined to assess the previous [1] recommendations.

Uneven openness in the false ceiling

- The numerical study that was conducted for the uneven openings in the false ceilings evaluated only an axisymmetric fire in the middle of the symmetrical compartment. A parametric study should be carried out for the design models studied here for comparison purposes. Preliminarily, it is hypothesised that results from the further study will give different results from those assessed in this study.

5 References

- [1] P.. Hinkley, Some notes on the control of smoke in enclosed shopping centres, 1971.
- [2] H.P. Morgan, J.P. Gardner, Design principles for smoke ventilation in enclosed shopping centres, Watford, 1990.
- [3] J.A. Milke, Smoke management for covered malls and atria, *Fire Technol.* 26 (1990) 223–243. <https://doi.org/10.1007/BF01040110>.
- [4] National Fire Protection Association, NFPA 92A Recommended Practice for Smoke-Control Systems 2000 Edition, (2000).
- [5] National Fire Protection Association, NFPA 92B Guide for Smoke Management Systems in Malls , Atria , and Large Areas, (2000) 60.
- [6] H.P. Morgan, B.K. Ghosh, G. Garrad, R. Pamlichka, J.-C.D. Smedt, L.R. Schoonbaert, Design methodologies for smoke and heat exhaust ventilation, Building Research Establishment, Watford, 1999.
- [7] R. Harrison, M. Spearpoint, Smoke management issues in buildings with large enclosures, *Fire Aust.* (2006) 1–3.
- [8] P.. Hinkley, WORK BY THE FIRE RESEARCH STATION ON THE CONTROL OF SMOKE IN COVERED, 1975.
- [9] G.O. Hansell, H.P. Morgan, Design approaches for smoke control in atrium buildings, Borehamwood, 1994.
- [10] N.R. Marshall, S.Q. Feng, H.P. Morgan, The influence of a perforated false ceiling on the performance of smoke ventilation systems, *Fire Saf. J.* 8 (1985) 227–237. [https://doi.org/10.1016/0379-7112\(85\)90017-7](https://doi.org/10.1016/0379-7112(85)90017-7).
- [11] A. Morten, B. Persson, Experimental investigation of influence of porosity in suspended ceiling on smoke detection. Remarks on the effect of a porous suspended ceiling on smoke detector response, in: Department of Fire Safety Engineering. Lund University, Lund, 1994.
- [12] S. Isaksson, B. Persson, H. Tuovinen, CFD simulations of fire detection in a room with a perforated suspended ceiling.pdf, (1997).
- [13] S.C. Fiona, W.K. Tsue, N.K. Chow, Y. Fong, H. Gao, H. Dong, G.W. Zou, Experimental Room Fire Studies with Perforated Suspended Ceiling, in: International Association for Fire Safety Science, 2011: pp. 1235–1248.
- [14] H.P. Morgan, Smoke control methods in enclosed shopping centres of one or more storeys_design summary, 1979.
- [15] D. Adler, Metric Handbook Planning and Design Data, Second Edi, Reed Educational and Professional Publishing Ltd., 1999. <https://doi.org/10.5130/sj.v1i2.618>.
- [16] H.H. Hu, Chapter 10 - Computational Fluid Dynamics, Fifth Edit, Elsevier, 2012. <https://doi.org/10.1016/B978-0-12-382100-3.10010-1>.

- [17] K. McGrattan, S. Hostikka, R. McDermott, J. Floyd, C. Weinschenk, K. Overhold, Fire Dynamics Simulator User's Guide (FDS), NIST Spec. Publ. 1019. Sixth Edit (2019). <https://doi.org/10.6028/NIST.SP.1019>.
- [18] Thunderbird engineering, PyroSim User Manual, (2014). www.thunderheadeng.com.
- [19] G.P. Forney, Smokeview (Version 5) A Tool for Visualizing Fire Dynamics Simulation Data Volume I : User's Guide, I (2020) 162. <https://doi.org/10.6028/NIST.SP.1017-1>.
- [20] G.H. Yeoh, K.K. Yuen, Advance Technique in Field Modeling, in: Comput. Fluid Dyn. Fire Eng., Butterworth-Heinemann, 2009: pp. 367–423.
- [21] BSI, PD 7974-1 : 2019 BSI Standards Publication. Application of fire safety engineering principles to the design of buildings, 2019.
- [22] W. Węgrzyński, G. Vigne, Experimental and numerical evaluation of the influence of the soot yield on the visibility in smoke in CFD analysis, Fire Saf. J. 91 (2017) 389–398. <https://doi.org/10.1016/j.firesaf.2017.03.053>.
- [23] M.J. Hurley, D. Gottuk, J.R. Hall, K. Harada, E. Kuligowski, M. Puchovsky, J. Torero, Jj.M. Watts, C. Wieczorek, SFPE handbook of fire protection engineering, fifth edition, 2016. <https://doi.org/10.1007/978-1-4939-2565-0>.
- [24] K. McGrattan, S. Hostikka, J. Floyd, R. McDermott, M. Vanella, Fire Dynamics Simulator Technical Reference Guide Volume 3: Validation, 3 (2019). <http://dx.doi.org/10.6028/NIST.SP.1018>.
- [25] R. Sinclair, CFD Simulation in Atrium Smoke Management System Design, ASHRAE Winter Meet. CD, Tech. Symp. Pap. (2001) 843–850.
- [26] B. Karlsson, J. Quintiere, Enclosure Fire Dynamics, 1999. <https://doi.org/10.1201/9781420050219>.
- [27] D. Drysdale, An Introduction to Fire Dynamics: Third Edition, 2011. <https://doi.org/10.1002/9781119975465>.
- [28] P. Van Hees, Validation and verification of fire models for fire safety engineering, Procedia Eng. 62 (2013) 154–168. <https://doi.org/10.1016/j.proeng.2013.08.052>.

6 Appendix A: Slice files from all test runs

Table 16. Temperature, velocity, and visibility scales for the following tables of horizontal and vertical planes.

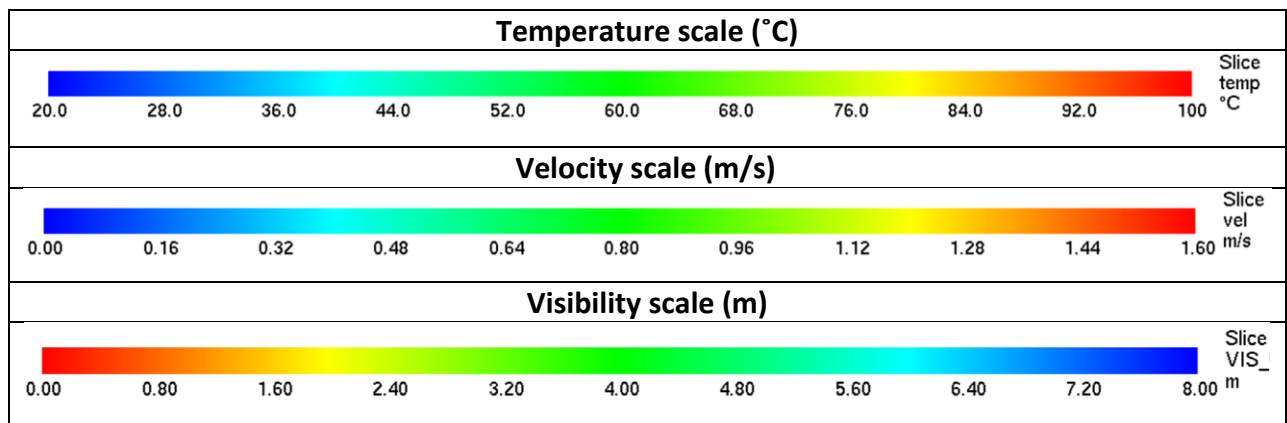


Table 17. Temperature slices at various locations with truncated temperatures below 30°C for 2 MW fire. Time-averaged steady-state results (50 s. of the averaging period). Slice cut is at 2.5 m on the X-axis. Blackline on the temperature slices is false ceiling locations. Colour bar scale is given in Table 16

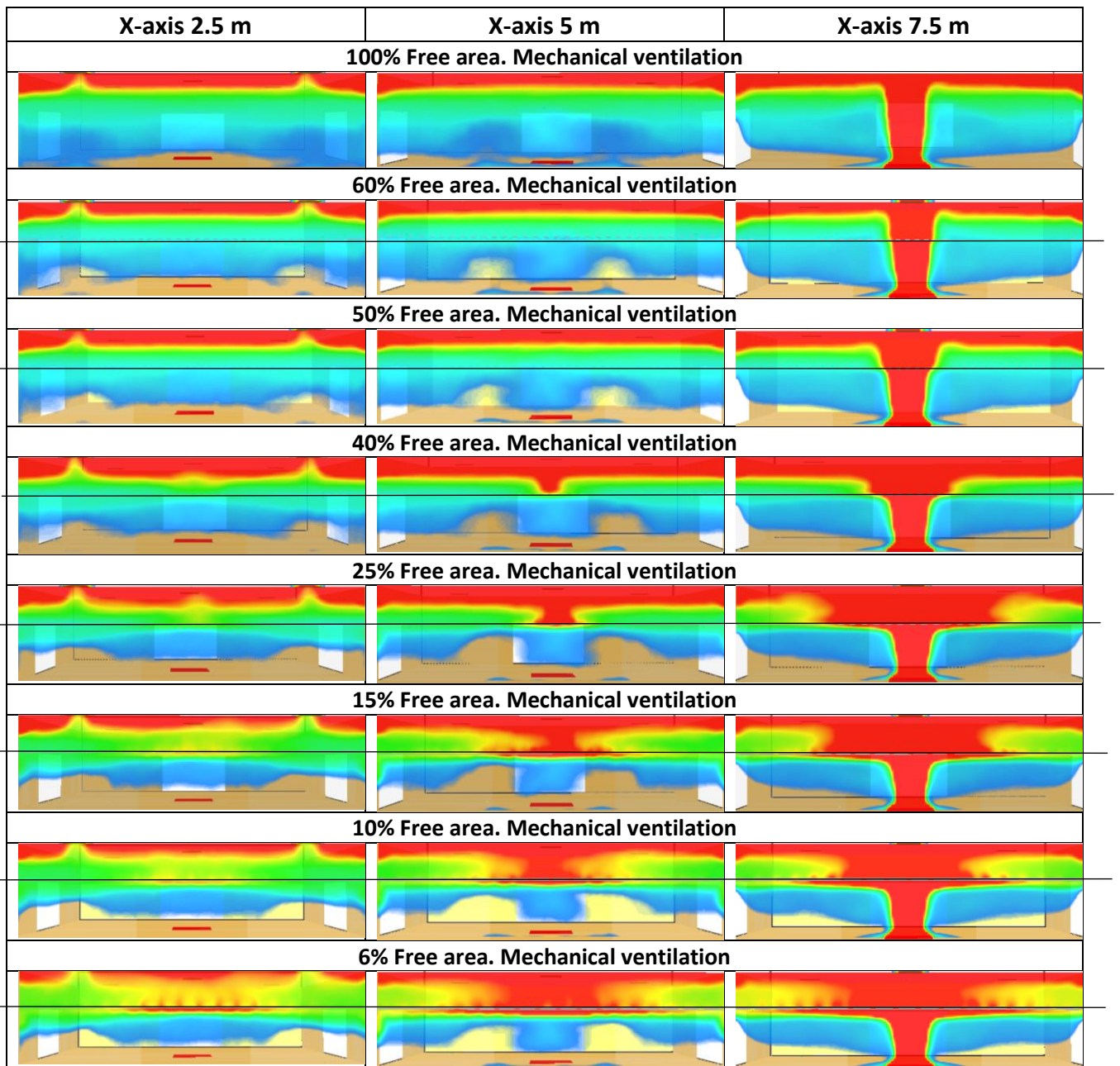
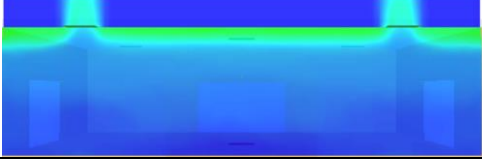
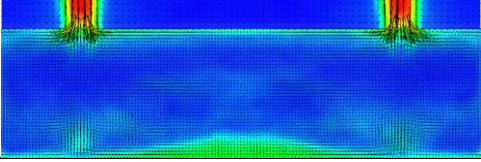
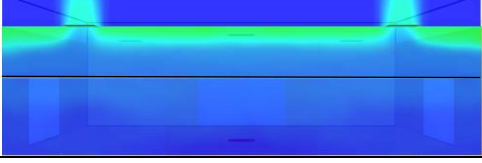
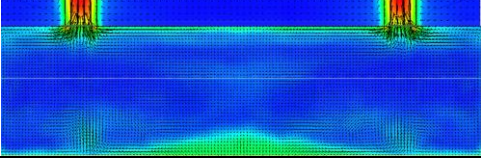
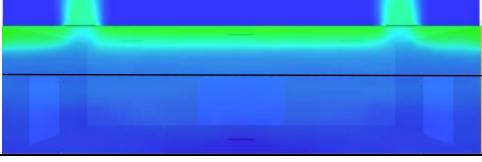
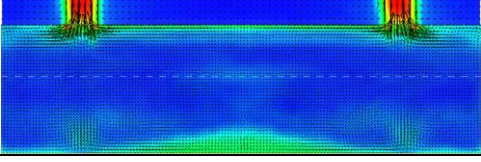
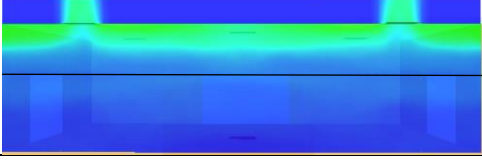
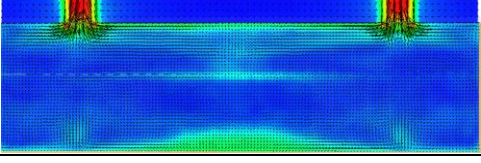
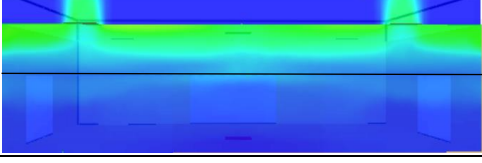
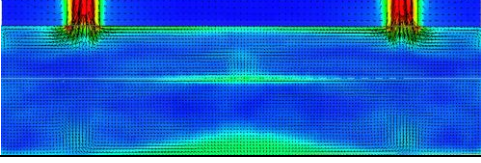
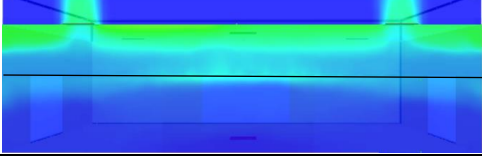
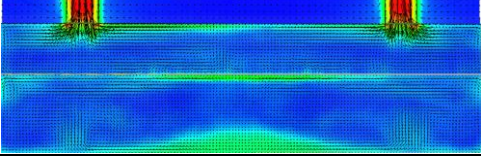
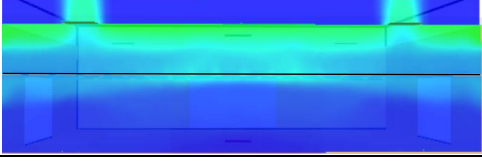
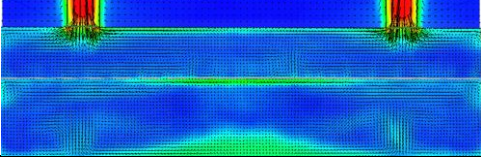
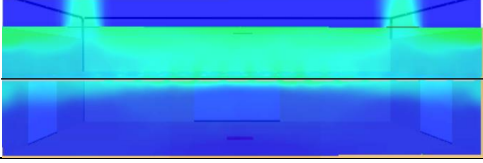
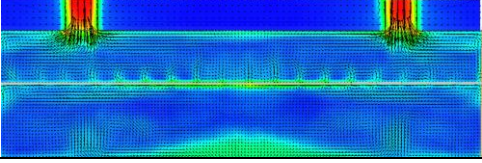


Table 18. Temperature and velocity fields of perforated false ceilings for 500 kW design fire. Time-averaged steady-state results (50 s. of the averaging period). Slice cut is at 2.5 m on the X-axis. The black line on the temperature slices is false ceiling

Temperature slice	Velocity vector slice
100% Free area	
	
60% Free area	
	
50% Free area	
	
40% Free area	
	
25% Free area	
	
15% Free area	
	
10% Free area	
	
6% Free area	
	

locations. Colour bar scale is given in Table 16

Table 19. Temperature and velocity fields of perforated false ceilings for 500 kW design fire. Time-averaged steady-state results (50 s. of the averaging period). Slice cut is at the middle of the fire source ($X=7.5$ m). A black line on the temperature slices is false ceiling locations. Colour bar scale is given in Table 16

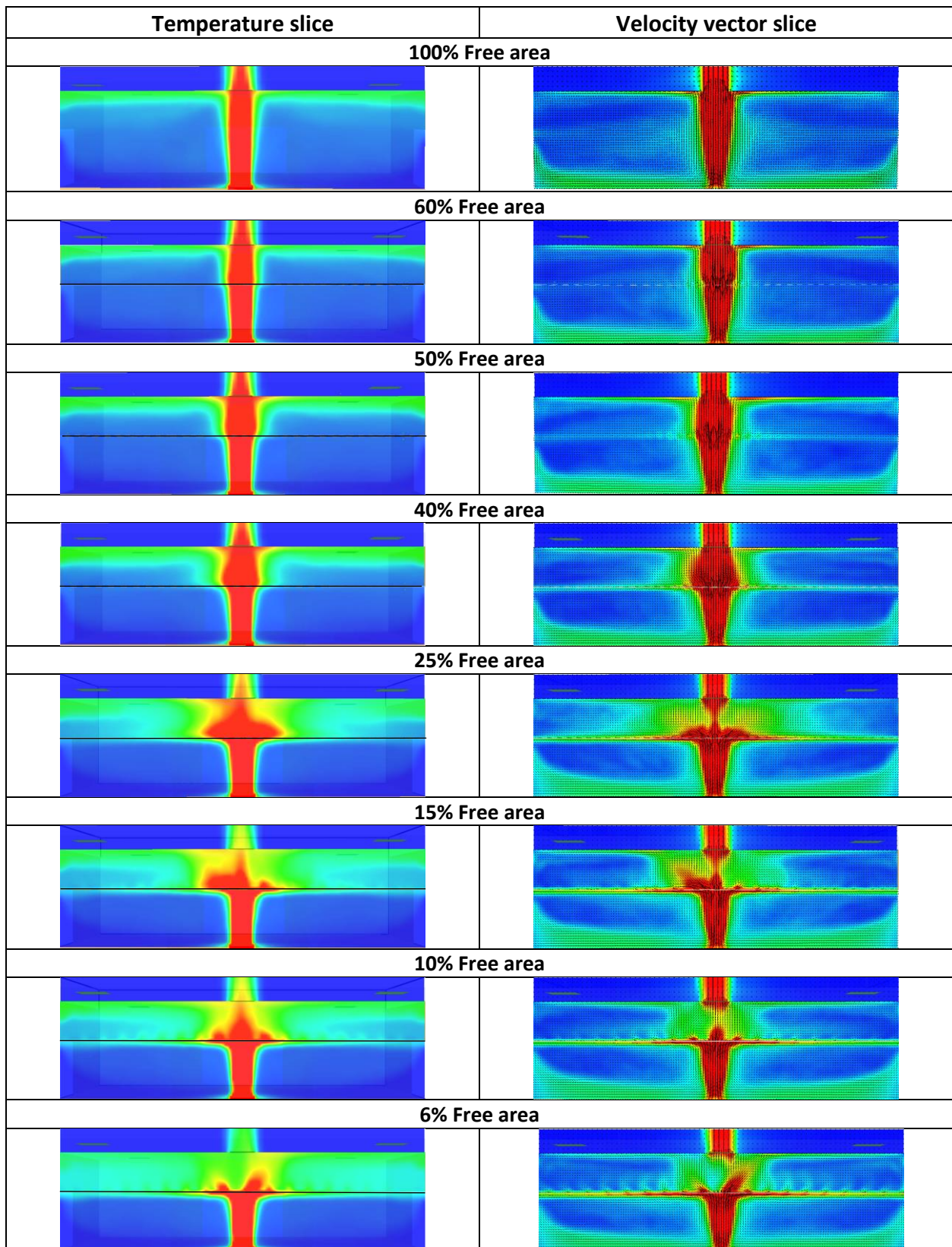


Table 20. The temperature on horizontal fields at 2.0, 2.3, 2.5, and 3.0 m heights for perforated false ceilings with 500 kW design fire. Time-averaged steady-state results (50 s. of the averaging period). Colour bar scale is given in Table 16

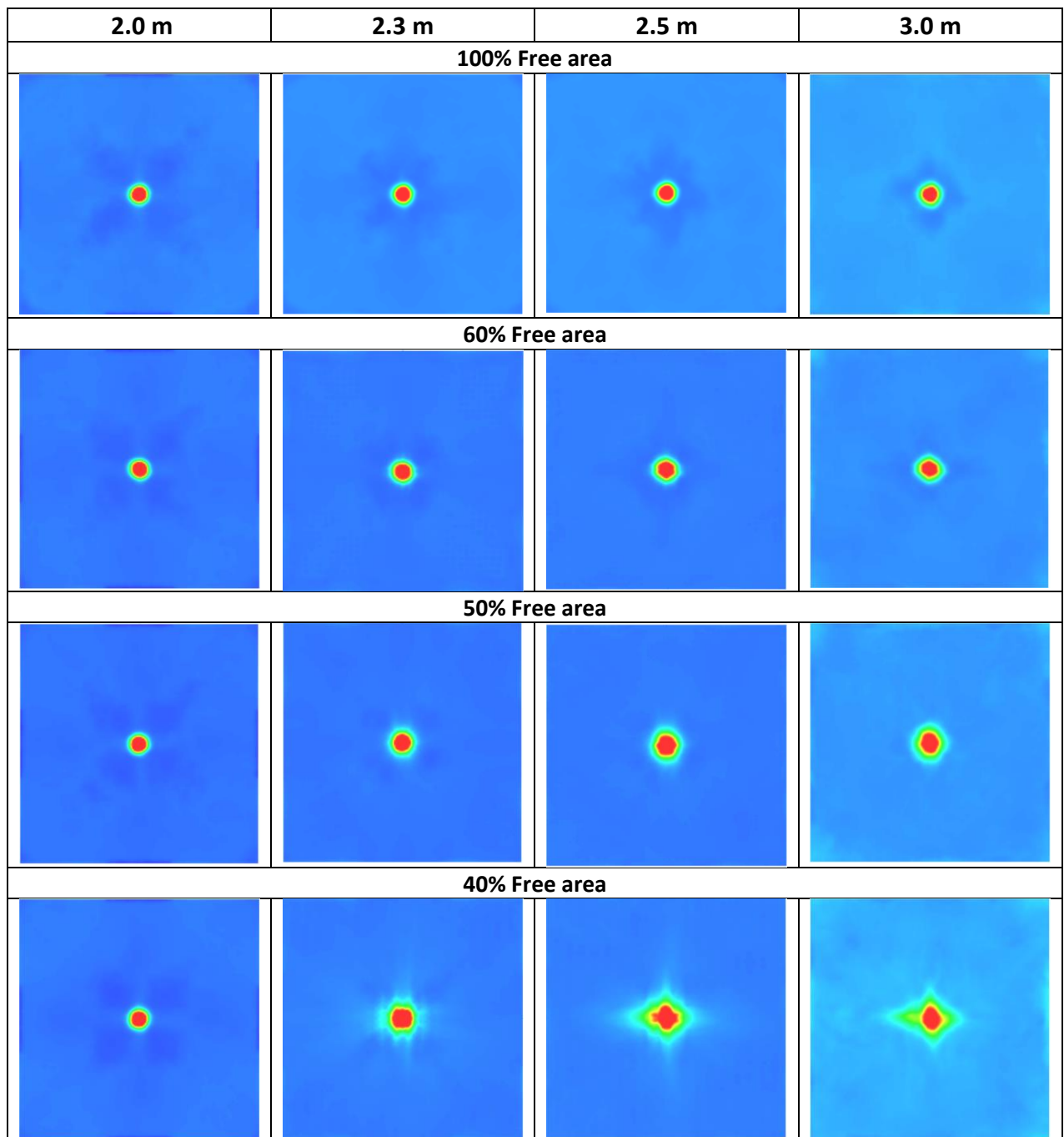


Table 20 (Continued). The temperature on horizontal fields at 2.0, 2.3, 2.5, and 3.0 m heights for perforated false ceilings with 500 kW design fire. Time-averaged steady-state results (50 s. of the averaging period). Colour bar scale is given in Table 16

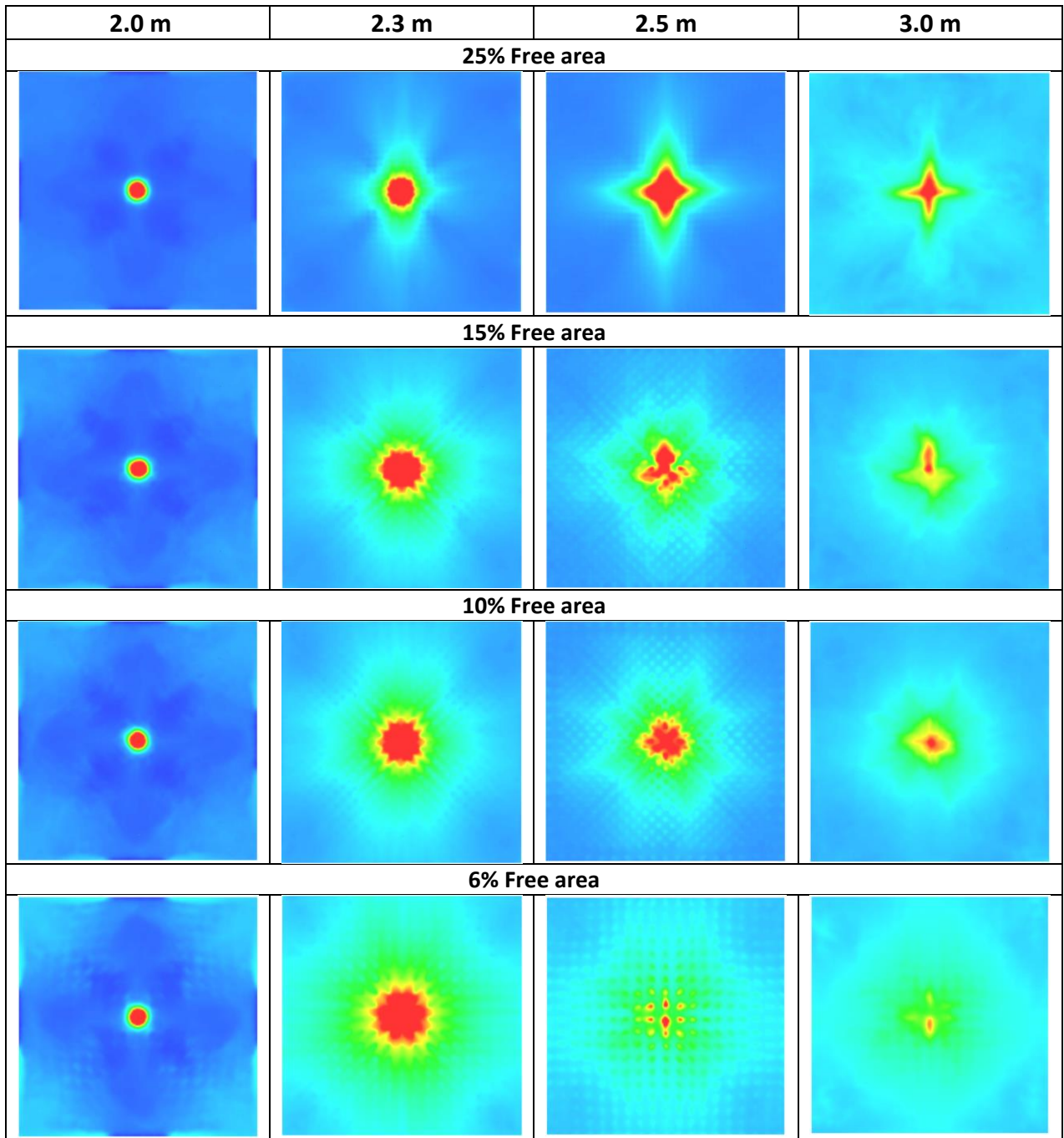


Table 21. Temperature and velocity fields of perforated false ceilings for 2 MW design fire. Time-averaged steady-state results (50 s. of the averaging period). Slice cut is at 2.5 m on the X-axis. Blackline on the temperature slices is false ceiling locations. Colour bar scale is given in Table 16

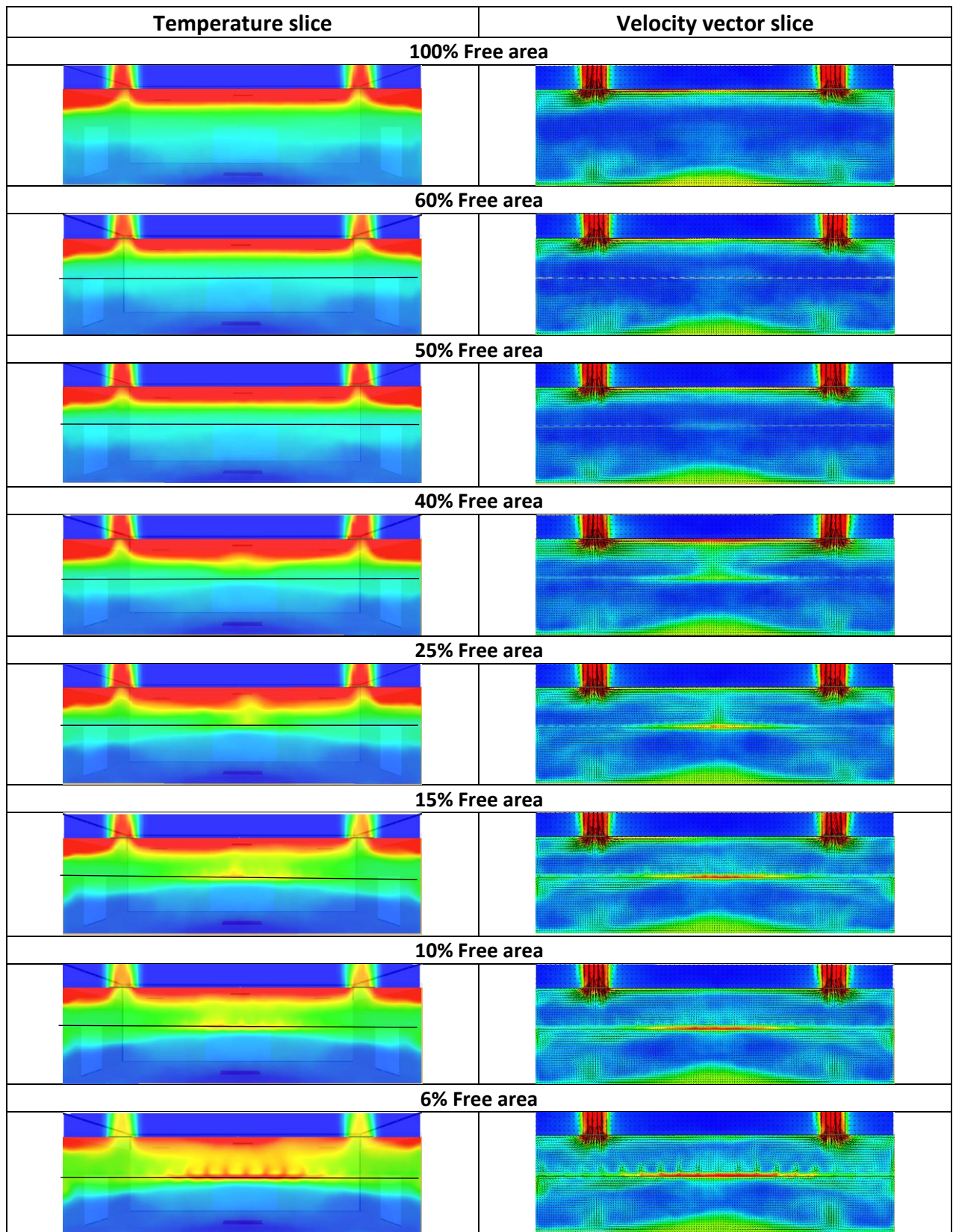


Table 22. Temperature and velocity fields of perforated false ceilings for 2 MW design fire. Time-averaged steady-state results (50 s. of the averaging period). Slice cut is at the middle of the fire source ($X=7.5$ m). Blackline on the temperature slices is false ceiling locations. Colour bar scale is given in Table 16

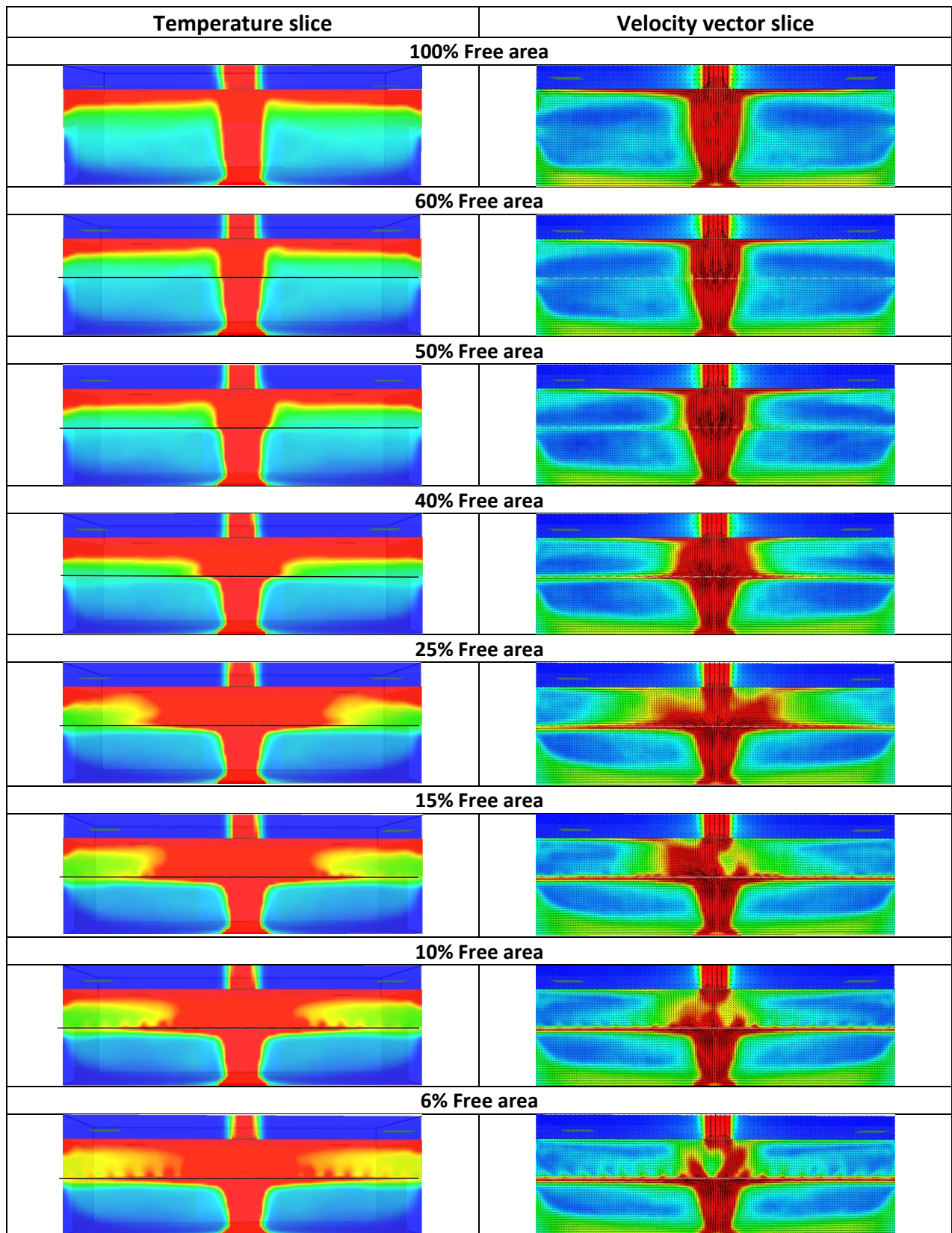


Table 23. The temperature on horizontal fields at 2.0, 2.3, 2.5, and 3.0 m heights for perforated false ceilings with 2 MW design fire. Time-averaged steady-state results (50 s. of the averaging period). Colour bar scale is given in Table 16

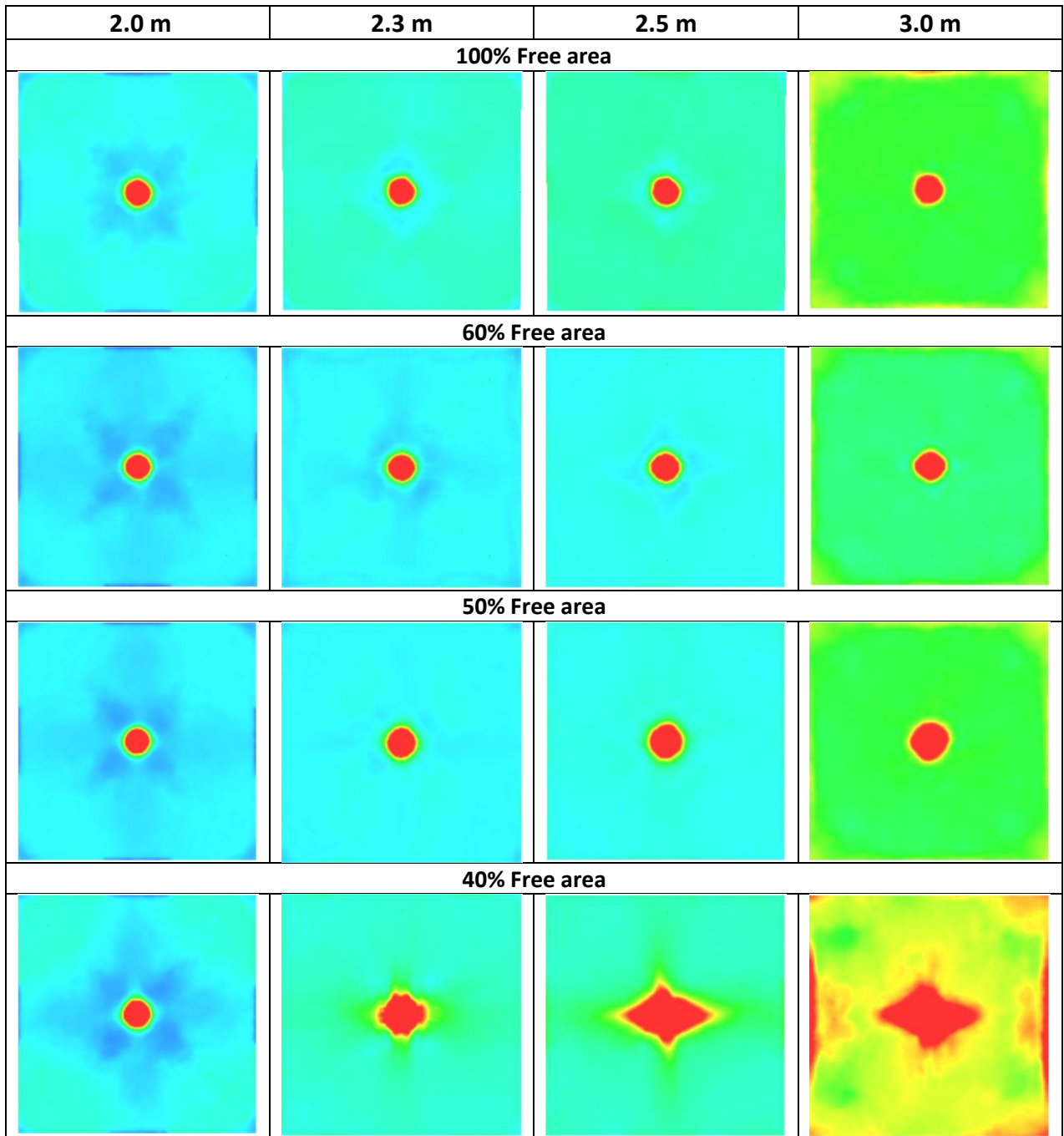


Table 23 (Continued). The temperature on horizontal fields at 2.0, 2.3, 2.5, and 3.0 m heights for perforated false ceilings with 2 MW design fire. Time-averaged steady-state results (50 s. of the averaging period). Colour bar scale is given in Table 16

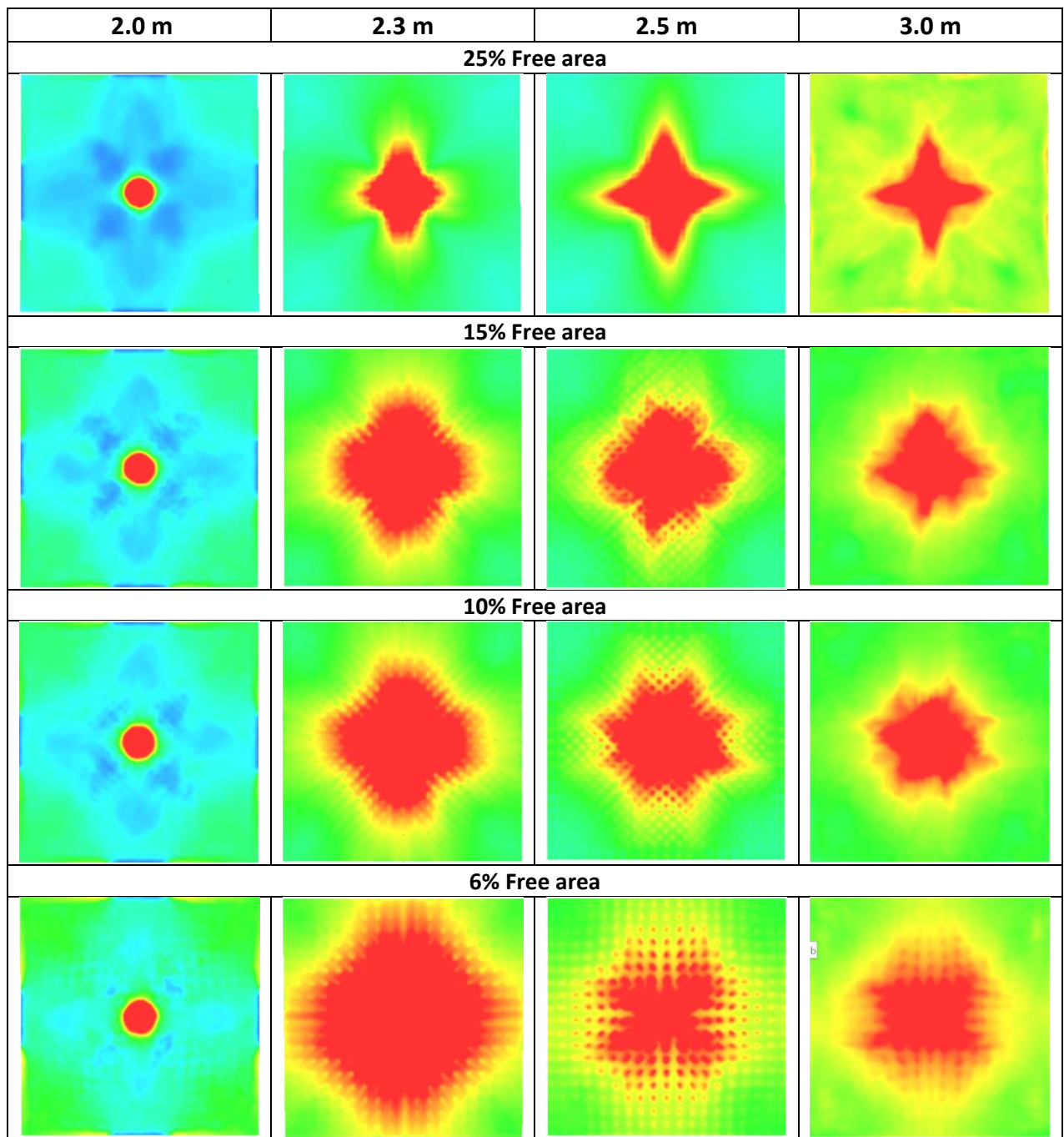


Table 24. Visibility on horizontal fields at 2.0, 2.3, 2.5 m heights for perforated false ceilings with 500 kW design fire. Time-averaged steady-state results (50 s. of the averaging period). Colour bar scale is given in Table 16

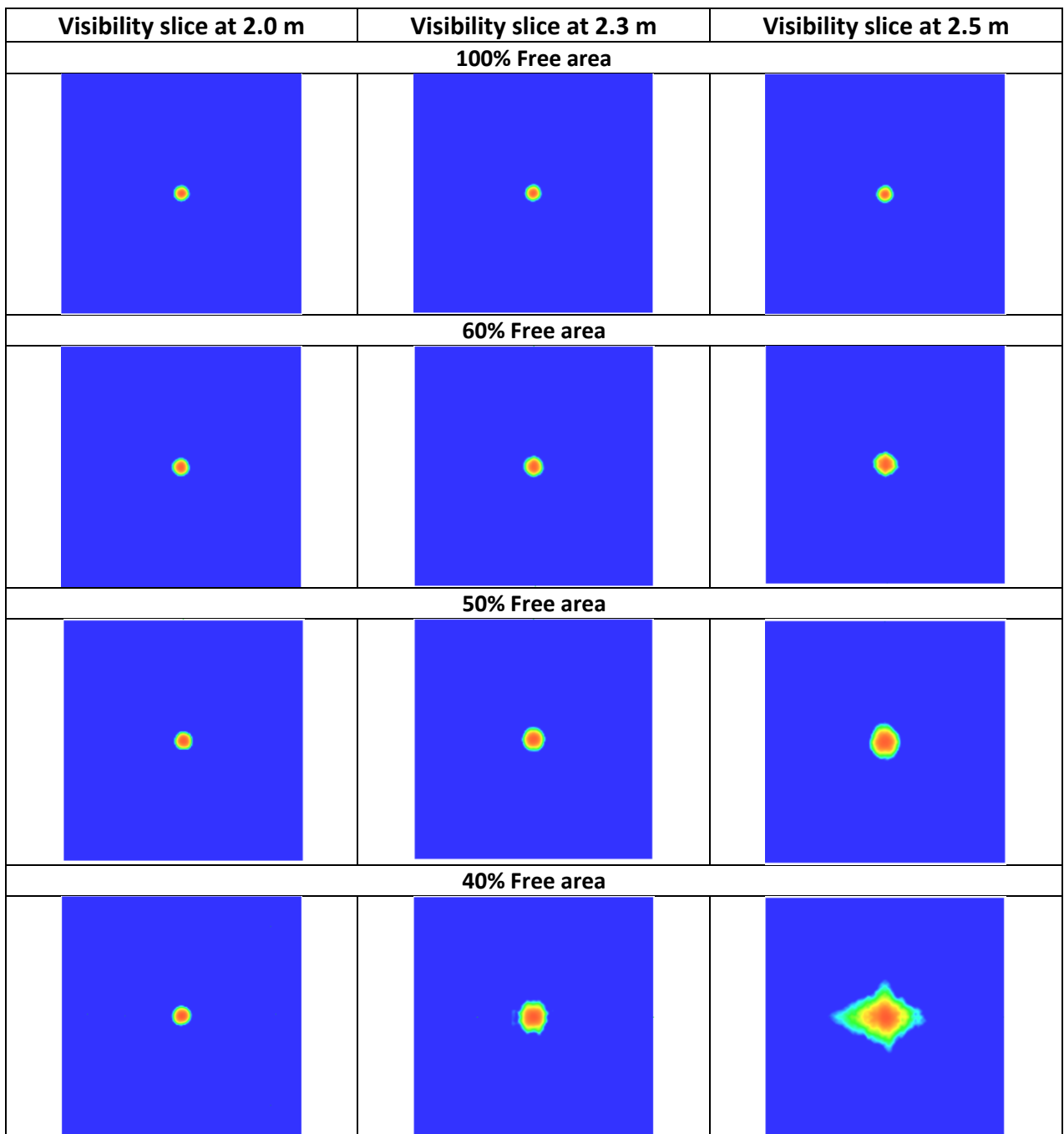


Table 24 (Continued). Visibility on horizontal fields at 2.0, 2.3, 2.5 m heights for perforated false ceilings with 500 kW design fire. Time-averaged steady-state results (50 s. of the averaging period). Colour bar scale is given in Table 16

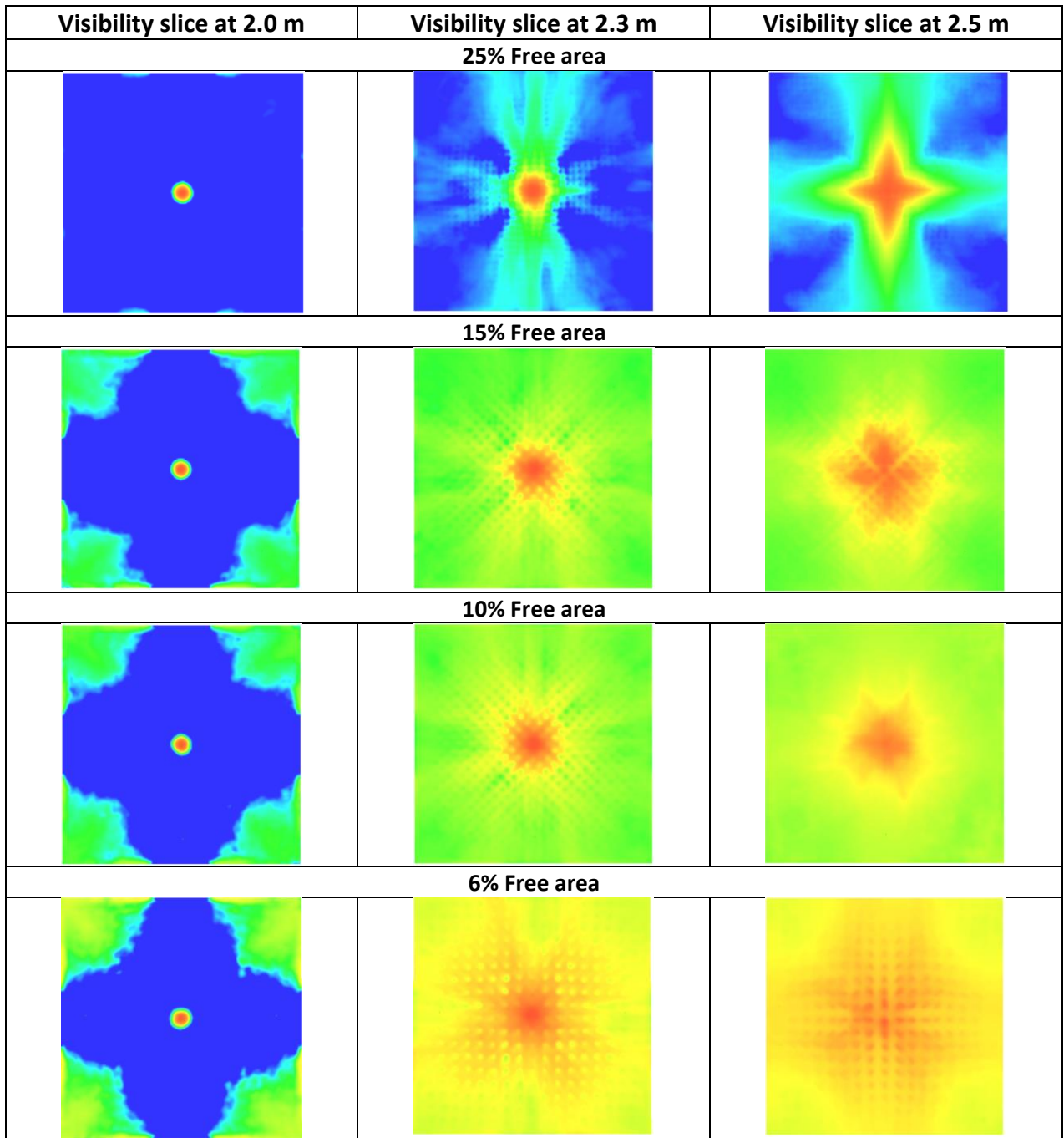


Table 25. Visibility on horizontal fields at 2.0, 2.3, 2.5 m heights for perforated false ceilings with 2 MW design fire. Time-averaged steady-state results (50 s. of the averaging period). Colour bar scale is given in Table 16

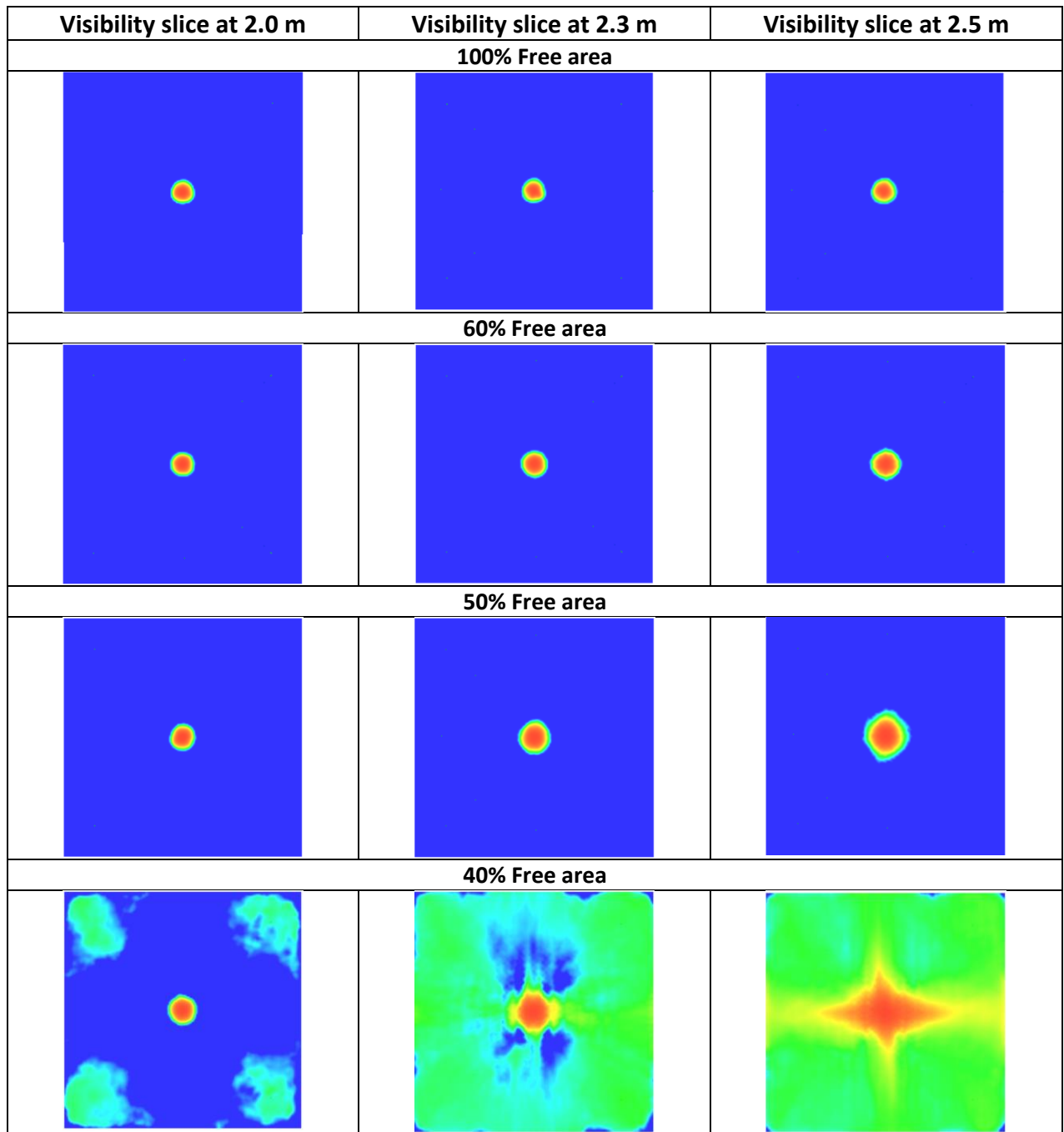


Table 25 (Continued). Visibility on horizontal fields at 2.0, 2.3, 2.5 m heights for perforated false ceilings with 2 MW design fire. Time-averaged steady-state results (50 s. of the averaging period). Colour bar scale is given in Table 16

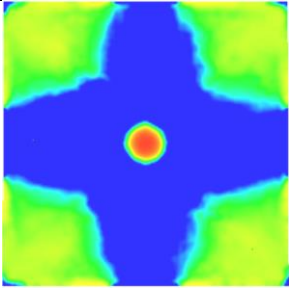
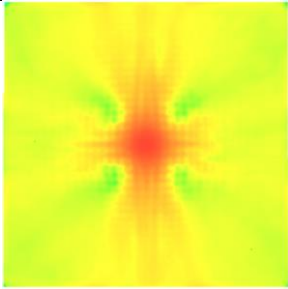
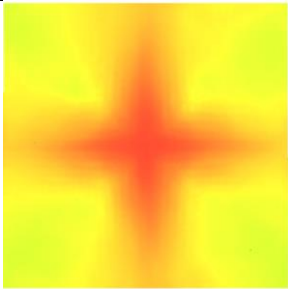
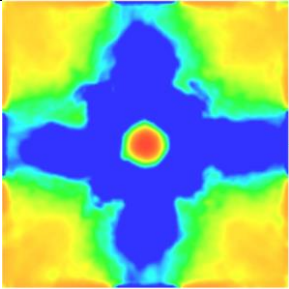
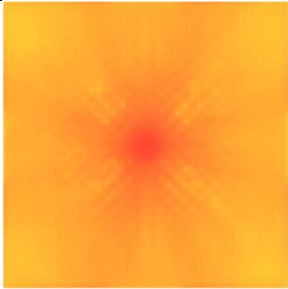

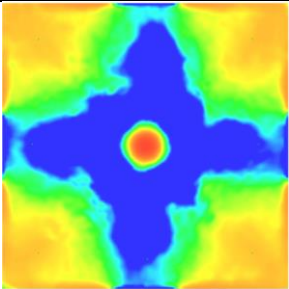
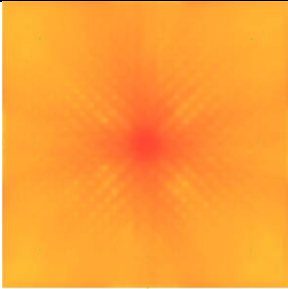

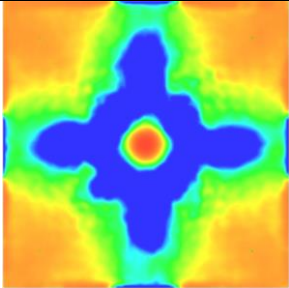
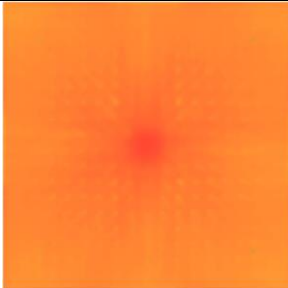
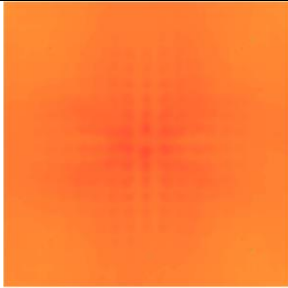
Visibility slice at 2.0 m	Visibility slice at 2.3 m	Visibility slice at 2.5 m
25% Free area		
		
15% Free area		
		
10% Free area		
		
6% Free area		
		

Table 26. Velocity vector slices at 1.5 m and 2.2 m for 50, 40, 25, 15% for 2 MW fire. Time-averaged steady-state results (50 s. of the averaging period). Colour bar scale is given in Table 16

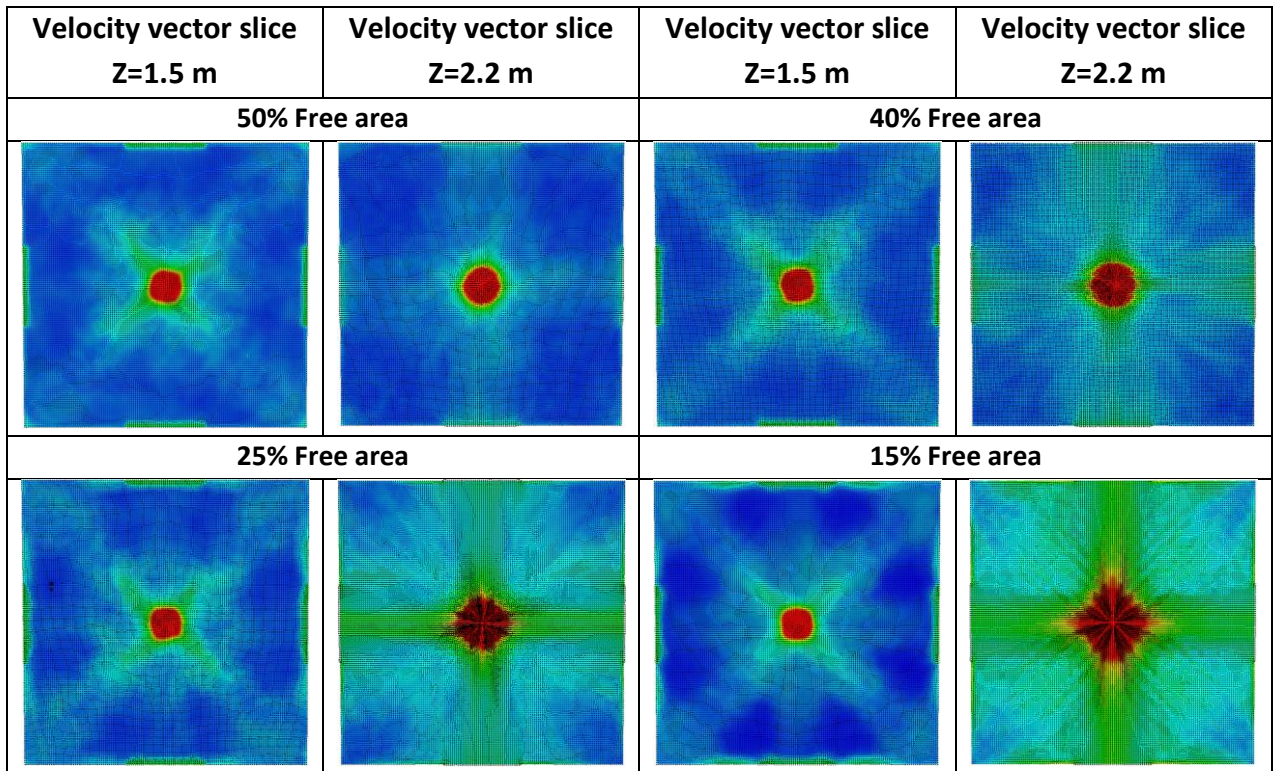


Table 27. Temperature and velocity fields of uneven openings in the false ceilings for relative openness of 40% (2 MW design fire). Time-averaged steady-state results (50 s. of the averaging period). Slice cut is at 2.5 m on the Y-axis. The black line on the temperature slices is false ceiling locations. Colour bar scale is given in Table 16

Temperature slice	Velocity vector slice
40% Free area. EVEN perforation.	
40% Free area UNEVEN openings. Design #1	
40% Free area UNEVEN openings. Design #2	
40% Free area UNEVEN openings. Design #3	
40% Free area UNEVEN openings. Design #4	
40% Free area UNEVEN openings. Design #5	
40% Free area UNEVEN openings. Design #6	
40% Free area UNEVEN openings. Design #7	

Table 28. Temperature and velocity fields of uneven openings in the false ceilings for relative openness of 40% (2 MW design fire). Time-averaged steady-state results (50 s. of the averaging period). Slice cut is at 7.5 m on the Y-axis. The black line on the temperature slices is false ceiling locations. Colour bar scale is given in Table 16

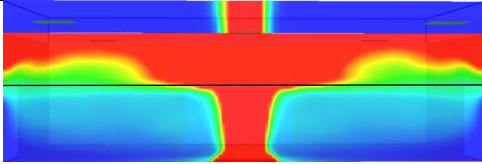
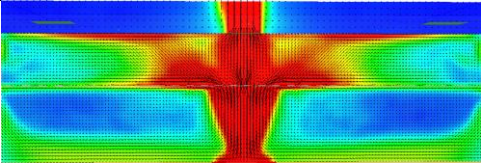
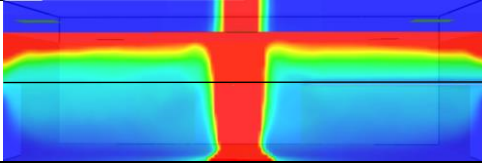
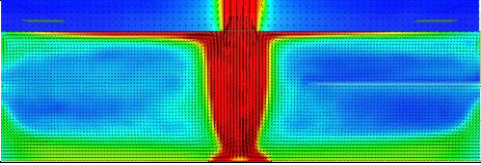
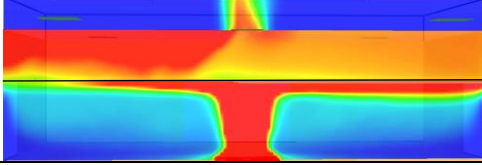
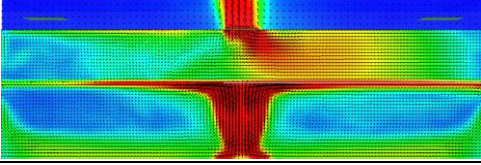
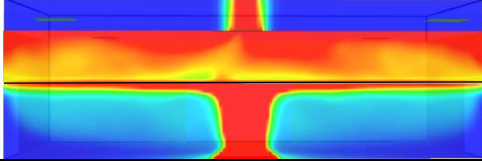
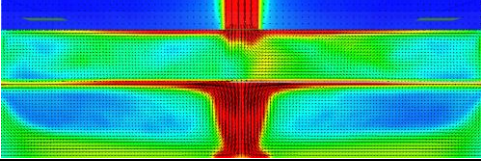
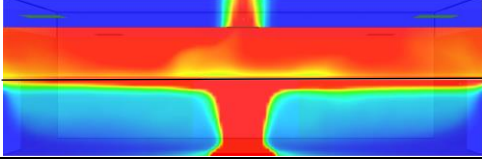
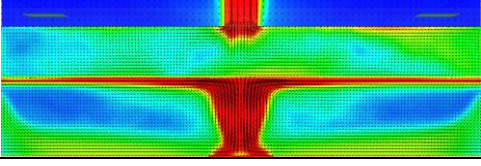
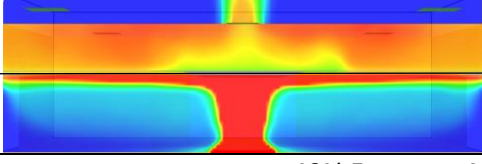
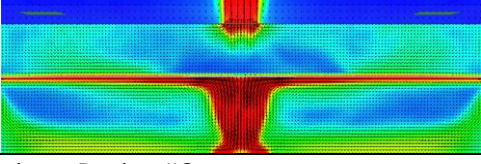
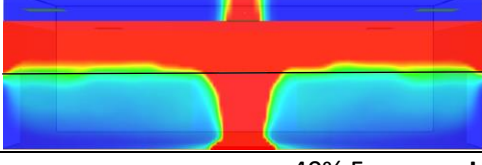
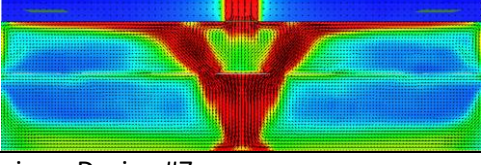
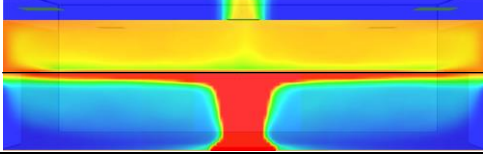
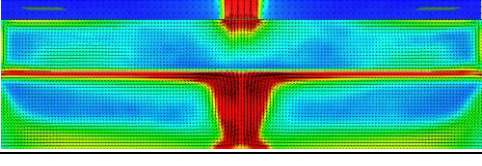
Temperature slice	Velocity vector slice
40% Free area. EVEN perforation.	
	
40% Free area UNEVEN openings. Design #1	
	
40% Free area UNEVEN openings. Design #2	
	
40% Free area UNEVEN openings. Design #3	
	
40% Free area UNEVEN openings. Design #4	
	
40% Free area UNEVEN openings. Design #5	
	
40% Free area UNEVEN openings. Design #6	
	
40% Free area UNEVEN openings. Design #7	
	

Table 29. Temperature and velocity fields of uneven openings in the false ceilings for relative openness of 25%. Time-averaged steady-state results (50 s. of the averaging period). Slice cut is at 2.5 m on the Y-axis. The black line on the temperature slices is false ceiling locations. Colour bar scale is given in Table 16

Temperature slice	Velocity vector slice
25% Free area. EVEN perforation.	
25% Free area UNEVEN openings. Design #1	
25% Free area UNEVEN openings. Design #2	
25% Free area UNEVEN openings. Design #3	
25% Free area UNEVEN openings. Design #4	
25% Free area UNEVEN openings. Design #5	
25% Free area UNEVEN openings. Design #6	
25% Free area UNEVEN openings. Design #7	

Table 29 (Continued). Temperature and velocity fields of uneven openings in the false ceilings for relative openness of 25%. Time-averaged steady-state results (50 s. of the averaging period). Slice cut is at 2.5 m on the Y-axis. The black line on the temperature slices is false ceiling locations. Colour bar scale is given in Table 16

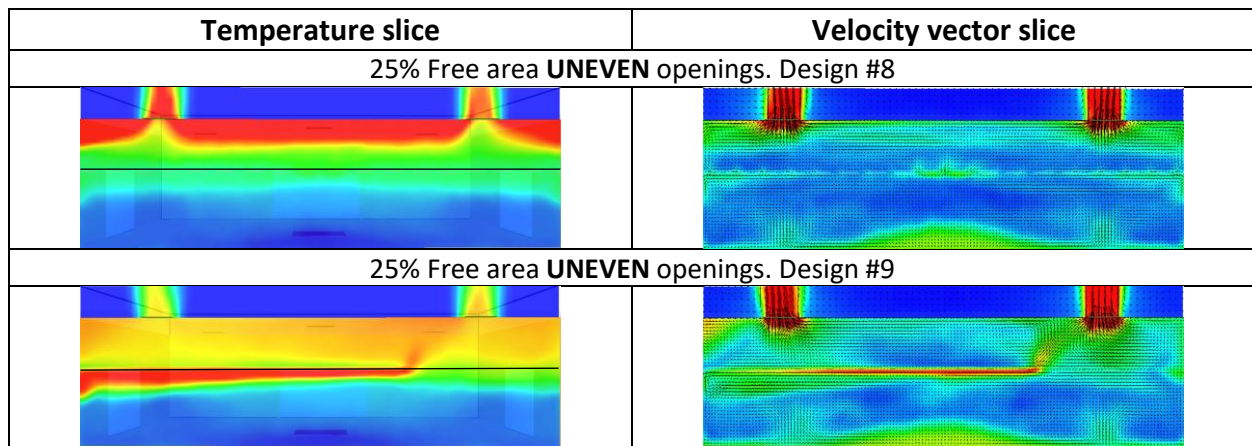


Table 30. Temperature and velocity fields of uneven openings in the false ceilings for relative openness of 25%. Time-averaged steady-state results (50 s. of the averaging period). Slice cut is at 7.5 m on the Y-axis. The black line on the temperature slices is false ceiling locations. Colour bar scale is given in Table 16

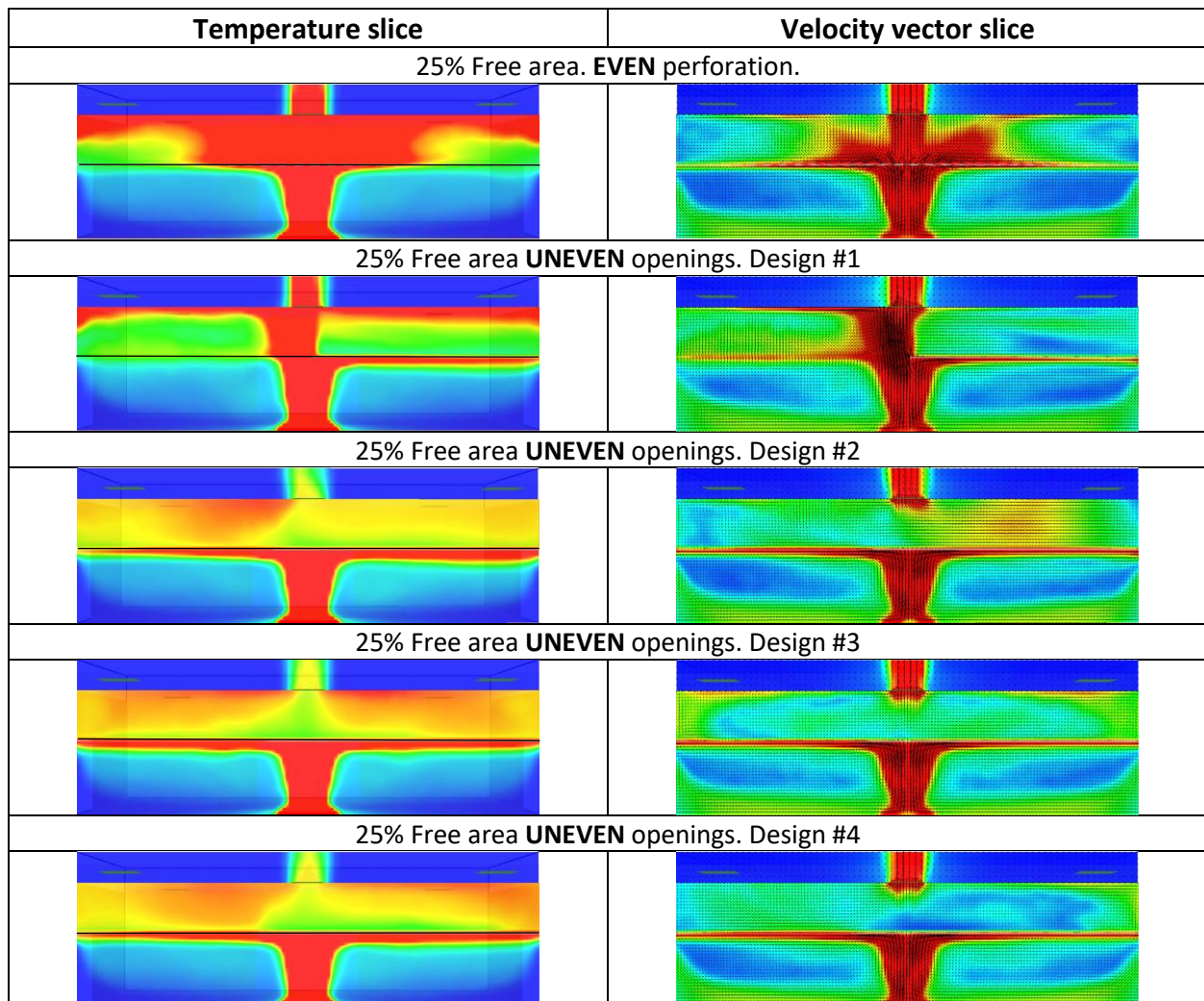


Table 30 (Continued). Temperature and velocity fields of uneven openings in the false ceilings for relative openness of 25%. Time-averaged steady-state results (50 s. of the averaging period). Slice cut is at 7.5 m on the Y-axis. The black line on the temperature slices is false ceiling locations. Colour bar scale is given in Table 16

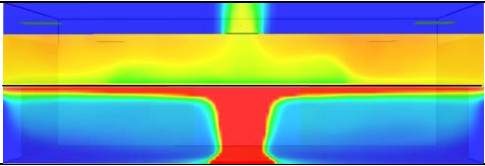
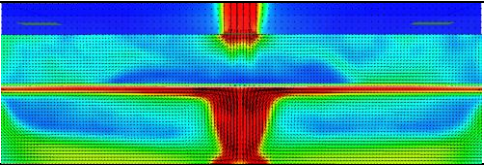
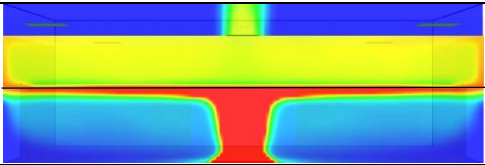
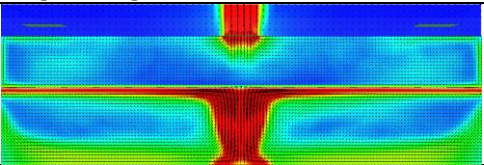
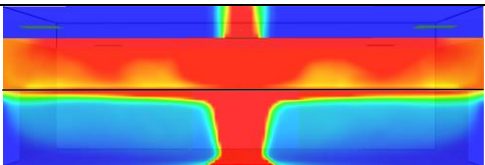
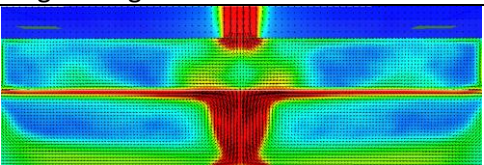
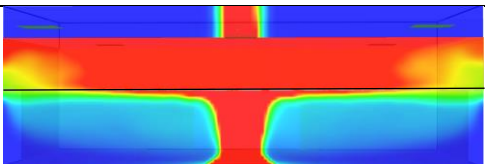
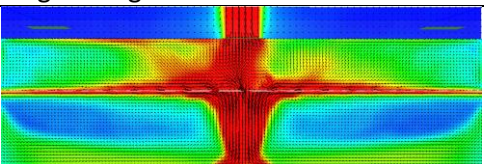
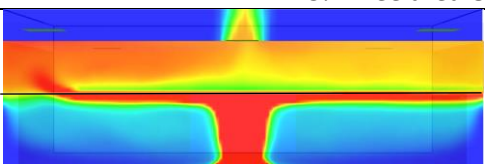
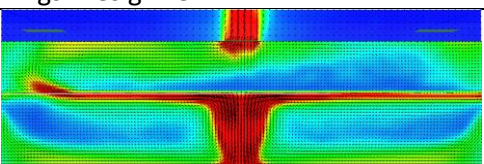
Temperature slice	Velocity vector slice
25% Free area UNEVEN openings. Design #5	
	
25% Free area UNEVEN openings. Design #6	
	
25% Free area UNEVEN openings. Design #7	
	
25% Free area UNEVEN openings. Design #8	
	
25% Free area UNEVEN openings. Design #9	
	

Table 31. The temperature on horizontal fields at 2.0, 2.3, 2.5, and 3.0 m height for uneven openings in the false ceilings for relative openness of 40%. Time-averaged steady-state results (50 s. of the averaging period). Colour bar scale is given in Table 16

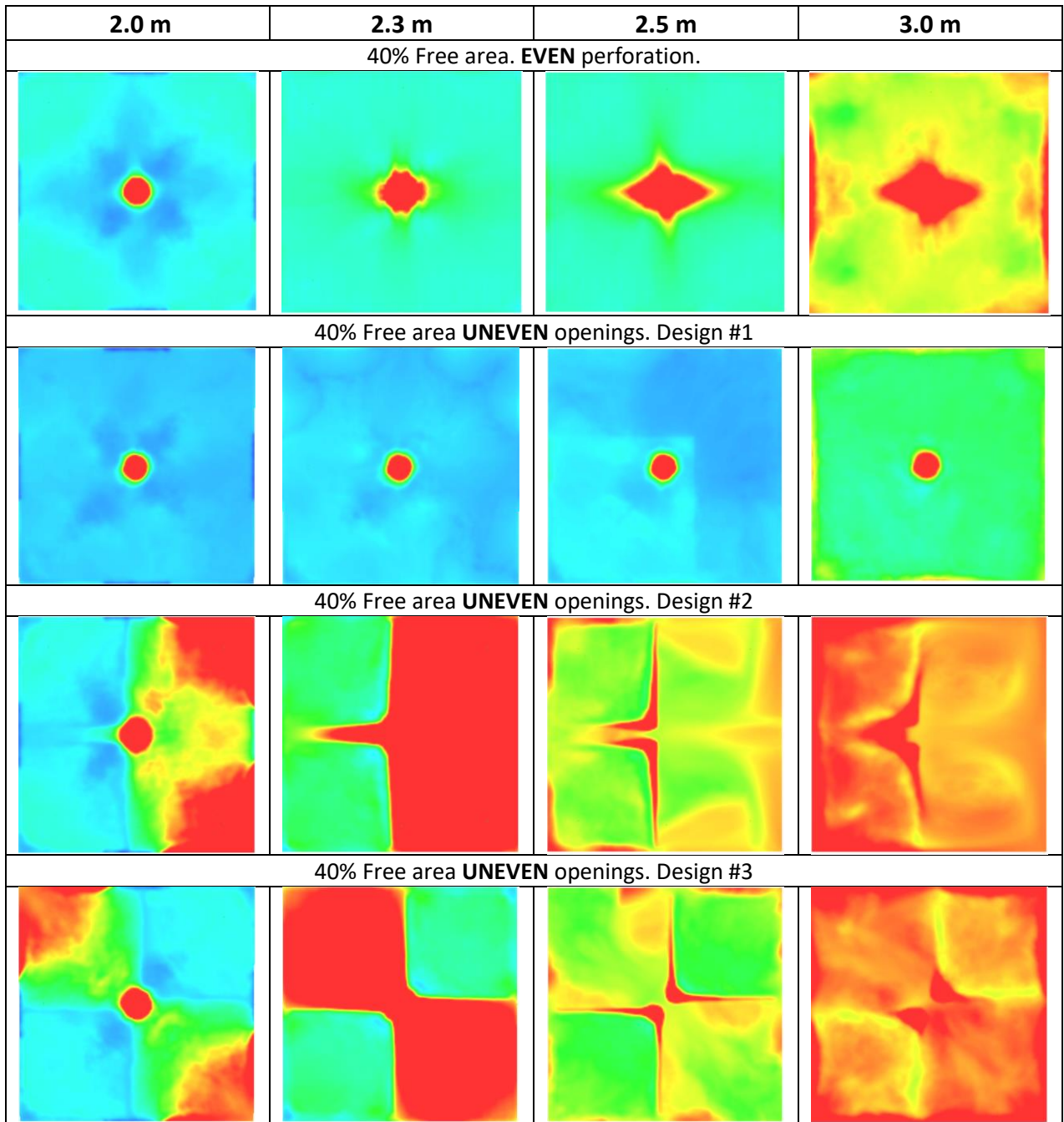


Table 31 (Continued). The temperature on horizontal fields at 2.0, 2.3, 2.5, and 3.0 m height for uneven openings in the false ceilings for relative openness of 40%. Time-averaged steady-state results (50 s. of the averaging period). Colour bar scale is given in Table 16

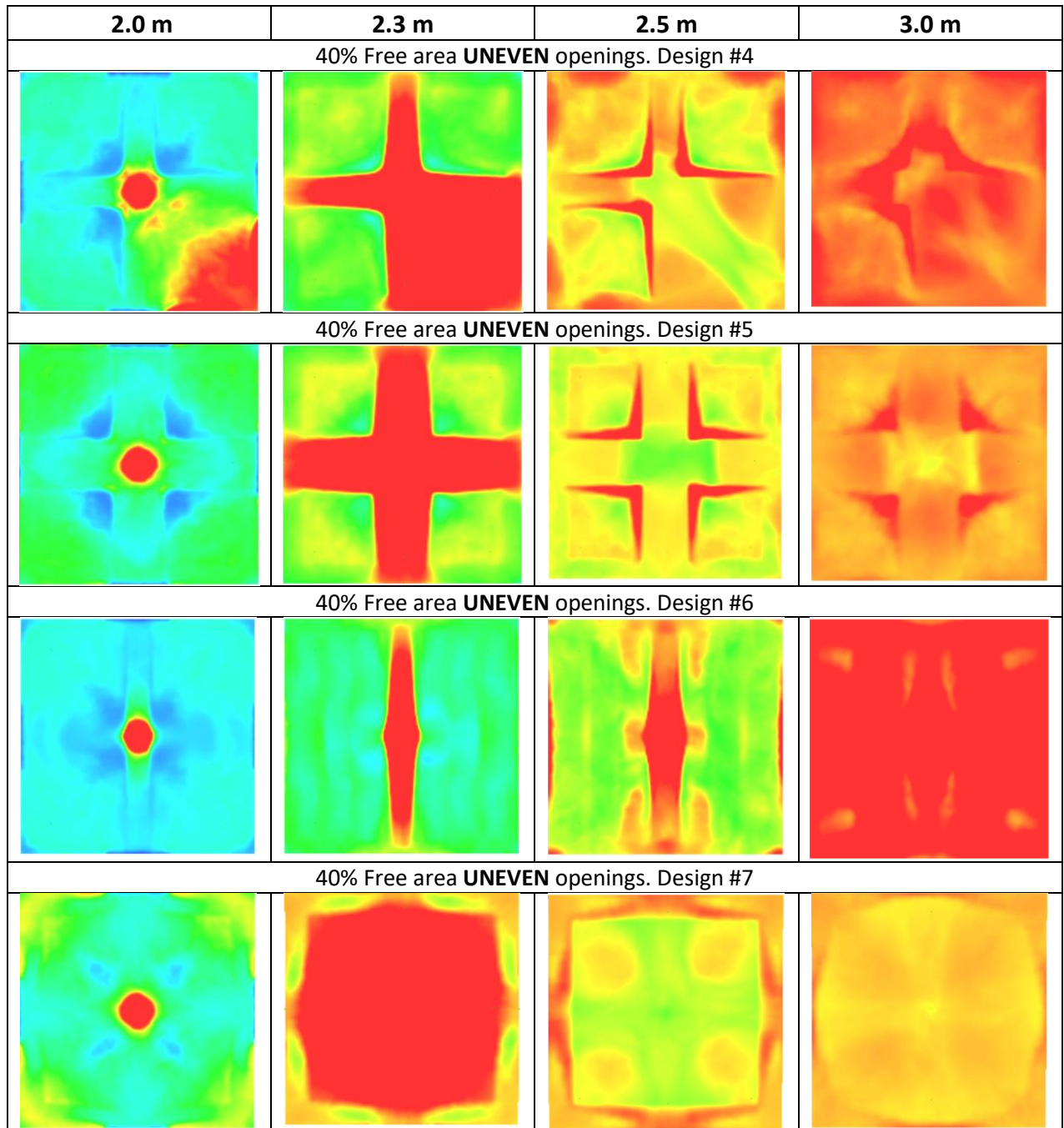


Table 32. The temperature on horizontal fields at 2.0, 2.3, 2.5, and 3.0 m height for 25% uneven openings in the false ceilings. Time-averaged steady-state results (50 s. of the averaging period). Colour bar scale is given in Table 16

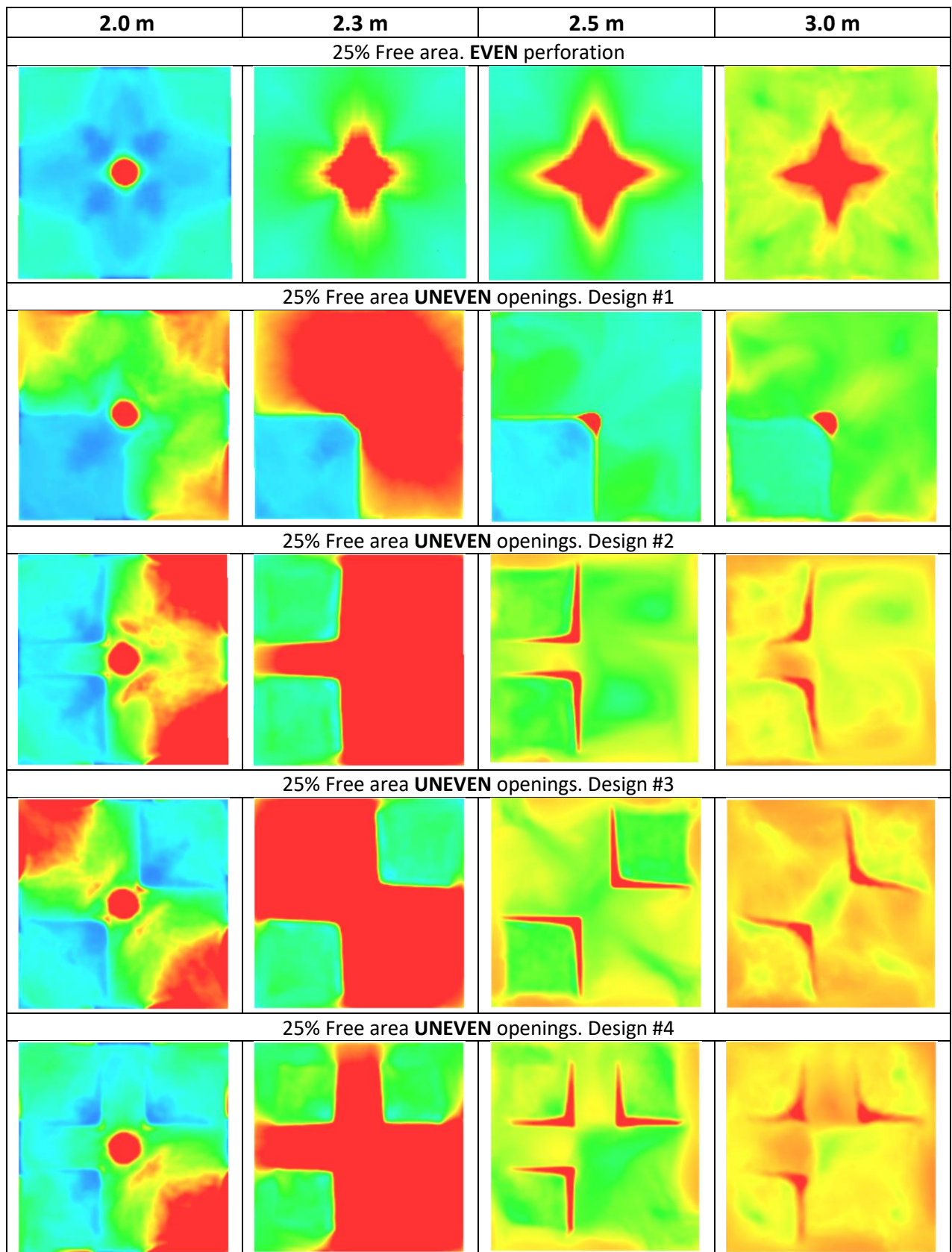


Table 32 (Continued). The temperature on horizontal fields at 2.0, 2.3, 2.5, and 3.0 m height for 25% uneven openings in the false ceilings. Time-averaged steady-state results (50 s. of the averaging period). Colour bar scale is given in Table 16

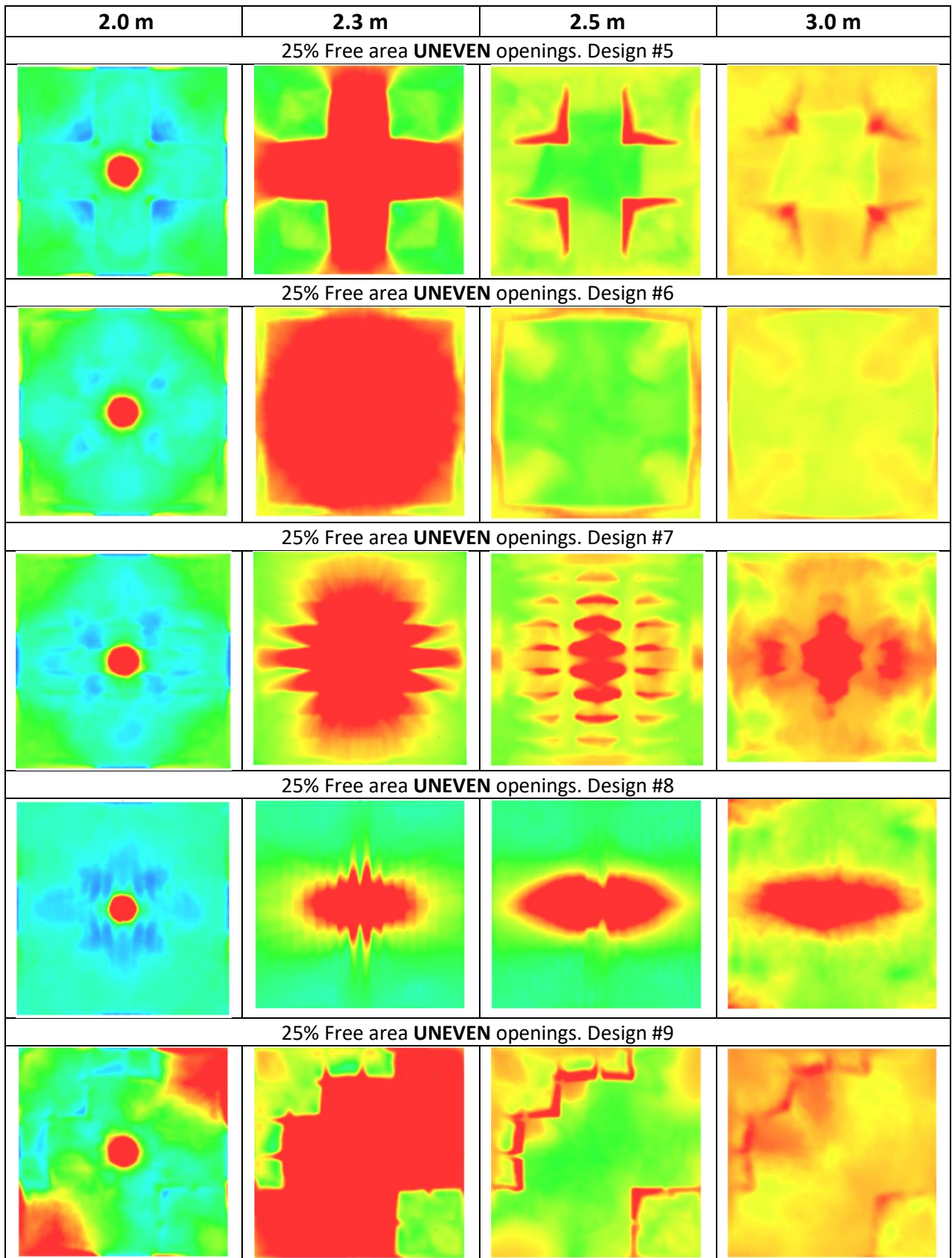


Table 33. Visibility on horizontal fields at 2.0, 2.3, and 2.5 m height for uneven openings in the false ceilings for relative openness of 40%. Time-averaged steady-state results (50 s. of the averaging period). Colour bar scale is given in Table 16

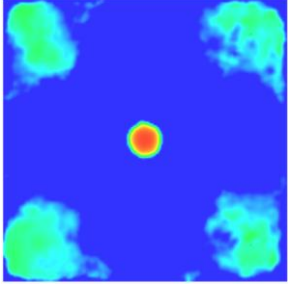
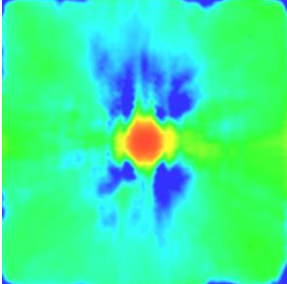
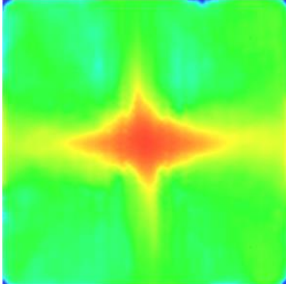
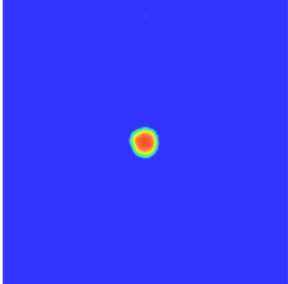
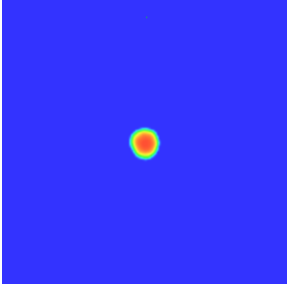
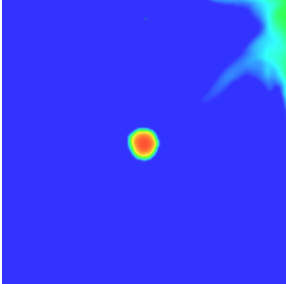
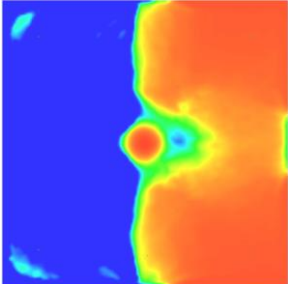
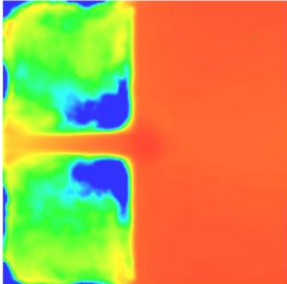
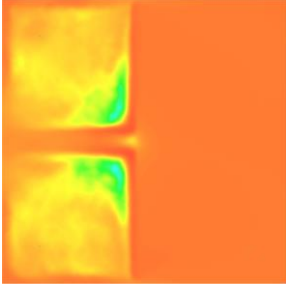
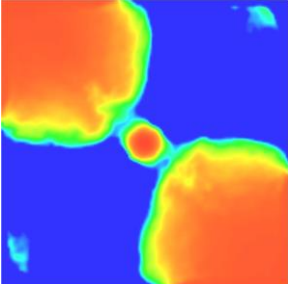
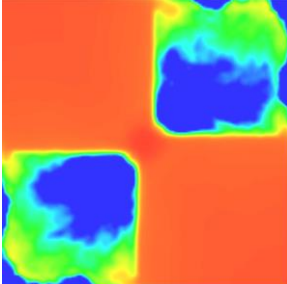
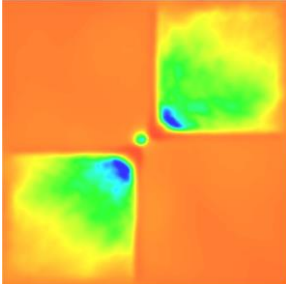
Visibility slice at 2.0 m	Visibility slice at 2.3 m	Visibility slice at 2.5 m
40% Free area. EVEN perforation		
		
40% Free area UNEVEN openings. Design #1		
		
40% Free area UNEVEN openings. Design #2		
		
40% Free area UNEVEN openings. Design #3		
		

Table 33 (Continued). Visibility on horizontal fields at 2.0, 2.3, and 2.5 m height for uneven openings in the false ceilings for relative openness of 40%. Time-averaged steady-state results (50 s. of the averaging period). Colour bar scale is given in Table 16

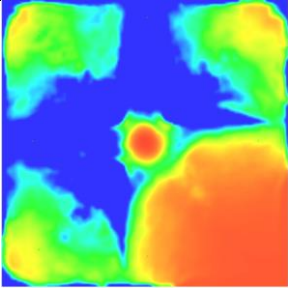
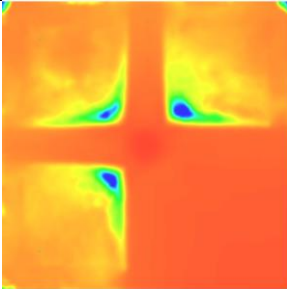
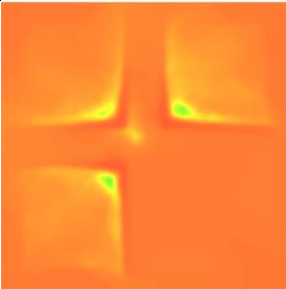
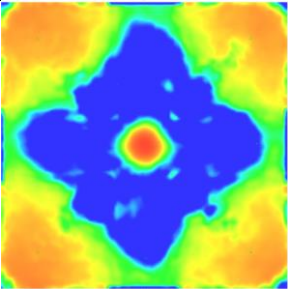
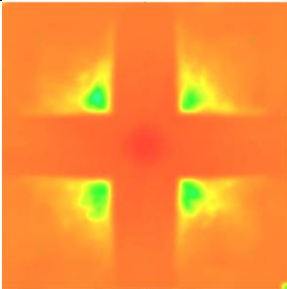
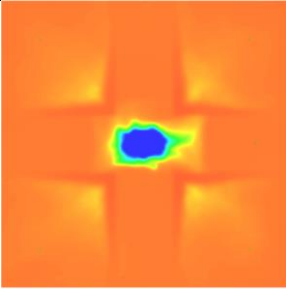
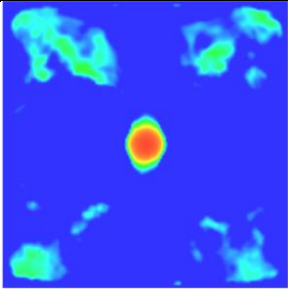
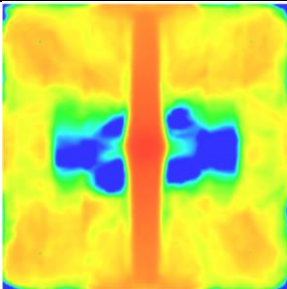
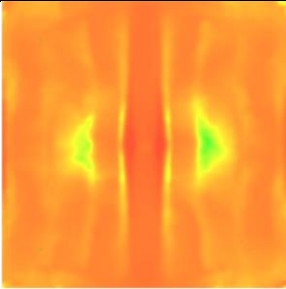
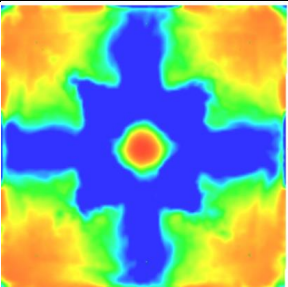
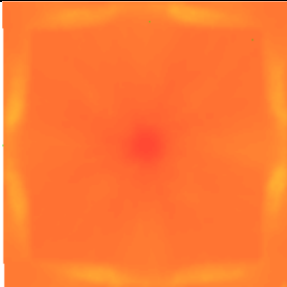
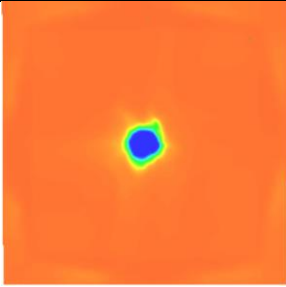
Visibility slice at 2.0 m	Visibility slice at 2.3 m	Visibility slice at 2.5 m
40% Free area UNEVEN openings. Design #4		
		
40% Free area UNEVEN openings. Design #5		
		
40% Free area UNEVEN openings. Design #6		
		
40% Free area UNEVEN openings. Design #7		
		

Table 34. Visibility on horizontal fields at 2.0, 2.3, and 2.5 m height for uneven openings in the false ceilings for relative openness of 25%. Time-averaged steady-state results (50 s. of the averaging period). Colour bar scale is given in Table 16

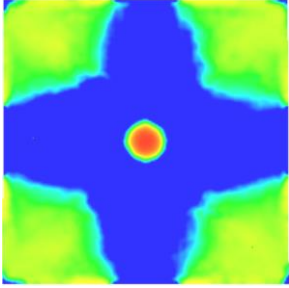
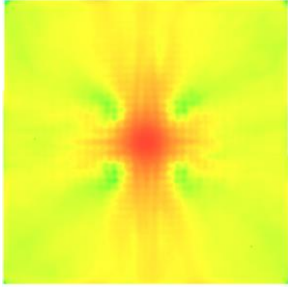
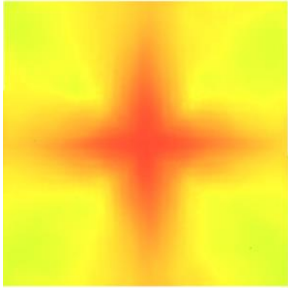
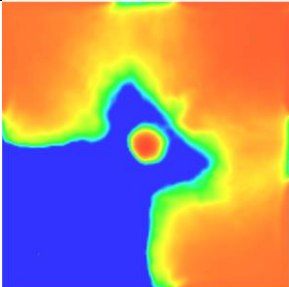
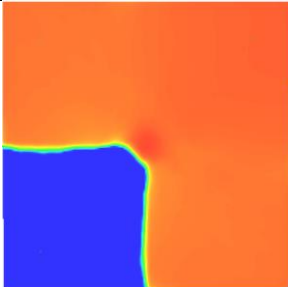
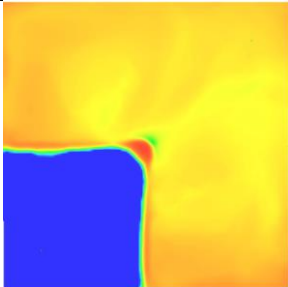
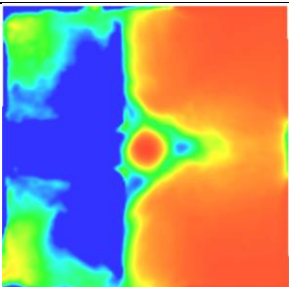
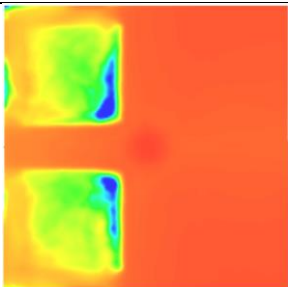
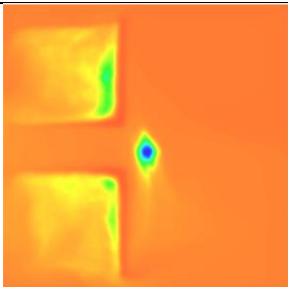
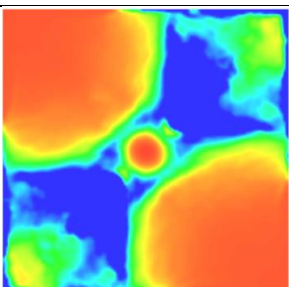
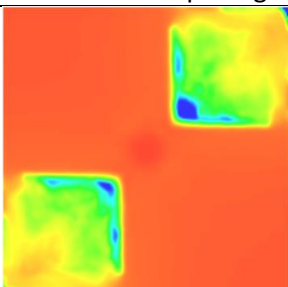
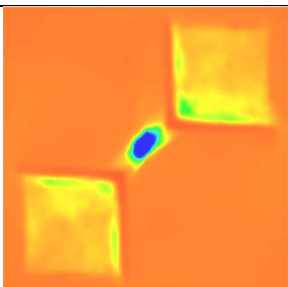
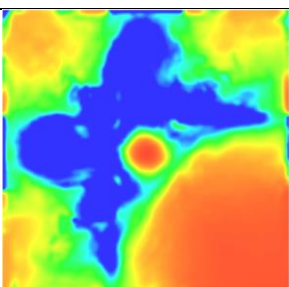
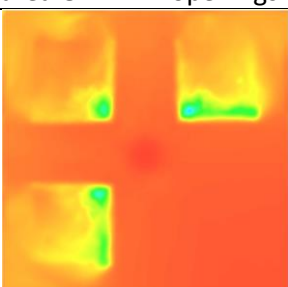
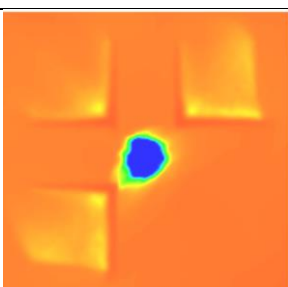
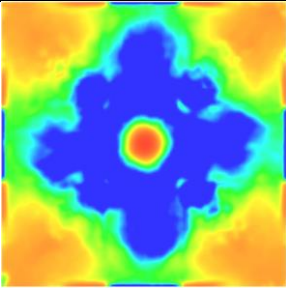
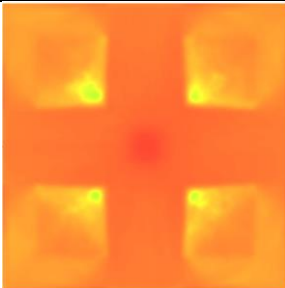
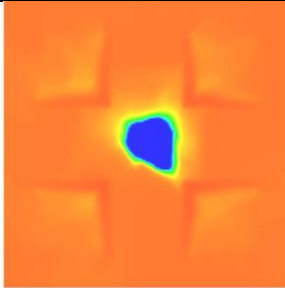
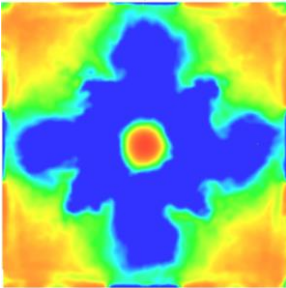
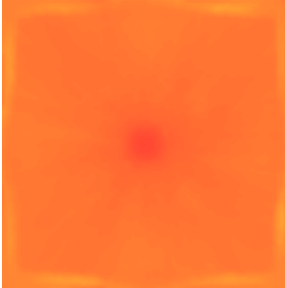
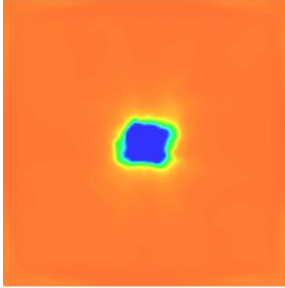
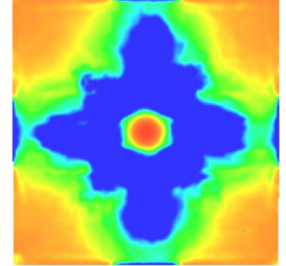
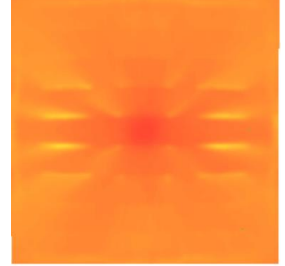
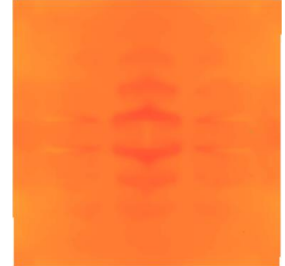
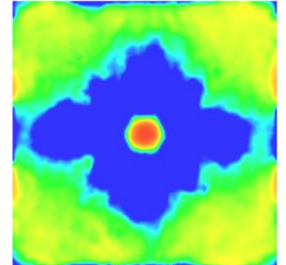
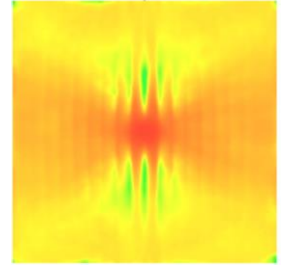
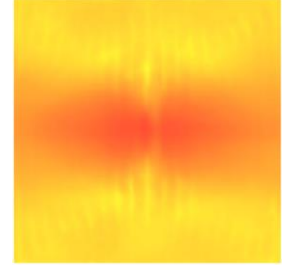
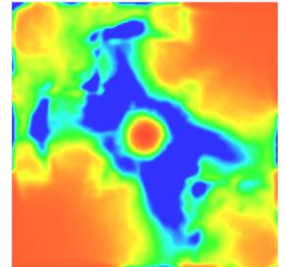
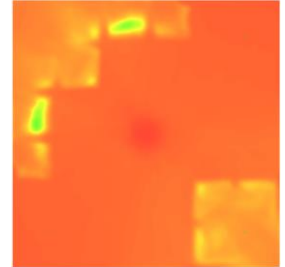
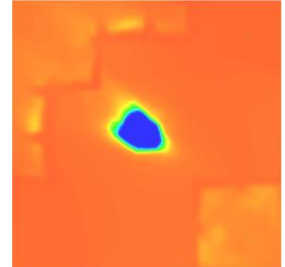
Visibility slice at 2.0 m	Visibility slice at 2.3 m	Visibility slice at 2.5 m
25% Free area EVEN perforation		
		
25% Free area UNEVEN openings. Design #1		
		
25% Free area UNEVEN openings. Design #2		
		
25% Free area UNEVEN openings. Design #3		
		
25% Free area UNEVEN openings. Design #4		
		

Table 34 (Continued). Visibility on horizontal fields at 2.0, 2.3, and 2.5 m height for uneven openings in the false ceilings for relative openness of 25%. Time-averaged steady-state results (50 s. of the averaging period). Colour bar scale is given in Table 16

Visibility slice at 2.0 m	Visibility slice at 2.3 m	Visibility slice at 2.5 m
25% Free area UNEVEN openings. Design #5		
		
25% Free area UNEVEN openings. Design #6		
		
25% Free area UNEVEN openings. Design #7		
		
25% Free area UNEVEN openings. Design #8		
		
25% Free area UNEVEN openings. Design #9		
		

7 Appendix B. Design extraction rate calculation.

Design criteria for the rate of smoke extraction and number of vents were identified with the following steps:

1. According to Section 5.1.1, if equation 5.1 is satisfied, then the plume is above large fire:

$$Y \leq 10(A_f)^{0.5} \text{ (m)}$$

$$Y \leq 10(4)^{0.5} \text{ (m)}$$

$$3 \leq 20 \text{ (m)}$$

Where,

Y – height of plume rise, m

A_f – area of the fire, m²

2. Rate of air entrainment into a plume of smoke rising above the fire can be obtained by equation 5.2:

$$M_f = C_e * P * Y^{3/2} \text{ (kgs}^{-1}\text{)}$$

$$M_f = 0.21 * 8 * 3^{3/2} \text{ (kgs}^{-1}\text{)}$$

$$M_f = 8.73 \text{ (kgs}^{-1}\text{)}$$

Where,

M_f – rate of air entrainment into the plume, kgs⁻¹

C_e – 0.19 (kgs⁻¹m^{-5/2}) for large areas such as auditoria, open
– plan offices, stadia, and atria

C_e – 0.21 (kgs⁻¹m^{-5/2}) for large areas where the ceiling is close to the fire

C_e – 0.34 (kgs⁻¹m^{-5/2}) for small rooms (unit shops, hotel rooms, cellular offices) where
ventilation openings are on one side of the fire.

P – the perimeter of the fire, m

3. Mean temperature rise of the smoke layer above ambient temperature, can be calculated with equation 5.10 in Section 5.4:

$$\theta = \frac{Q_w}{M * c} \text{ (K)}$$

$$\theta = \frac{500 \text{ kWm}^{-2} * 4 \text{ m}^2}{8.73} \text{ (K)}$$

$$\theta = 229 \text{ (K)}$$

Where,

θ – mean temperature rise, K

Q_w – convective heat flux in the gases, kW

M – the mass flow of smoke, kgs^{-1}

c – specific heat capacity of gases $(\text{kJ (kg)}^{-1}\text{K}^{-1})$

4. According to Section 5.10, it is important to identify the number of exhaust points within the reservoir because, for any specific smoke layer depth, there is a maximum rate (M_{crit}) for each exhaust point. This implies that if the exhaust rate is increased any further that a critical value could result in “plug-holing”. Presence of plug-holing in the design means ineffective usage of the design capacity of the exhaust system, which draws clean air from the compartment, instead of hot smoke gases. Equation 5.14 gives more pessimistic result based on Heselden’s analysis which can be considered the worst-case method to calculate the number of ventilators close to the wall:

$$M_{crit} = 1.3 \left(\frac{g * D^5 * T_0 * \theta_l}{T_l^2} \right)^{1/2} (\text{kgs}^{-1})$$

$$M_{crit} = 1.3 \left(\frac{9.81 * 1^5 * 293 * 229}{522^2} \right)^{1/2} (\text{kgs}^{-1})$$

$$M_{crit} = 2.02 (\text{kgs}^{-1})$$

Then, the number of exhaust points can be found with:

$$N \geq \frac{M_e}{M_{crit}}$$

$$N \geq \frac{8.73}{2.02}$$

$$N \geq 4.32, \text{ hence 5 exhaust points}$$

Where,

M_{crit} – critical exhaust rate at an exhaust point, kgs^{-1}

M_e – mass flow rate, ei M_f or M_B (kg s^{-1})

g – acceleration due to gravity, ms^{-2}

D – the depth of smoke layer below the exhaust point, m

T_0 – ambient temperature, K

θ_l – smoke layer temperature rise, $^{\circ}\text{C}$

$$T_l = T_0 + \theta_l \text{ (K)}$$

5. Design exhaust rate for mechanical ventilation system is found according to equation 5.16 in Section 5.13:

$$V_l = \frac{M_l * T_l}{\rho_0 * T_0} \text{ (m}^3\text{s}^{-1}\text{)}$$
$$V_l = \frac{8.73 * 522}{1.225 * 293} \text{ (m}^3\text{s}^{-1}\text{)}$$
$$V_l = 12.7 \text{ (m}^3\text{s}^{-1}\text{)}$$

Where,

V_l – volumetric exhaust rate, m^3s^{-1}

M_l – mass flow rate, ei M_f or M_B

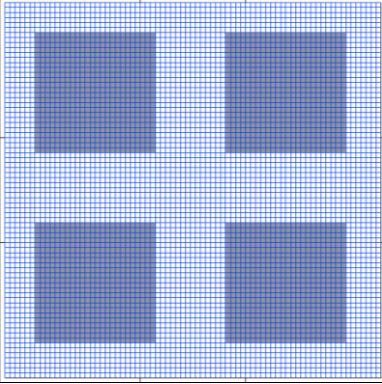
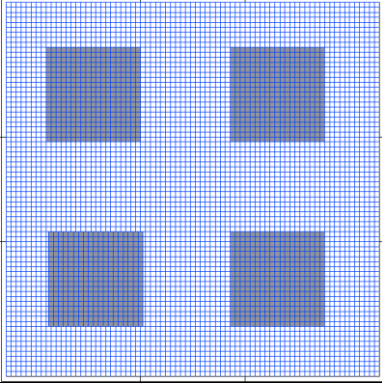
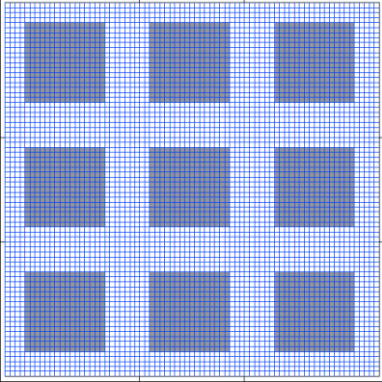
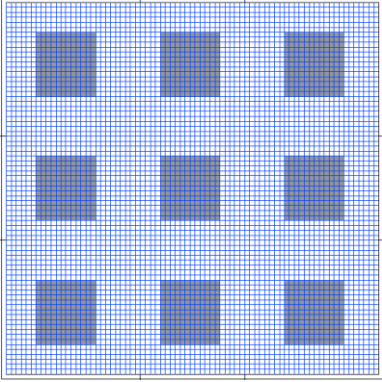
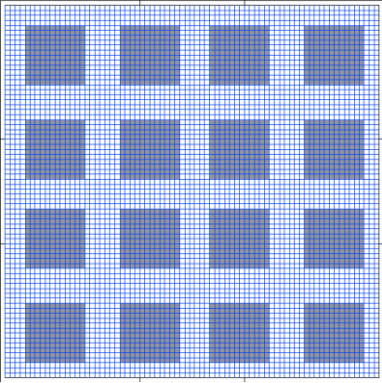
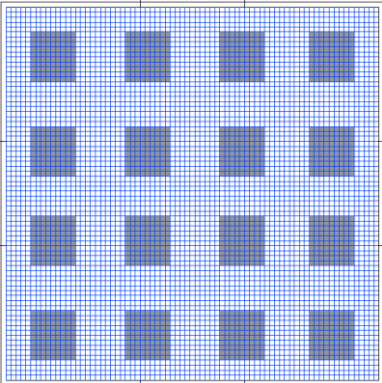
ρ_0 – the density of ambient air, kg m^{-3}

6. Finally, the total exhaust rate of $12.7 \text{ m}^3\text{s}^{-1}$ divided by five exhaust points gives $2.54 \text{ m}^3\text{s}^{-1}$ per each exhaust point. Mechanical exhaust points were modelled as exhaust surface with a volume flow rate of $2.54 \text{ m}^3\text{s}^{-1}$ and default ramp-up time of 1s, whereas inlet openings were modelled as open vents.

8 Appendix C: Additional simulations

Additional simulations have been performed to see how the temperatures at various locations and visibility improve if number of openness in the false ceiling increase and become fore symmetric. For this purpose, 40% Design #5 and 25% Design #5 were further continued with pattern in a similar manner. If Design #5 consists of openings that form a pattern of 2 x 2, further amendment of the design is 3 x 3, 4 x 4, and 5 x 5.

Table 35. The geometry of additional performed simulation.

	40% uneven openness	25% uneven openness
	Area of each opening: 22.5 m ²	Area of each opening: 14 m ²
Design #5 2 x 2		
	Area of each opening: 10 m ²	Area of each opening: 6.25 m ²
3 x 3		
	Area of each opening: 5.6 m ²	Area of each opening: 3.5 m ²
4 x 4		
	Area of each opening: 3.6 m ²	Area of each opening: 2.3 m ²

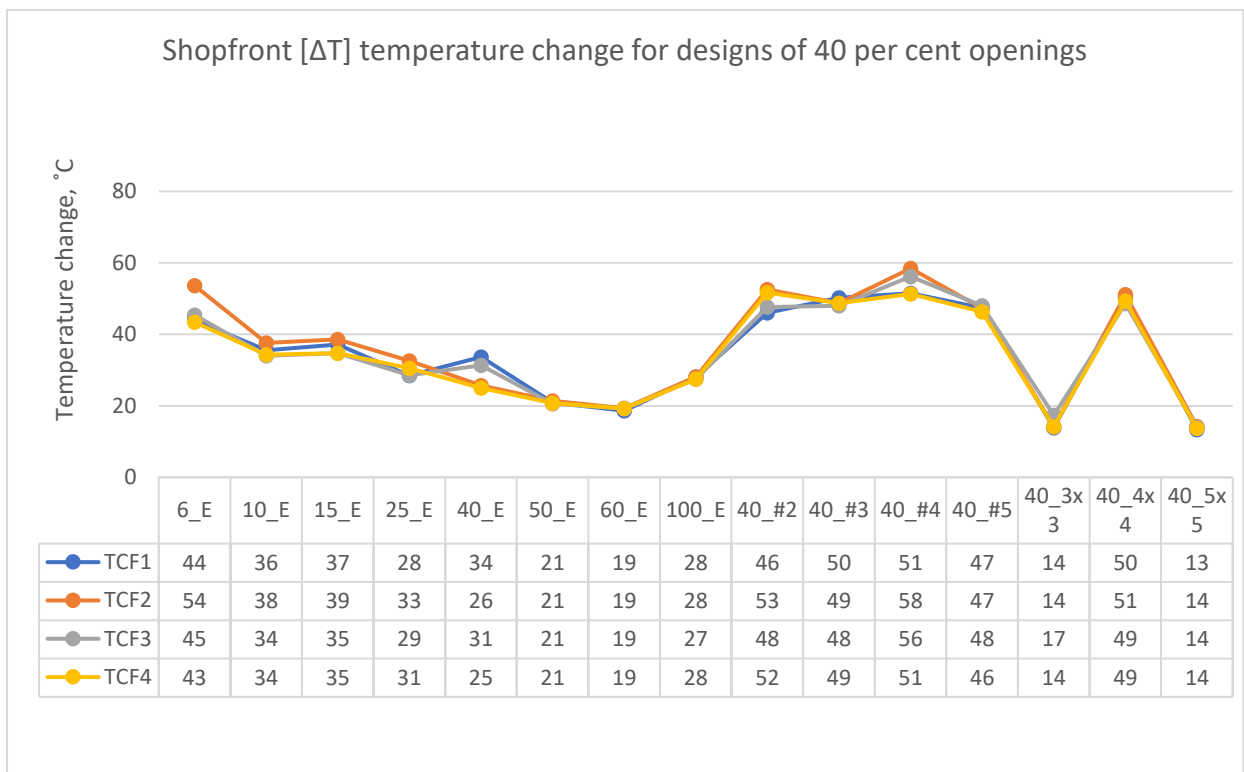
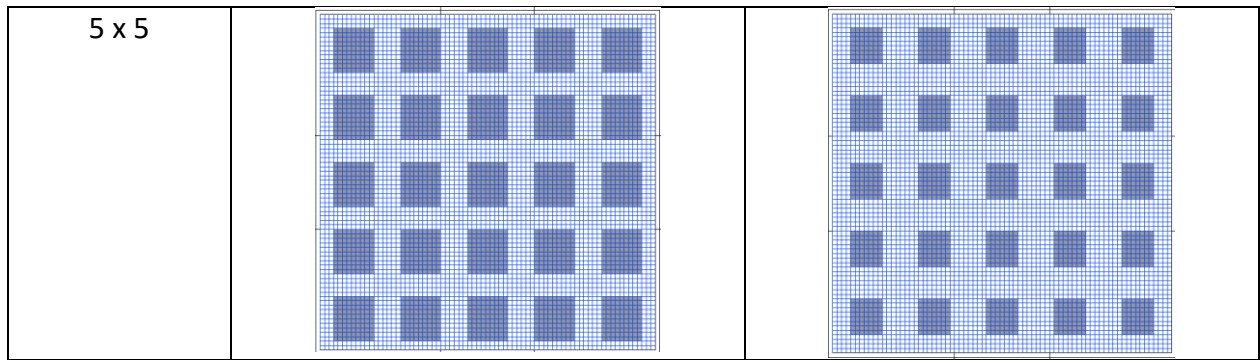


Figure 31. Comparison of temperatures for perforated false ceiling with 6, 10, 15, 25, 40, 50, and 60% free area and uneven openness of 40% with various designs. Temperature readings are from thermocouples located at each of the four shopfront downstands. TCF1, TCF2, TCF3, and TCF4 are thermocouple names. Time-averaged steady-state results (50 s. of the averaging period)

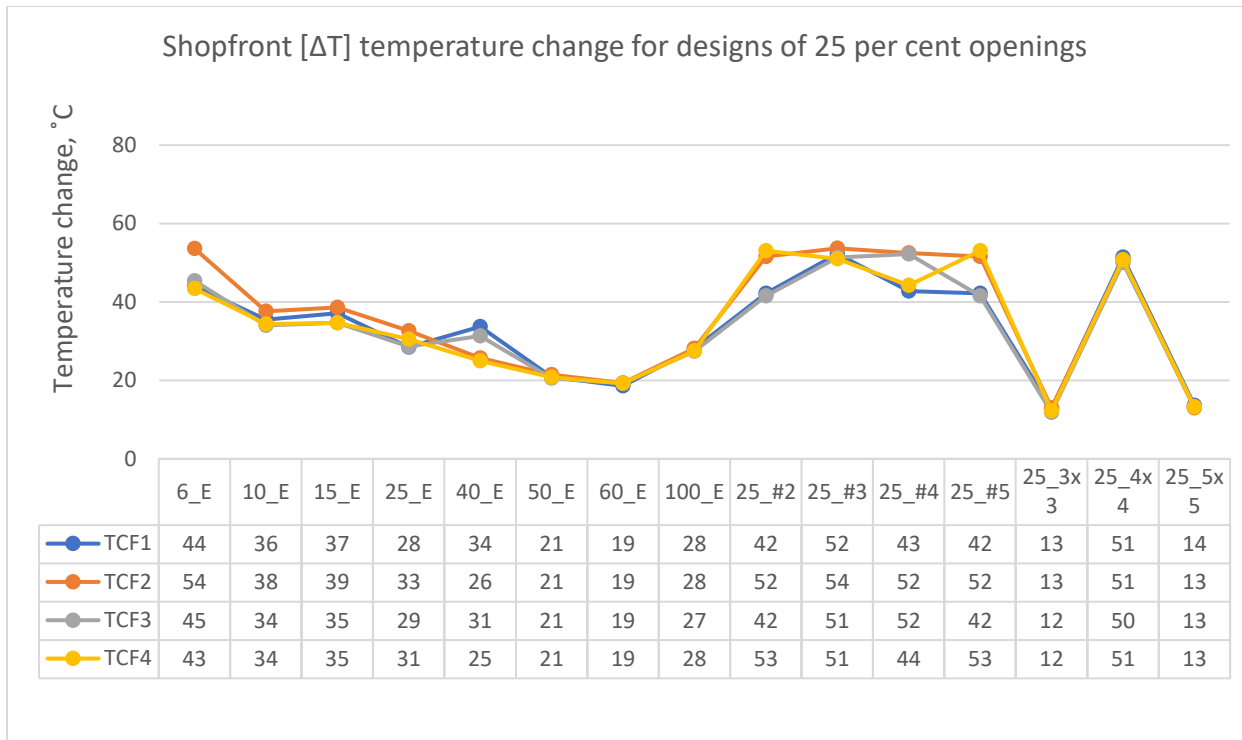


Figure 32. Comparison of temperatures for perforated false ceiling with 6, 10, 15, 25, 40, 50, and 60% free area and uneven openness of 25% with various designs. Temperature readings are from thermocouples located at each of the four shopfront downstands. TCF1, TCF2, TCF3, and TCF4 are thermocouple names. Time-averaged steady-state results (50 s. of the averaging period)

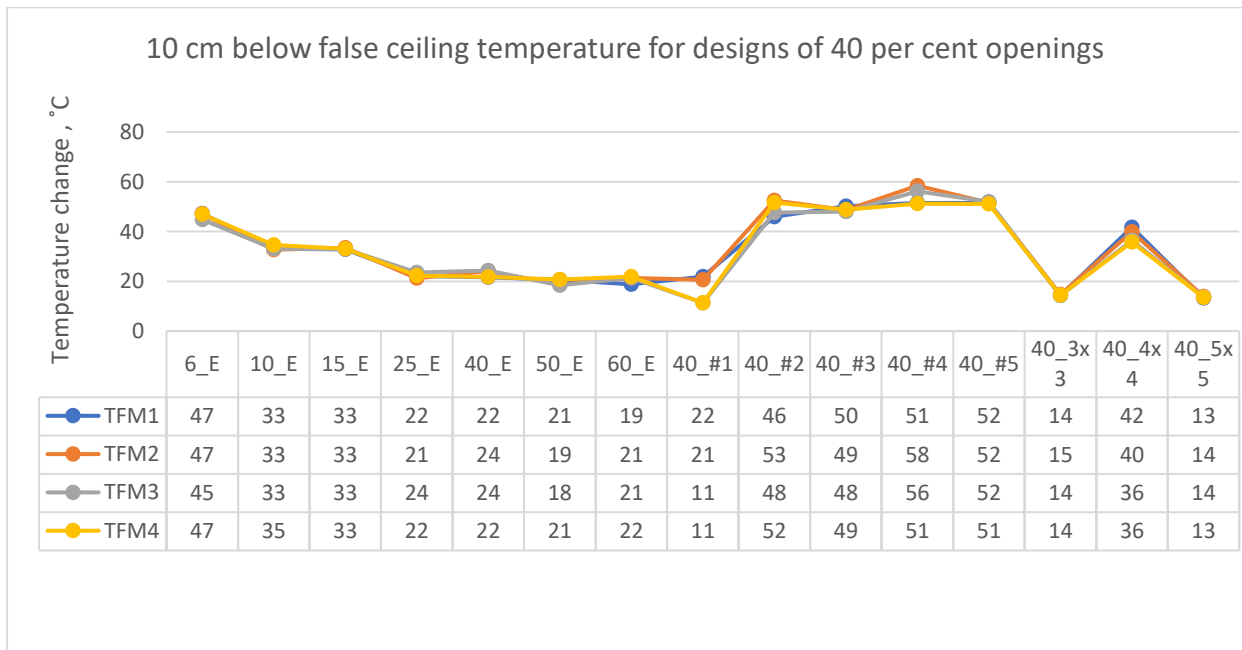


Figure 33. Comparison of temperatures for perforated false ceiling with 6, 10, 15, 25, 40, 50, and 60% free area and uneven openness of 40% with various designs. Temperature readings are from thermocouples located 10 cm below false ceiling. TFM1, TFM2, TFM3, and TFM4 are thermocouple names. Time-averaged steady-state results (50 s. of the averaging period)

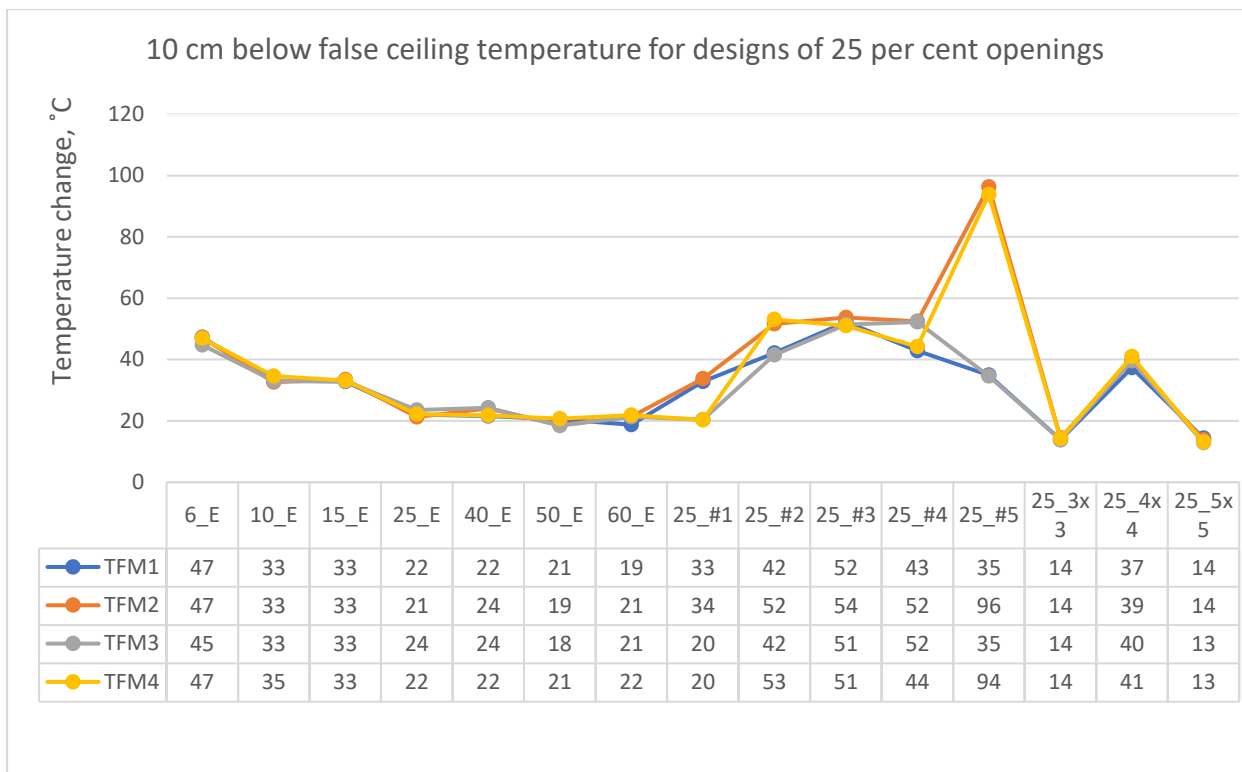


Figure 34. Comparison of temperatures for perforated false ceiling with 6, 10, 15, 25, 40, 50, and 60% free area and uneven openness of 25% with various designs. Temperature readings are from thermocouples located 10 cm below false ceiling. TFM1, TFM2, TFM3, and TFM4 are thermocouple names. Time-averaged steady-state results (50 s. of the averaging period)

9 Appendix D. FDS input for 40% free area uneven openness in the false ceiling. Design #5

Mech2_405a.fds

Generated by PyroSim - Version 2019.3.1204

Jun 16, 2020 12:58:14 AM

&HEAD CHID='Mech2_405a'/

&TIME T_END=200.0/

&DUMP COLUMN_DUMP_LIMIT=.TRUE., DT_RESTART=10.0, DT_SL3D=0.25/

&MESH ID='Mesh 0-1', IJK=10,150,40, XB=0.0,1.0,0.0,15.0,0.0,4.0/

&MESH ID='Mesh 1-2', IJK=10,150,40, XB=1.0,2.0,0.0,15.0,0.0,4.0/

&MESH ID='Mesh 2-3', IJK=10,150,40, XB=2.0,3.0,0.0,15.0,0.0,4.0/

&MESH ID='Mesh 3-4', IJK=10,150,40, XB=3.0,4.0,0.0,15.0,0.0,4.0/

&MESH ID='Mesh 4-5', IJK=10,150,40, XB=4.0,5.0,0.0,15.0,0.0,4.0/

&MESH ID='Mesh 5-6', IJK=10,150,40, XB=5.0,6.0,0.0,15.0,0.0,4.0/

&MESH ID='Mesh 6-7', IJK=10,150,40, XB=6.0,7.0,0.0,15.0,0.0,4.0/

&MESH ID='Mesh 7-8', IJK=10,150,40, XB=7.0,8.0,0.0,15.0,0.0,4.0/

&MESH ID='Mesh 8-9', IJK=10,150,40, XB=8.0,9.0,0.0,15.0,0.0,4.0/

&MESH ID='Mesh 9-10', IJK=10,150,40, XB=9.0,10.0,0.0,15.0,0.0,4.0/

&MESH ID='Mesh 10-11', IJK=10,150,40, XB=10.0,11.0,0.0,15.0,0.0,4.0/

&MESH ID='Mesh 11-12', IJK=10,150,40, XB=11.0,12.0,0.0,15.0,0.0,4.0/

&MESH ID='Mesh 12-13', IJK=10,150,40, XB=12.0,13.0,0.0,15.0,0.0,4.0/

&MESH ID='Mesh 13-14', IJK=10,150,40, XB=13.0,14.0,0.0,15.0,0.0,4.0/

&MESH ID='Mesh 14-15', IJK=10,150,40, XB=14.0,15.0,0.0,15.0,0.0,4.0/

&MESH ID='Extra Mesh for smoke', IJK=75,75,5, XB=0.0,15.0,0.0,15.0,4.0,5.0/

&REAC ID='POLYURETHANE_GM37',

 FYI='SFPE Handbook, GM37',

 FUEL='REAC_FUEL',

C=1.0,
H=1.2,
O=0.2,
N=0.08,
CO_YIELD=0.024,
SOOT_YIELD=0.113,
RADIATIVE_FRACTION=0.35/

&PROP ID='TCF1 props', BEAD_DIAMETER=5.0E-3/
&PROP ID='TCF2 props', BEAD_DIAMETER=5.0E-3/
&PROP ID='TCF3 props', BEAD_DIAMETER=5.0E-3/
&PROP ID='TCF4 props', BEAD_DIAMETER=5.0E-3/
&PROP ID='TCC1 props', BEAD_DIAMETER=5.0E-3/
&PROP ID='TCC2 props', BEAD_DIAMETER=5.0E-3/
&PROP ID='TCC4 props', BEAD_DIAMETER=5.0E-3/
&PROP ID='TCC5 props', BEAD_DIAMETER=5.0E-3/
&PROP ID='TCA1 props', BEAD_DIAMETER=5.0E-3/
&PROP ID='TCA2 props', BEAD_DIAMETER=5.0E-3/
&PROP ID='TCA3 props', BEAD_DIAMETER=5.0E-3/
&PROP ID='TCA4 props', BEAD_DIAMETER=5.0E-3/
&PROP ID='TFM1 props', BEAD_DIAMETER=5.0E-3/
&PROP ID='TFM2 props', BEAD_DIAMETER=5.0E-3/
&PROP ID='TFM3 props', BEAD_DIAMETER=5.0E-3/
&PROP ID='TFM4 props', BEAD_DIAMETER=5.0E-3/
&PROP ID='TFM01 props', BEAD_DIAMETER=5.0E-3/
&PROP ID='TFM02 props', BEAD_DIAMETER=5.0E-3/
&PROP ID='TFM03 props', BEAD_DIAMETER=5.0E-3/
&PROP ID='TFM04 props', BEAD_DIAMETER=5.0E-3/
&DEVC ID='TCF1', PROP_ID='TCF1 props', QUANTITY='THERMOCOUPLE', XYZ=0.0,7.5,2.4/
&DEVC ID='TCF2', PROP_ID='TCF2 props', QUANTITY='THERMOCOUPLE', XYZ=7.6,0.0,2.4/
&DEVC ID='TCF3', PROP_ID='TCF3 props', QUANTITY='THERMOCOUPLE', XYZ=15.0,7.5,2.4/
&DEVC ID='TCF4', PROP_ID='TCF4 props', QUANTITY='THERMOCOUPLE', XYZ=7.5,15.0,2.4/

&DEVC ID='TCC1', PROP_ID='TCC1 props', QUANTITY='THERMOCOUPLE', XYZ=7.6,2.0,3.9/
&DEVC ID='TCC2', PROP_ID='TCC2 props', QUANTITY='THERMOCOUPLE', XYZ=2.0,7.6,3.9/
&DEVC ID='TCC4', PROP_ID='TCC4 props', QUANTITY='THERMOCOUPLE', XYZ=13.0,7.6,3.9/
&DEVC ID='TCC5', PROP_ID='TCC5 props', QUANTITY='THERMOCOUPLE', XYZ=7.6,13.6,3.98/
&DEVC ID='TCA1', PROP_ID='TCA1 props', QUANTITY='THERMOCOUPLE', XYZ=2.0,2.0,0.1/
&DEVC ID='TCA2', PROP_ID='TCA2 props', QUANTITY='THERMOCOUPLE', XYZ=13.0,2.0,0.1/
&DEVC ID='TCA3', PROP_ID='TCA3 props', QUANTITY='THERMOCOUPLE', XYZ=2.0,13.0,0.1/
&DEVC ID='TCA4', PROP_ID='TCA4 props', QUANTITY='THERMOCOUPLE', XYZ=13.0,13.0,0.1/
&DEVC ID='TFM1', PROP_ID='TFM1 props', QUANTITY='THERMOCOUPLE', XYZ=2.0,2.0,2.3/
&DEVC ID='TFM2', PROP_ID='TFM2 props', QUANTITY='THERMOCOUPLE', XYZ=13.0,2.0,2.3/
&DEVC ID='TFM3', PROP_ID='TFM3 props', QUANTITY='THERMOCOUPLE', XYZ=2.0,13.0,2.3/
&DEVC ID='TFM4', PROP_ID='TFM4 props', QUANTITY='THERMOCOUPLE', XYZ=13.0,13.0,2.3/
&DEVC ID='TFM01', PROP_ID='TFM01 props', QUANTITY='THERMOCOUPLE', XYZ=2.0,2.0,2.5/
&DEVC ID='TFM02', PROP_ID='TFM02 props', QUANTITY='THERMOCOUPLE', XYZ=13.0,13.0,2.5/
&DEVC ID='TFM03', PROP_ID='TFM03 props', QUANTITY='THERMOCOUPLE', XYZ=2.0,13.0,2.5/
&DEVC ID='TFM04', PROP_ID='TFM04 props', QUANTITY='THERMOCOUPLE', XYZ=13.0,2.0,2.5/

&SURF ID='ADIABATIC',
 COLOR='GRAY 80',
 ADIABATIC=.TRUE./

&SURF ID='Mechanical exhaust',
 RGB=26,128,26,
 VOLUME_FLOW=2.54/

&SURF ID='Fire',
 COLOR='RED',
 HRRPUA=500.0,
 TMP_FRONT=300.0/

&OBST ID='Obstruction', XB=0.0,5.4,0.0,0.0,0.0,4.0, RGB=240,240,240, TRANSPARENCY=0.156863,
SURF_ID='ADIABATIC'/

&OBST ID='Obstruction', XB=0.0,5.4,15.0,15.0,0.0,4.0, RGB=240,240,240, TRANSPARENCY=0.156863,
SURF_ID='ADIABATIC'/

&OBST ID='Obstruction', XB=0.0,0.0,0.0,5.4,0.0,4.0, RGB=240,240,240, TRANSPARENCY=0.156863, SURF_ID='ADIABATIC'/

&OBST ID='Obstruction', XB=0.0,0.0,9.6,15.0,0.0,4.0, RGB=240,240,240, TRANSPARENCY=0.156863, SURF_ID='ADIABATIC'/

&OBST ID='Obstruction', XB=15.0,15.0,0.0,5.4,0.0,4.0, RGB=240,240,240, TRANSPARENCY=0.156863, SURF_ID='ADIABATIC'/

&OBST ID='Obstruction', XB=9.6,15.0,15.0,15.0,0.0,4.0, RGB=240,240,240, TRANSPARENCY=0.156863, SURF_ID='ADIABATIC'/

&OBST ID='Obstruction', XB=9.6,15.0,0.0,0.0,0.0,4.0, RGB=240,240,240, TRANSPARENCY=0.156863, SURF_ID='ADIABATIC'/

&OBST ID='Obstruction', XB=5.4,9.6,0.0,0.0,2.4,4.0, RGB=240,240,240, TRANSPARENCY=0.156863, SURF_ID='ADIABATIC'/

&OBST ID='Obstruction', XB=5.4,9.6,15.0,15.0,2.4,4.0, RGB=240,240,240, TRANSPARENCY=0.156863, SURF_ID='ADIABATIC'/

&OBST ID='Obstruction', XB=0.0,0.0,5.4,9.6,2.4,4.0, RGB=240,240,240, TRANSPARENCY=0.156863, SURF_ID='ADIABATIC'/

&OBST ID='Obstruction', XB=15.0,15.0,5.4,9.6,2.4,4.0, RGB=240,240,240, TRANSPARENCY=0.156863, SURF_ID='ADIABATIC'/

&OBST ID='Obstruction', XB=15.0,15.0,9.6,15.0,0.0,4.0, RGB=240,240,240, TRANSPARENCY=0.156863, SURF_ID='ADIABATIC'/

&OBST ID='Ceiling', XB=0.0,15.0,0.0,2.0,4.0,4.0, RGB=240,240,240, TRANSPARENCY=0.156863, SURF_ID='ADIABATIC'/

&OBST ID='Ceiling', XB=0.0,15.0,13.0,15.0,4.0,4.0, RGB=240,240,240, TRANSPARENCY=0.156863, SURF_ID='ADIABATIC'/

&OBST ID='Ceiling', XB=3.0,7.0,2.0,13.0,4.0,4.0, RGB=240,240,240, TRANSPARENCY=0.156863, SURF_ID='ADIABATIC'/

&OBST ID='Ceiling', XB=0.0,2.0,2.0,13.0,4.0,4.0, RGB=240,240,240, TRANSPARENCY=0.156863, SURF_ID='ADIABATIC'/

&OBST ID='Ceiling', XB=13.0,15.0,2.0,13.0,4.0,4.0, RGB=240,240,240, TRANSPARENCY=0.156863, SURF_ID='ADIABATIC'/

&OBST ID='Ceiling', XB=12.0,13.0,3.0,12.0,4.0,4.0, RGB=240,240,240, TRANSPARENCY=0.156863, SURF_ID='ADIABATIC'/

&OBST ID='Ceiling', XB=2.0,3.0,3.0,12.0,4.0,4.0, RGB=240,240,240, TRANSPARENCY=0.156863, SURF_ID='ADIABATIC'/

&OBST ID='Ceiling', XB=8.0,12.0,2.0,13.0,4.0,4.0, RGB=240,240,240, TRANSPARENCY=0.156863, SURF_ID='ADIABATIC'/

&OBST ID='Ceiling', XB=7.0,8.0,2.0,7.0,4.0,4.0, RGB=240,240,240, TRANSPARENCY=0.156863, SURF_ID='ADIABATIC'/

&OBST ID='Ceiling', XB=7.0,8.0,8.0,13.0,4.0,4.0, RGB=240,240,240, TRANSPARENCY=0.156863, SURF_ID='ADIABATIC'/

&OBST ID='Floor', XB=0.0,15.0,0.0,15.0,0.0,0.0, RGB=240,240,240, TRANSPARENCY=0.156863, SURF_ID='ADIABATIC'/

&OBST ID='Obstruction', XB=0.0,1.2,0.0,15.0,2.4,2.4, COLOR='GRAY 80', SURF_ID='INERT'/

&OBST ID='Obstruction', XB=6.0,9.0,0.0,15.0,2.4,2.4, COLOR='GRAY 80', SURF_ID='INERT'/

&OBST ID='Obstruction', XB=1.2,6.0,0.0,1.2,2.4,2.4, COLOR='GRAY 80', SURF_ID='INERT'/

&OBST ID='Obstruction', XB=9.0,13.8,13.8,15.0,2.4,2.4, COLOR='GRAY 80', SURF_ID='INERT'/

&OBST ID='Obstruction', XB=1.2,6.0,6.0,9.0,2.4,2.4, COLOR='GRAY 80', SURF_ID='INERT'/

&OBST ID='Obstruction', XB=13.8,15.0,0.0,15.0,2.4,2.4, COLOR='GRAY 80', SURF_ID='INERT'/

&OBST ID='Obstruction', XB=9.0,13.8,6.0,9.0,2.4,2.4, COLOR='GRAY 80', SURF_ID='INERT'/

&OBST ID='Obstruction', XB=1.2,6.0,13.8,15.0,2.4,2.4, COLOR='GRAY 80', SURF_ID='INERT'/

&OBST ID='Obstruction', XB=9.0,13.8,0.0,1.2,2.4,2.4, COLOR='GRAY 80', SURF_ID='INERT'/

&HOLE ID='FC', XB=1.2,6.01,1.2,6.0,2.4,2.5/

&HOLE ID='FC', XB=8.99,13.8,9.0,13.8,2.4,2.5/

&HOLE ID='FC', XB=1.2,6.01,9.0,13.8,2.4,2.5/

&HOLE ID='FC', XB=8.99,13.8,1.2,6.0,2.4,2.5/

&HOLE ID='Hole', XB=5.4,9.6,-0.1,0.1,-0.01,2.4/

&HOLE ID='Hole', XB=5.4,9.6,14.9,15.1,-0.01,2.4/

&HOLE ID='Hole', XB=14.9,15.1,5.4,9.6,-0.01,2.4/

&HOLE ID='Hole', XB=-0.1,0.1,5.4,9.6,-0.01,2.4/

&VENT ID='Vent01', SURF_ID='OPEN', XB=0.0,0.0,5.4,9.6,0.0,2.4/

&VENT ID='Vent02', SURF_ID='OPEN', XB=15.0,15.0,5.4,9.6,0.0,2.4/

&VENT ID='Vent03', SURF_ID='OPEN', XB=5.4,9.6,15.0,15.0,0.0,2.4/

&VENT ID='Vent04', SURF_ID='OPEN', XB=5.4,9.6,0.0,0.0,0.0,2.4/

&VENT ID='Vent05', SURF_ID='Mechanical exhaust', XB=2.0,3.0,2.0,3.0,4.0,4.0/

&VENT ID='Vent06', SURF_ID='Mechanical exhaust', XB=2.0,3.0,12.0,13.0,4.0,4.0/

&VENT ID='Vent07', SURF_ID='Mechanical exhaust', XB=12.0,13.0,12.0,13.0,4.0,4.0/

&VENT ID='Vent08', SURF_ID='Mechanical exhaust', XB=12.0,13.0,2.0,3.0,4.0,4.0/

&VENT ID='Vent09', SURF_ID='Mechanical exhaust', XB=7.0,8.0,7.0,8.0,4.0,4.0/

&VENT ID='Fire', SURF_ID='Fire', XB=6.5,8.5,6.5,8.5,0.0,0.0/
&VENT ID='Roof', SURF_ID='OPEN', XB=0.0,15.0,0.0,15.0,5.0,5.0/
&VENT ID='Roof extra', SURF_ID='OPEN', XB=0.0,15.0,0.0,0.0,4.0,5.0/
&VENT ID='Roof extra01', SURF_ID='OPEN', XB=0.0,15.0,15.0,15.0,4.0,5.0/
&VENT ID='Roof extra02', SURF_ID='OPEN', XB=0.0,0.0,0.0,15.0,4.0,5.0/
&VENT ID='Roof extra03', SURF_ID='OPEN', XB=15.0,15.0,0.0,15.0,4.0,5.0/

&SLCF QUANTITY='TEMPERATURE', PBY=5.0/
&SLCF QUANTITY='TEMPERATURE', PBX=5.0/
&SLCF QUANTITY='TEMPERATURE', PBX=2.5/
&SLCF QUANTITY='TEMPERATURE', PBZ=1.5/
&SLCF QUANTITY='TEMPERATURE', PBZ=2.0/
&SLCF QUANTITY='TEMPERATURE', PBZ=2.2/
&SLCF QUANTITY='TEMPERATURE', PBZ=2.3/
&SLCF QUANTITY='TEMPERATURE', PBZ=2.4/
&SLCF QUANTITY='TEMPERATURE', PBZ=2.5/
&SLCF QUANTITY='TEMPERATURE', PBZ=2.6/
&SLCF QUANTITY='TEMPERATURE', PBZ=2.7/
&SLCF QUANTITY='TEMPERATURE', PBZ=2.8/
&SLCF QUANTITY='TEMPERATURE', PBZ=2.9/
&SLCF QUANTITY='TEMPERATURE', PBZ=3.0/
&SLCF QUANTITY='TEMPERATURE', PBZ=3.1/
&SLCF QUANTITY='TEMPERATURE', PBZ=3.2/
&SLCF QUANTITY='TEMPERATURE', PBZ=3.3/
&SLCF QUANTITY='TEMPERATURE', PBZ=3.4/
&SLCF QUANTITY='TEMPERATURE', PBZ=3.5/
&SLCF QUANTITY='TEMPERATURE', PBZ=3.6/
&SLCF QUANTITY='TEMPERATURE', PBZ=3.7/
&SLCF QUANTITY='TEMPERATURE', PBZ=3.8/
&SLCF QUANTITY='TEMPERATURE', PBZ=3.9/
&SLCF QUANTITY='TEMPERATURE', PBX=7.5/
&SLCF QUANTITY='TEMPERATURE', PBY=7.5/

&SLCF QUANTITY='TEMPERATURE', PBY=2.5/
&SLCF QUANTITY='VISIBILITY', PBX=5.0/
&SLCF QUANTITY='VISIBILITY', PBY=5.0/
&SLCF QUANTITY='VISIBILITY', PBX=2.5/
&SLCF QUANTITY='VISIBILITY', PBY=2.5/
&SLCF QUANTITY='VISIBILITY', PBY=7.5/
&SLCF QUANTITY='VISIBILITY', PBX=7.5/
&SLCF QUANTITY='VISIBILITY', PBZ=2.0/
&SLCF QUANTITY='VISIBILITY', PBZ=2.2/
&SLCF QUANTITY='VISIBILITY', PBZ=2.3/
&SLCF QUANTITY='VISIBILITY', PBZ=2.4/
&SLCF QUANTITY='VISIBILITY', PBZ=2.5/
&SLCF QUANTITY='VISIBILITY', PBZ=2.6/
&SLCF QUANTITY='VISIBILITY', PBZ=2.7/
&SLCF QUANTITY='VISIBILITY', PBZ=2.8/
&SLCF QUANTITY='VISIBILITY', PBZ=2.9/
&SLCF QUANTITY='VISIBILITY', PBZ=3.0/
&SLCF QUANTITY='VISIBILITY', PBZ=3.1/
&SLCF QUANTITY='VISIBILITY', PBZ=3.2/
&SLCF QUANTITY='VISIBILITY', PBZ=3.3/
&SLCF QUANTITY='VISIBILITY', PBZ=3.4/
&SLCF QUANTITY='VISIBILITY', PBZ=3.5/
&SLCF QUANTITY='VISIBILITY', PBZ=3.6/
&SLCF QUANTITY='VISIBILITY', PBZ=3.7/
&SLCF QUANTITY='VISIBILITY', PBZ=3.8/
&SLCF QUANTITY='VISIBILITY', PBZ=3.9/
&SLCF QUANTITY='VELOCITY', VECTOR=.TRUE., PBY=5.0/
&SLCF QUANTITY='VELOCITY', VECTOR=.TRUE., PBX=5.0/
&SLCF QUANTITY='VELOCITY', VECTOR=.TRUE., PBX=2.5/
&SLCF QUANTITY='VELOCITY', VECTOR=.TRUE., PBY=2.5/
&SLCF QUANTITY='VELOCITY', VECTOR=.TRUE., PBX=7.5/
&SLCF QUANTITY='VELOCITY', VECTOR=.TRUE., PBY=7.5/

&SLCF QUANTITY='VELOCITY', VECTOR=.TRUE., PBZ=0.5/
&SLCF QUANTITY='VELOCITY', VECTOR=.TRUE., PBZ=1.5/
&SLCF QUANTITY='VELOCITY', VECTOR=.TRUE., PBZ=2.2/
&SLCF QUANTITY='VELOCITY', VECTOR=.TRUE., PBZ=2.4/
&SLCF QUANTITY='VELOCITY', VECTOR=.TRUE., PBZ=2.5/
&SLCF QUANTITY='VELOCITY', VECTOR=.TRUE., PBZ=2.6/
&SLCF QUANTITY='VELOCITY', VECTOR=.TRUE., PBZ=3.0/
&SLCF QUANTITY='VELOCITY', VECTOR=.TRUE., PBZ=3.9/

&TAIL /